The role of the Sunda Strait in the glacial to Holocene development of the eastern tropical Indian Ocean hydrography

Dissertation

zur Erlangung des Doktorgrades der Naturwissenschaften

Dr. rer. nat.

im Fachbereich Geowissenschaften

der Universität Bremen

vorgelegt von

Riza Yuliratno Setiawan

Bremen, August 2015

Tag des öffentlichen Kolloquiums

31.09.2015

15:15 Uhr, GEO Hörsaal 1550

Gutachter der Dissertation

Prof. Dr. Dierk Hebbeln

Prof. Dr. Heiko Pälike

Prüfer

Prof. Dr. Tobias Mörz

PD Dr. Christian Winter

Weitere Mitglieder des Prüfungsausschusses

Dr. Mahyar Mohtadi

Maren Bender

N a m e : Riza Yuliratno Setiawan Datum : 04.08.2015

Anschrift : MARUM- Center for Marine Environmental Sciences

E r k l ä r u n g

Hiermit versichere ich, dass ich

1. die Arbeit ohne unerlaubte fremde Hilfe angefertigt habe

2. keine anderen als die von mir angegebenen Quellen und Hilfsmittel benutzt habe und

3. die den benutzten Werken wörtlich oder inhaltlich entnommenen Stellen als solche kenntlich gemacht habe.

Bremen, den 04.08.2015

Riza Yuliratno Setiawan

ACKNOWLEDGEMENTS

I would like to thank my supervisors Prof. Dierk Hebbeln, Dr. Mahyar Mohtadi, Dr. Stephan Steinke and Prof. Michal Kucera for being so incredibly patient and supportive. I would like to thank Dr. Jeroen Groeneveld, Dr. Henning Kuhnert and Cornelia Kwiatkowski. I have greatly enjoyed working with you and I have learnt an enormous amount on the Mg/Ca and Ba/Ca analyses and ICP-OES. Thank you also to Dr. Ed Hathorne and Dr. Katharina Pahnke for introducing me to the neodymium world and providing me many supports.

Thank you also needs to go to those organisations from which I received funding, namely the Deutscher Akademischer Austauschdienst (DAAD), MARUM and, GLOMAR for funding this research and also for providing excellent opportunities for research training courses and career development. It was privilege to be a student in the Department of Geosciences, GLOMAR-MARUM, University of Bremen. The staffs and the PhD students were very helpful and supportive.

A huge thanks to the members of the working group of Marine Sedimentology "AG Hebbeln": Gema Martínez Méndez, Claudia Wienberg, Jürgen Titschack, Daniela Pittauer, Lydie Dupont, Martin Bartels, Lelia Matos, M. Yusuf Awaluddin, Florian Boxberg, Martina Hollstein, Roshan Zaidan, and Hiske Fink. Special thank you needs to go to my office mates, Carmen Friese, Inka Meyer, and Jan-Berend Stuut. You all have provided me a perfect working environment. You have all been fantastic.

Finally a big thank you to my amazing family. To my wife and daughter: Venny and Alyssa, my parents: Amin Sutaryo and Surati, my little brothers: Yosi, Oni, and Ifan, who have lovingly and steadfastly supported and encouraged me throughout the years. I could not have done this without your endless love and support. Furthermore, thank you goes to CATOR group and Indonesian community in Bremen for your friendships. Family and friends support and encouragement have played a major role in completing what will be my last ever thesis.

CONTENTS

Abstract 9

Zusammenfassung 11

1 Introduction

1.1. The Indonesian Seas and major climate phenomena 13

1.2. Eastern tropical Indian Ocean 17

1.3 Paleoceanographic reconstruction of the eastern tropical Indian Ocean 19

1.3.1. Paleogeographic changes since the Last Glacial Maximum (LGM) 21

1.4. Dissertation objectives 22

1.5. Dissertation structure and contribution to publications 24

2 Regional Hydrography

2.1. Ocean circulation 27

2.2. Water masses 28

3 Materials and Methods

3.1. Materials of study and sediment sampling 30

3.2. Methods

3.2.1. Accelerator mass spectrometry (AMS) dating 30

3.2.2. Stable isotope, Mg/Ca and Ba/Ca analyses 31

3.2.3. Neodymium and strontium isotope analyses

3.2.3.1. Neodymium extraction from mixed planktonic foraminifera 32

3.2.3.2. Neodymium and Strontium extraction from detrital fraction 32

3.2.3.3. Neodymium and strontium isotope measurements 32

3.2.4. X-Ray Fluorescence (XRF) core scanning 33

4 The consequences of opening the Sunda Strait on the hydrography of the eastern tropical Indian Ocean 34

1. Introduction 35

2. Study Area 36

3. Materials and Method

3.1. Sediment cores GeoB 10042-1 and GeoB 10043-3 39

3.2. Radiocarbon dating 39

3.3. Stable Isotope and Mg/Ca Analyses 41

3.4. X-Ray Fluorescence (XRF) Core Scanning 43

3.5. Spliced records and published data 43

4. Results

4.1. Age Model 44

4.2. Shell $\delta^{18}O$ and Mg/Ca ratio of *G. ruber* s.s. 46

4.3. Seawater $\delta^{18}O$ ($\delta^{18}O_{sw}$) 47

4.4. XRF Measurements 47

5. Discussion

5.1. Hydrologic conditions off the Sunda Strait prior to the Sunda Shelf flooding (10 kyr BP) 49

5.2. The flooding of the Sunda Shelf 53

5.3. Hydrologic conditions off the Sunda Strait after the Sunda Shelf Flooding 54

5.4. The impact of the Sunda Strait opening on regional hydrography 55

6. Conclusion 57

5 Modification of the deep water neodymium isotope composition along the eastern margin of the tropical Indian Ocean 58

1. Introduction 59

2. Study Area 60
3. Materials and Methods
3.1. Sediment cores GeoB 10042-1 and GeoB 10043-3 62
3.2. Age Model 63
3.3. Neodymium and strontium isotope analyses
3.3.1. Neodymium extraction from mixed planktonic foraminifera 63
3.3.2. Neodymium and Strontium extraction from detrital fraction 63
3.3.3. Column chromatography and isotope measurement 64
4. Results
4.1. Neodymium Isotope Composition of Mixed Planktic Foraminifera 64
4.2. Neodymium and Strontium Isotope Composition of the Detrital Silicates 65
5. Discussion
5.1. Modification of the foraminifera ε_{Nd} off the Sunda Strait 69
5.2. Variability of the detrital ε_{Nd} off the Sunda Strait 73
6. Conclusion 75

6 Testing the applicability of *G. sacculifer* Ba/Ca as an indicator of freshwater discharge in the eastern tropical Indian Ocean

1. Introduction 77
2. Study Area 79
3. Materials and Methods
3.1. Surface sediments samples 80
3.2. Cleaning of foraminifera shells 80
3.3. Measurement 82
3.4. Calculation of seawater $\delta^{18}O$ 82
4. Results
4.1. Planktic foraminifera *G. sacculifer* element to calcium ratios 83
4.2. Planktic foraminifera *G. sacculifer* $\delta^{18}O_{sw}$ 86
5. Discussion 86
5.1. Testing G. sacculifer Ba/Ca as a proxy for salinity 87

5.2. Testing G. sacculifer Ba/Ca as an indicator for marine productivity 89
6. Conclusion 93

7 Synthesis 95

8 Outlook 97

9 References 99

Abstract

The eastern tropical Indian Ocean (ETIO) off southern Indonesia is a very important region for the global thermohaline circulation as it hosts the exit pathway of the Indonesian Throughflow (ITF). From this region cool and fresh ITF waters are advected by the South Equatorial Current (SEC) to the Indian Ocean. Consequently, the ITF water freshens the Indian Ocean. Nevertheless, the hydrology condition was different during the Last Glacial Maximum (LGM). During this period the sea level was low and the Sunda Shelf was an exposed land. Marine records and simulation study suggest that the exposure of the Sunda Shelf caused a significant reduction in convection over the Indonesian region, resulting arid condition and saltier sea surface condition off south Java. Armed with two sedimentary archives collected from the ETIO off the Sunda Strait, this dissertation investigates the evolution of hydrological changes in the ETIO during the past ~40 kyr B.P. with respect to the flooding of the Sunda Shelf. Furthermore, this dissertation examines the applicability of planktic foraminifera Ba/Ca ratio as a tracer for freshwater discharge.

New results of Mg/Ca-based sea surface temperature (SST), seawater $\delta^{18}O$ ($\delta^{18}O_{sw}$), and XRF-Ti/Ca ratio of GeoB 10042-1 and GeoB 10043-3 collected from off the Sunda Strait revealed that the region has experienced prominent hydrological changes during the past ~40 kyr B.P. The results show that sea surface conditions off the Sunda Strait were cooler and saltier conditions during the last glacial compared to the Holocene, and support previous finding that suggests slowdowns of the Atlantic meridional overturning circulation (AMOC) during the Heinrich stadials 1-3 and the Younger Dryas have caused dry conditions in the ETIO region. Whereas during the Holocene sea surface conditions off the Sunda Strait exhibit warmer and fresher conditions, particularly after the opening of the Sunda Strait at ~10 kyr B.P. This fresher sea surface condition is maintained until today as a consequence of persistent transport of low salinity Java Sea water into the ETIO via the Sunda Strait.

Novel millennial-scale reconstruction of past bottom water conditions (foraminifera ε_{Nd}) show distinct modifications of the bottom water (2171 m) off the Sunda Strait during the past 19 kyr. Modifications of the bottom water during the last deglaciation and the Holocene correspond to a strong- and a weak thermocline ITF flow, respectively. Furthermore, the results imply that the variability of the detrital ε_{Nd} data off the Sunda Strait is susceptible to the ITF flow and large terrigenous material supply from the Sunda Strait.

Planktic foraminifera Ba/Ca ratio has been recently used to reconstruct modern and past freshwater discharge. The application of this proxy is based on the observation that suggests that the Ba/Ca ratio of seawater is directly incorporated into foraminifera calcite, and river water has a distinctly higher Ba/Ca ratio than seawater. However, cleaning experiments results on planktic foraminifera *G. sacculifer* collected from the ETIO revealed that the Ba/Ca ratio of *G. sacculifer* cannot be used as a tracer for modern and past salinity changes due to the appearance of seasonal upwelling complicates the interpretation of the proxy.

Zusammenfassung

Seewärts vor Süd-Indonesien befindet sich der östliche tropische Indische Ozean (ETIO). Diese Ozeanregion ist von besonderer Bedeutung für die globale thermohaline Ozeanzirkulation, da sich hier der Durchgang des indonesischen Durchflusses (ITF) befindet. In dieser Region werden kühle und salzarme ITF Gewässer mit dem Südäquatorialstrom (SEC) in den Indischen Ozean advektiert. Durch den Einfluss der ITF Gewässer erniedrigt sich der Salzgehalt im Indischen Ozean. Die Hydrologie war jedoch während des letzten glazialen Maximums (LGM) anders. Während dieser Zeit war der Meeresspiegel niedrig und der Sunda Schelf lag frei. Marine Archive und Simulationsstudien zeigen, dass die Freilegung des Sunda Schelfes zu einer signifikanten Verringerung der Konvektion innerhalb der indonesischen Region führte. Dadurch kam es zu verringertem Niederschlag und einer salzigeren Meeresoberfläche seewärts vor Süd-Java. Mit Hilfe von zwei Sedimentarchiven, die aus der Region ETIO seewärts der Sundastraße gezogen wurden, untersucht diese Dissertation die Entwicklung der hydrologischen Veränderungen im ETIO während der letzten ~ 40 ka in Bezug auf die Überflutung des Sunda-Schelfes. Darüber hinaus untersucht die Dissertation die Anwendbarkeit von Ba/Ca-Verhältnissen in planktischen Foraminiferenschalen als einen Proxy für Süßwassereintrag.

Neue Ergebnisse der Mg/Ca-basierten Meeresoberflächentemperatur (SST), Meerwasser ^{18}O ($\delta^{18}O_{sw}$) und XRF-Ti/Ca-Verhältnis von den Sedimentkernen GeoB 10042-1 und 10043-3 GeoB ergeben, dass die Gewässer vor der Sundastraße bedeutenden hydrologischen Veränderungen während der vergangenen ~ 40 ka unterlagen. Die Meeresoberflächentemperaturen waren kühler und das Oberflächenwasser war salziger während der letzten Eiszeit im Vergleich zum Holozän. Diese Ergebnisse unterstützen die frühere Feststellung, dass die Verlangsamung der Atlantischen meridionalen Umwälzbewegung (Atlantic overturning circulation = AMOC) während der Heinrich Stadialen

1-3 und der jüngeren Dryas zu niederschlagsärmeren Bedingungen in der ETIO-Region geführt hat. Im Gegensatz dazu herrschten während des Holozäns wärmere und salzärmere Meeresoberflächenbedingungen vor der Sundastraße vor, insbesondere nach der Eröffnung der Sundastraße vor ~ 10 ka. Diese salzärmeren Meeresoberflächenbedingungen halten sich bis heute als Folge des anhaltenden Transportes von salzarmen Javasee-Gewässern in die ETIO Region über die Sundastraße.

Neue jahrtausend-skalige Rekonstruktionen von vergangenen Tiefenwasserbedingungen (Foraminiferen εNd) zeigen deutliche Modifikationen im Tiefenwasser (2170 m) seewärts der Sundastraße während der letzten 19 ka. Diese Modifikationen des Tiefenwassers entsprechen jeweils stärkeren und schwächeren thermoklinen ITF-Flüssen. Darüber hinaus lassen die Ergebnisse erkennen, dass die Variabilität der εNd-Daten seewärts der Sundastraße anfällig für den ITF-Fluss und großem terrigenen Materialeintrag von der Sundastraße ist.

Das Ba/Ca-Verhältnis in planktischen Foraminiferenschalen wurde kürzlich verwendet, um modernen und vergangenen Süßwassereintrag zu rekonstruieren. Die Anwendung dieses Proxies basiert auf folgenden Beobachtungen: Das Ba/Ca-Verhältnis von Seewasser baut sich direkt in das Kalzit der Foraminiferenschalen ein und Flusswasser hat ein deutlich höheres Ba/Ca-Verhältnis als Meerwasser. Allerdings zeigen Reinigungs-Experimente an der planktischen Foraminifere *G. sacculifer*, die aus dem ETIO gesammelt wurde, dass das Ba/Ca-Verhältnis in den Schalen der *G. sacculifer* nicht als Anzeiger für moderne und vergangene Salinitäts-Veränderungen verwendet werden kann. Dies hängt damit zusammen, dass das Vorkommen von saisonalem Auftrieb die Interpretation des Proxies verkompliziert.

1. Introduction

1.1. The Indonesian Seas and major climate phenomena

The Indonesian Seas play a significant role in the global climate as they lie beneath the major atmospheric deep convection center (Neale and Slingo, 2003; Qu et al., 2005; Kida and Richards, 2009) and within the Indo-Pacific Warm Pool (IPWP), the region of the warmest (>28°C) global sea surface temperatures (SSTs) (Pierrehumber, 2000). As a consequence, the Indonesian region provides heat and water vapor for the globe (Qu et al., 2005). Most importantly, the Indonesian Seas are the only low-latitude oceanic connection between the Pacific and Indian Oceans, known as the Indonesian throughflow (ITF). Today the estimated ITF transport is ~15 Sv (1 Sv = 10^6 m^3 s^{-1}) and roughly 80% of that is transported via the main pathway, the Makassar Strait (Gordon et al., 2010). From the Makassar Strait, the ITF water can exit via Lombok Strait or circulate through the Banda and Flores Seas and enter the Indian Ocean via Ombai Strait or Timor Passage (Sprintall et al. 2014).

The Indonesian Seas are also situated at the center of the Australian-Indonesian Monsoon (AIM) system. The sea surface currents in the Indonesian Seas flow according to the seasonally reversing monsoon winds (Figure 1). Furthermore, this monsoon system has been suggested to impact sea surface conditions of the Indonesian Seas (Figure 1; e.g. Setiawan and Kawamura, 2011a; Setiawan and Habibi, 2011b). The southeast monsoon (SEM) (June–August) is associated with the dry season due to southeasterly winds from Australia carrying warm and dry air across Indonesia (Figure 1a). Whereas the northwest monsoon (NWM) is associated with the wet season as westerlies from the Asian continent carry warm and moist air to the Indonesian region (Figure 1b) (Susanto et al., 2006). In addition, also the ITF reveals a seasonal pattern with maximum ITF transport occurring during the SEM (e.g. Meyers et al., 1995).

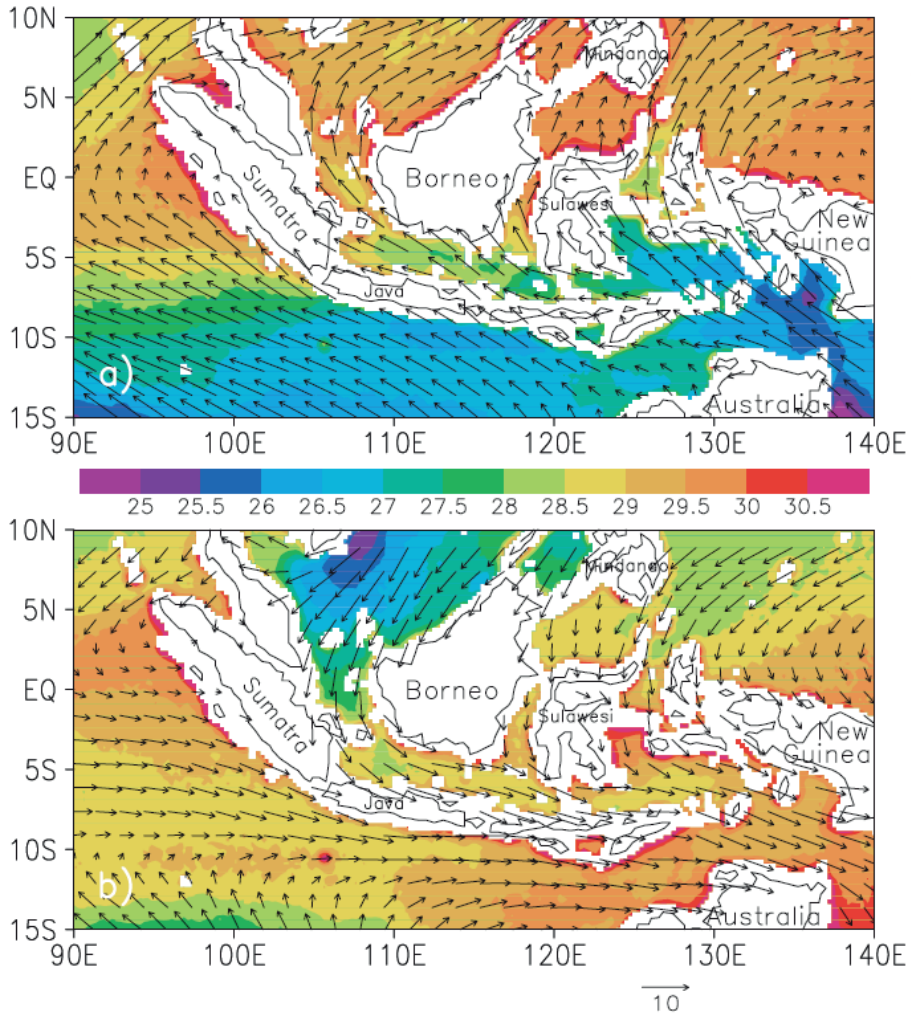

Figure 1. Monthly mean SST superimposed with sea surface wind (QuikSCAT) (m/s) in (a) August and (b) February (Qu et al., 2005). During the SEM season the southeasterly winds blow from Australia northwestward towards the Asian continent. The SEM winds induce significant sea surface cooling in the internal Indonesian Seas and the ETIO. While during the NWM season the northwesterly winds blow from the Asian continent to Australia. During this season prominent sea surface cooling only appears in the South China Sea.

The Indonesian Seas are significantly influenced by the El Niño–Southern Oscillation (ENSO) and the Indian Ocean Dipole (IOD). The ENSO and IOD are primary controlling factors of interannual variability of the climate over the Indonesia region (Gordon et al., 2003; Saji et al. 1999). ENSO is a climate variability associated with a disturbance of the Walker circulation over the tropical Pacific Ocean (Figure 2; Rasmusson and Carpenter, 1982). During the warm El Niño phase of ENSO, the position of maximum rainfall in the Indo-Pacific Warm Pool (IPWP) shifts eastward towards the central and eastern Pacific Ocean following an eastward

displacement of warmest SSTs (Figure 2) (Hendon, 2003; McBride et al., 2003). As a result, the Indonesian region experiences drought conditions and a strong SEM. In contrast to El Niño, La Niña conditions are characterized by intensified trade winds and warmer SSTs than usual in the IPWP. During La Niña the Walker circulation is much stronger, with a strong rising branch over Indonesia, bringing increased rainfall over the region (McBride et al., 2003). With respect to ITF, simulation and observation studies indicate a weaker ITF during El Niño in response to the Pacific trade-wind relaxations (Gordon et al., 1999). However, the relationship between ENSO and ITF at the exit portals is less clear as the ITF transport in the Lombok Strait, Ombai Strait, and Timor passage is also subject to Indian Ocean variability (Sprintall and Révelard, 2014).

The IOD is a zonal-asymmetric equatorial variability of SST (western cold-eastern warm) across the basin of the Indian Ocean (Saji et al., 1999; Webster et al., 1999). A positive phase of IOD is characterized by negative SST anomalies in the equatorial southeastern Indian Ocean and positive SST anomalies in the equatorial western Indian Ocean, and vice versa for a negative IOD phase. A positive IOD develops and peaks in the months from June-October/November (Meyers et al., 2007; Cai et al., 2013; Wang et al., 2015). During the positive IOD, normal convective activities over the eastern Indian Ocean shift westward (Liu et al., 2013), inducing heavy rainfall over the summer monsoon regions of eastern Africa and India (Ashok et al., 2004) and severe drought in Indonesia (Webster et al., 1999).

The IOD often interacts and frequently occurs with ENSO events (Figure 3), indicating the interactive nature of the two major climate phenomena (e.g. Yuan et al., 2011). Figure 3b and 3f show the strongest SST anomaly patterns occur for El Niño with positive IOD and for La Niña with negative IOD, respectively. In both figures, the equatorial Pacific SST anomaly indicates the widest band of latitude and the Java–Sumatra upwelling zone suggests the strongest signal along the coast (Meyers et al., 2007). For instance, the strong El Niños in 1997

and 2006 occurred concurrently with IODs, causing severe drought in Indonesia–Australia and floods in East Africa (Luo et al., 2010).

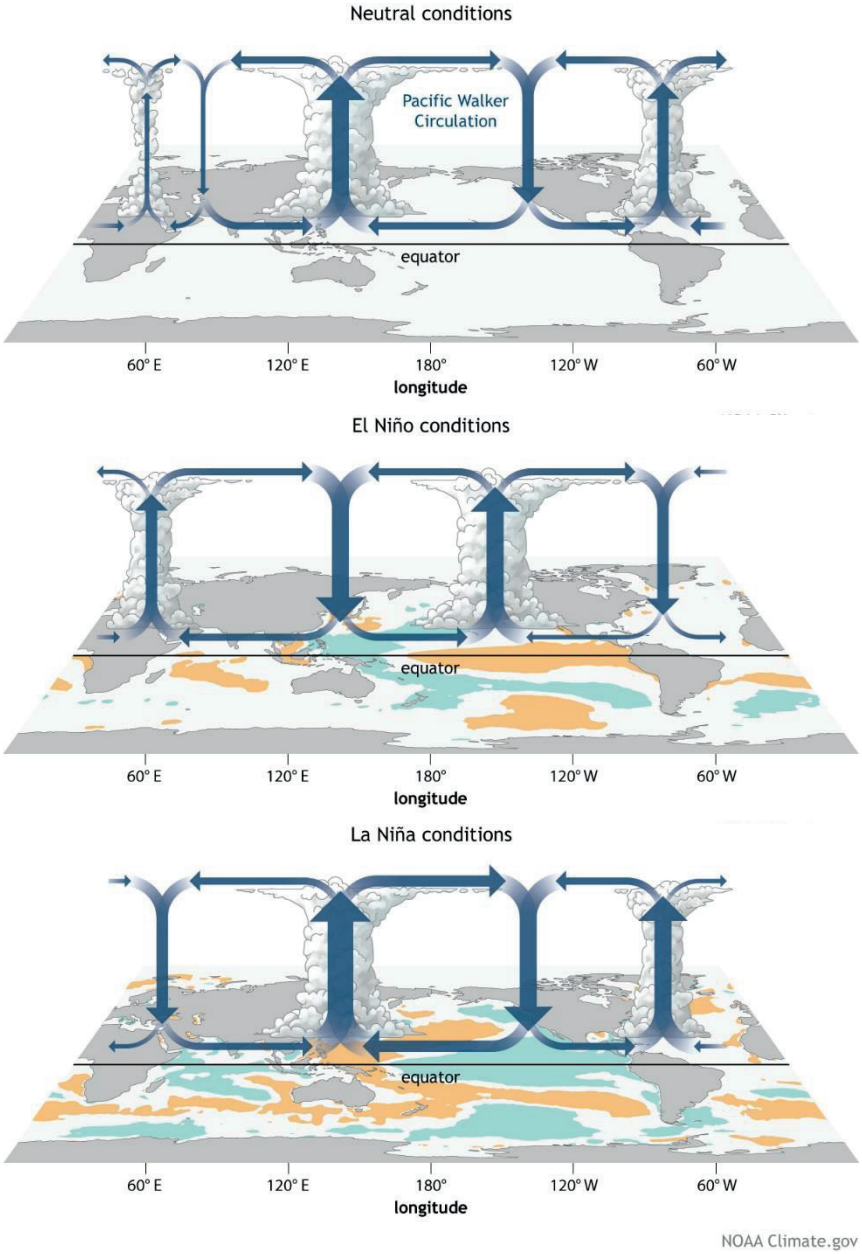

Figure 2. Generalized Walker Circulation (December-February) during neutral (top), El Niño (middle), La Niña (bottom) conditions. During neutral condition convection associated with rising branches of the Walker Circulation is found over the Maritime continent, northern South America, and eastern Africa. During El Niño events, overlaid on map of average sea surface temperature anomalies. Anomalous ocean warming in the central and eastern Pacific (orange) help to shift a rising branch of the Walker Circulation to east of 180°, while sinking branches shift to over the Maritime continent and northern South America. During La Niña events, anomalous ocean cooling (blue-green) in the central and eastern Pacific Ocean and warming over the western Pacific Ocean enhance the rising branch of the Walker circulation over the Maritime Continent and the sinking branch over the eastern Pacific Ocean. Enhanced rising motion is also observed over northern South America, while anomalous sinking motion is found

over eastern Africa (https://www.climate.gov/news-features/blogs/enso/walker-circulation-ensos-atmospheric-buddy).

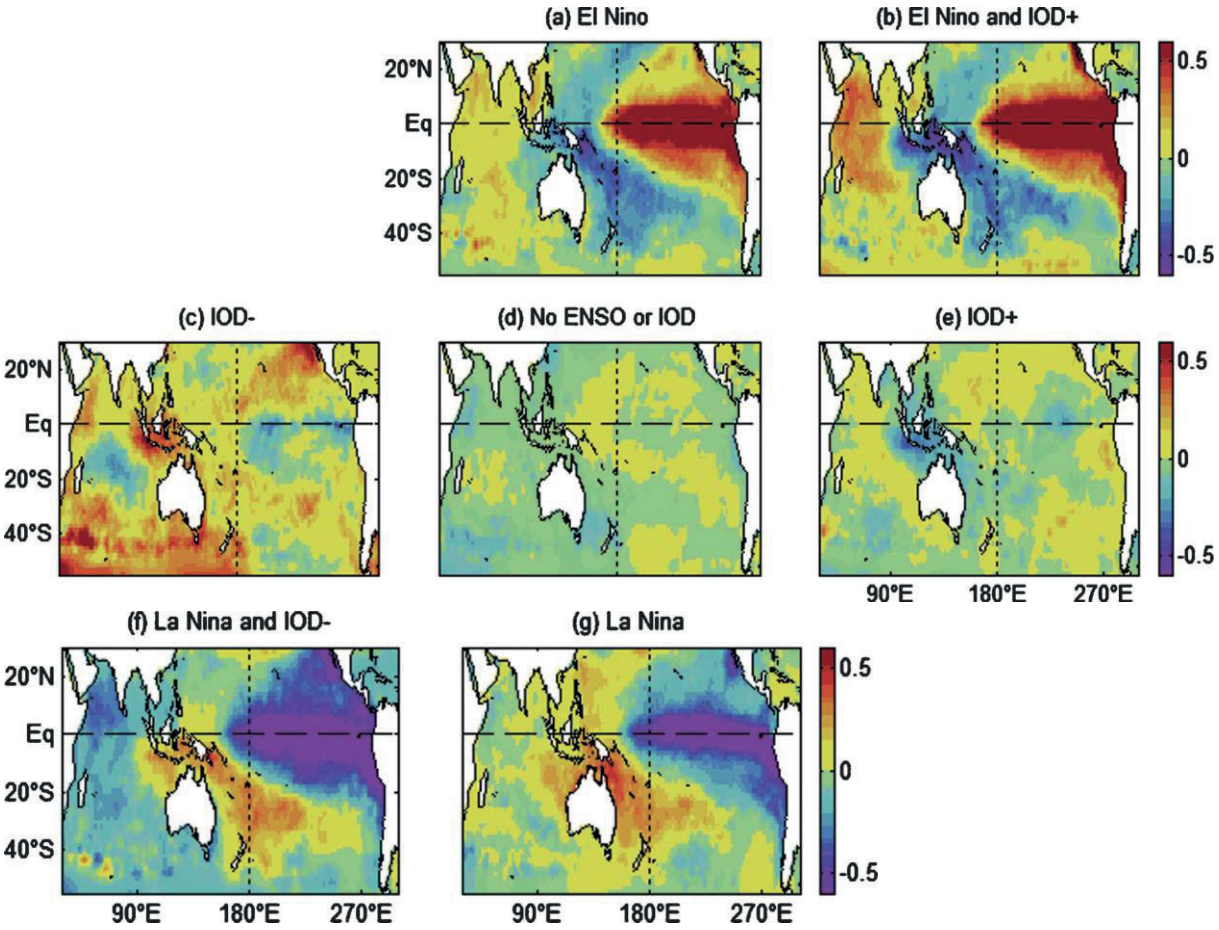

Figure 3. Composite maps of SST anomalies averaged for June-November (Meyers et al., 2007). The strongest SST anomaly patterns occur for El Niño with positive IOD (3b) and La Niña with negative IOD (3f). In the ETIO, the Java–Sumatra upwelling zone has the strongest signal during these events.

1.2. Eastern tropical Indian Ocean

The region of eastern tropical Indian Ocean region (ETIO) is a pivotal region as it hosts the exit portals of the ITF (e.g. Sprintall et al., 2014). Recent studies suggest that the ITF transport via Lombok Strait, Ombai Strait, and Timor Passage is about 2.6 Sv, 4.9 Sv, and 7.5 Sv, respectively (Sprintall et al., 2009). Around 88% ITF water transported to the ETIO exits the

Indian Ocean through the Agulhas Current after a 50-year period (Song et al., 2004), thereby forming an integral part of the global ocean conveyor belt (Talley and Sprintall, 2005).

The ETIO is also characterized by the presence of upwelling along the south coasts of Sumatra-Java-Lesser Sunda Island chain (Susanto et al., 2001). The existence of upwelling during the SEM has been suggested to enhance marine productivity (Hendiarti et al., 2004; Susanto and Marra, 2005) and pelagic fish catch (Hendiarti et al., 2005) in the ETIO region off south Java. With respect to ocean dynamics, upwelling is an important process influencing the mixed layer depth and barrier layer thickness in the ETIO region by uplifting the thermocline (Du et al., 2008). During a positive IOD event the ETIO region off Sumatra and Java experiences a strong SST depression (-3°C) initiated by an anomalous upwelling (Du et al., 2008). As a result, unusual high chlorophyll a concentrations are observed (Susanto and Marra, 2005; Iskandar et al., 2009), reflecting enhanced marine productivity in the region. In line with the IOD, ENSO also has been suggested to influence the strength of Sumatra-Java upwelling, with strong El Niño induces high chlorophyll a concentration (Susanto et al., 2001). These observations imply that upwelling in the ETIO region off Sumatra-Java is sensitive to IOD and ENSO (Meyers et al., 2007).

The ETIO is a region where precipitation (P) exceeds over evaporation (E) throughout the year (Hendon, 2003). Qu and Meyers (2005) suggest that a large P-E is confined to the coastal region of Indonesia, with a maximum >10 mm day^{-1} observed near the coast of Sumatra. According to Mohtadi et al. (2014), central-western Sumatra receives higher average monthly rainfall (~360 mm per month) compared to northwestern Sumatra (~135 mm per month). Furthermore they suggest that the contribution of the AIM to the total rainfall is insignificant in central and northern Sumatra. Hence, the ETIO regions off northern and central Sumatra are suitable areas to study the evolution of the hydrological changes without any significant biases introduced by AIM or ENSO (Mohtadi et al., 2014).

1.3. Paleoceanographic reconstruction of the eastern tropical Indian Ocean

Over the past decade, a number of paleoceanographic studies based on marine sedimentary archives have been published from different sites in the ETIO region. The longest time scale of reconstruction (300 kyr) was provided by sediment core SO139-74KL collected from off southern Sumatra (Lückge et al., 2009). Lückge et al. (2009) have used X-ray fluorescence, total organic carbon, and C_{37} alkenones to investigate past changes in marine productivity, freshwater budget, and SST at orbital time scales. The most important finding from this study is that during the past 300 kyr enhanced marine paleoproductivity in the ETIO region was directly related to strengthening of upwelling during SEM and periods of increased Northern Hemisphere summer insolation at a precessional cyclicity. In contrast, during insolation minima the atmospheric pressure gradient relaxed and monsoon winds weakened, decreasing the intensity of upwelling and marine productivity. Further they suggest that the good correspondence between paleoproductivity and solar insolation at precessional frequency is similar to today's seasonal upwelling off Sumatra and Java. This finding is in agreement with a study by Mohtadi et al. (2011a) that suggests that the upwelling off southern Java changed in accordance with upwelling of the Arabian Sea through variations in the strength of large-scale cross-equatorial boreal summer winds in response to Northern Hemisphere summer insolation.

Multidecadal to centennial-scale variability of the south Java upwelling during the past 2 kyr has been investigated by Steinke et al. (2014). This study suggests that upwelling was generally strong during the Little Ice Age (LIA) and weak during the Medieval Warm Period (MWP) and the Roman Warm Period (RWP). Furthermore the study reveals that periods of strengthened upwelling and more intense austral winter monsoon winds over southern Indonesia are associated with reduced East Asian summer monsoon (EASM) rainfall over north/central China during the last 2 kyr. This new study supports previous findings that suggest the importance of large-scale Australian/Indonesian cross-equatorial boreal summer winds in governing the

intensity of south Sumatra-Java upwelling. However, the influence of IOD on the upwelling variability off southern Indonesia cannot be resolved yet.

The past variability of IOD in the ETIO region is not well studied. Until today there are only three publications (Abram et al., 2007; 2009; Kwiatkowski et al., 2015) discussing the variations of IOD during the Holocene and one publication for the past 24 kyr (Niedermeyer et al., 2014). Abram et al. (2007; 2009) suggest that a good correspondence between the Asian monsoon system and IOD is implied by a longer duration of positive IOD events during stronger Asian summer monsoon. They also argue that sea surface cooling during a positive IOD event is constrained by the cross-equatorial wind reversal at the end of the Asian summer monsoon season, resulting in an abrupt termination of Ekman upwelling along the coast of Sumatra and Java. Abram et al. (2007; 2009) further postulate that the reversal winds may have played an important role in controlling the timing of peak cooling during positive IOD events during the Holocene. This finding supports the proxy record of plant wax stable hydrogen (δD) from off northwest Sumatra that suggests the Holocene variability of rainfall in the ETIO is coupled to changes in the IOD variations (Niedermeyer et al., 2014). Furthermore, a study by Kwiatkowski et al. (2015) shows a thermocline shoaling off western Sumatra during the positive IOD-like mean state.

Another important finding on hydrological changes in the ETIO region has been reported from the non-ENSO and monsoon regions, central and northern Sumatra (Mohtadi et al., 2014). Mohtadi et al. (2014) found that saltier sea surface conditions and reduced rainfall in the ETIO during Heinrich stadials and the Younger Dryas were due to a weakened and easterly displacement of the Hadley Circulation as a response to a slowdown of the Atlantic meridional overturning circulation (AMOC). Furthermore, they suggest that zonally asymmetric changes within the Indian Ocean were not the primary control on Indian Ocean hydrology during these periods.

1.3.1. Paleogeographic changes since the Last Glacial Maximum (LGM)

The Sunda Shelf is an important region in the IPWP as it forms the world's second largest submerged shelf (Molengraaff, 1921; Dickerson, 1941). The Sunda Shelf is located in the western Indonesian Archipelago and is surrounded by the coastal areas of Vietnam, Cambodia and Thailand, the Peninsular Malaysia, Singapore, and Indonesia (Hanebuth and Stattegger, 2004). Palaeoclimate records and simulation experiments show that both the exposure and the flooding of the Sunda Shelf have influenced the regional hydroclimate (Linsley et al., 2010; DiNezio and Tierney, 2013; Griffiths et al., 2013). During the Last Glacial Maximum (LGM), when sea level was approximately −123 m lower than today (Hanebuth et al., 2009), the Sunda Shelf was an exposed land-mass (so-called "Sundaland") connecting the islands of Borneo, Java, and Sumatra with continental Asia (Hanebuth et al., 2011). During this period Sundaland rainforests covered a greater area than today (Cannon et al., 2009; Hanebuth et al., 2011) while intertidal marine communities were being pushed seaward (Hanebuth et al., 2011). A simulation study suggests that the exposure of the Sunda Shelf altered the atmospheric circulation by weakening the Indian Ocean Walker Circulation, which was accompanied by increased aridity in the ETIO and higher sea surface salinity (SSS) south of Java (DiNezio and Tierney, 2013). Previous studies suggest that the Sunda Shelf was inundated during rapid deglacial sea-level rise (Hanebuth et al., 2000; Sathiamurthy and Voris, 2006). Around 14 kyr B.P. meltwater pulse 1A (MWP-1A) produced a sea level rise of 16 m within 300 years over the Sunda Shelf (Hanebuth et al., 2000). At ~ 9.5 kyr B.P. the flooding of the Sunda shelf reached the shallowest point, the Karimata Strait, allowing the connection of water masses of the South China Sea and the southern Makassar Strait via the Java Sea (Hanebuth et al., 2000; Sathiamurthy and Voris, 2006). As a result, the flooding affected the regional hydrology of the Makassar Strait (Linsley et al., 2010), the Timor Sea (Xu et al., 2008), the Savu Sea (Dubois et al., 2014), and in Flores (Griffiths et al., 2009; 2013). Moreover, some studies suggest that the flooding of the Sunda

Shelf influenced the ITF by changing a surface-dominated to a thermocline-dominated flow (Linsley et al., 2010; Xu et al., 2008).

1.4. Dissertation objectives

Hydrological changes in the eastern tropical Indian Ocean on different time scales have been investigated using marine sediment proxy and model simulation. Several studies have invoked flooding of the Sunda Shelf as well as opening of the Sunda Strait at ~ 10 kyr as possible drivers for changes in upper ocean condition in the eastern tropical Indian Ocean (Mohtadi et al., 2010a; 2010b; Lückge et al., 2009). Simulation studies show that the Sunda Strait transports a significant amount of low salinity Java Sea water into the Indian Ocean, impacting background state of the sea surface conditions in the region (Putri, 2005; Du and Qu, 2010). However, to date the impact of the opening of the Sunda Strait on sea surface conditions and the hydrological evolution off the Sunda Strait are not well constrained from marine sedimentary-based reconstructions in the ETIO.

The neodymium isotopic composition ($^{143}Nd/^{144}Nd$ ratio, expressed as ε_{Nd}) of planktic foraminifera has been successfully used to reconstruct past changes in oceanic circulation (Piotrowski et al., 2012; Osborne et al., 2014) and has been shown to reliably record the isotopic composition of bottom waters (Roberts et al., 2012; Kraft et al., 2013; Molina-Kescher et al., 2014). The ε_{Nd} of water masses is mainly controlled by the isotopic composition of the surrounding land masses at their origin. Specifically weathering and erosion of continental rocks ultimately have been suggested to play a primary role in controlling the ε_{Nd} of dissolved Nd in the oceans (Frank, 2002). The residence time of Nd in seawater is shorter than the mixing times of the oceans (200–1000 years) (Tachikawa et al., 1999; Arsouze et al., 2009; Rempfer et al., 2011). Until today past changes in the ε_{Nd} of bottom water in the ETIO and the impact of the opening of the Sunda Strait on bottom water are not known.

Foraminifera Ba/Ca ratio is a new geochemical proxy for continental runoff and freshwater discharges (Hall and Chan, 2004; Weldeab et al., 2007; Schmidt and Lynch-Stieglitz, 2011). It has been suggested that one of the primary sources of Ba in the oceans is riverine input due to dissolved Ba is enriched in riverine water compared to seawater (Weldeab et al., 2007). Since the early Holocene, specifically after the opening of the Sunda Strait at ~10 kyr B.P., sea surface conditions in the ETIO off the Sunda Strait are characterized by fresher surface conditions due to a continues import of low salinity Java Sea water. Thus, with respect to the Ba/Ca proxy, the modern oceanographic setting of the ETIO appears to be suitable its application. However, until to date no study on the Ba/Ca ratio in the ETIO have been reported.

The central purpose of this dissertation is to investigate hydrological changes in the eastern tropical Indian Ocean and to relate the changes to the opening of the Sunda Strait at ~10 kyr. The specific objectives of this dissertation are as follows:

1. How did sea surface conditions in the eastern tropical Indian Ocean off the Sunda Strait vary during the past ~40 kyr and respond to the opening of the Sunda Strait?
2. How did bottom water in the eastern tropical Indian Ocean off the Sunda Strait vary during the past ~19 kyr? What are the factors inducing modification of the bottom water (foraminifera ε_{Nd}) off the Sunda Strait?
3. Can the planktic foraminifera *G. sacculifer* Ba/Ca ratio be used as a tracer for present and past freshwater discharges in the ETIO off the Sunda Strait? What is the effect of using different reductive reagents on the *G. sacculifer* Ba/Ca ratio?

In order to tackle the above research questions two sediment cores (GeoB 10042-1 and GeoB 10043-3) and ten surface sediment samples collected from the ETIO region off the Sunda Strait and off western and southern Sumatra have been selected, respectively, permitting a detailed reconstruction of the hydrological changes off the Sunda Strait and providing first Ba/Ca ratios for the ETIO.

1.5. Dissertation structure and contribution to publications

Chapters 1-3 provide a general introduction of the research topic, the study area, and the materials and methods used in this study. Chapters 4-5 of this dissertation are written in a scientific style and format fitted for journal publication, and are thus presented as self-contained studies. Chapter 6 provides a technical report on Ba/Ca ratio cleaning experiment. Finally, chapter 7 and 8 provide a synthesis of the dissertation and an outlook.

Chapter 4: The consequences of opening the Sunda Strait on the hydrography of the eastern tropical Indian Ocean (re-submitted after revision to *Paleoceanography*)

R. Y. Setiawan, M. Mohtadi, J. Southon, J. Groeneveld, S. Steinke, D. Hebbeln

This chapter presents and discusses temporal variability of the Mg/Ca-based sea surface temperatures (SSTs; based on Mg/Ca measurements on *Globigerinoides ruber* sensu stricto (s.s.)), seawater $\delta^{18}O$ ($\delta^{18}O_{sw}$; based on $\delta^{18}O$ and Mg/Ca measurements on *G. ruber* s.s.), and the terrigenous supply (based on XRF-Ti/Ca ratios) in the eastern tropical Indian Ocean during the past ~40 kyr. Of particular interest here are evidence of the impacts of the opening of the Sunda Strait on these parameters. The results show that since the opening of the Sunda Strait at ~10 kyr B.P. SST and $\delta^{18}O_{sw}$ off the Sunda Strait indicate warmer and fresher surface conditions compared during the last glacial, suggesting persistent advection of low salinity Java Sea water.

Contributions: In this chapter R. Y. Setiawan contributed to perform all laboratory works. Specifically, the laboratory works include XRF and Mg/Ca measurements on bulk sediment and planktic foraminifera *G. ruber* s.s. R. Y. Setiawan wrote the paper with significant editorial contribution from all co-authors.

Chapter 5: Modification of the deep water neodymium isotope composition along the eastern margin of the tropical Indian Ocean (in preparation)

R. Y. Setiawan, E. C. Hathorne, K. Pahnke, M. Mohtadi, D. Hebbeln

This chapter presents and discusses the temporal variability of the bottom water circulation (based on planktic foraminifera ε_{Nd}) during the past ~19kyr, and investigates the factors inducing modification of the bottom water circulation and the provenance of the detrital materials off the Sunda Strait. The results demonstrate that during the last glacial and the period between ~7.7 and ~2.6 kyr B.P. bottom water off the Sunda Strait experienced significant modifications presumably due to a strong flow of the thermocline ITF and a large supply of terrigenous materials at ~10 kyr B.P., respectively. Furthermore, the results indicate that the South Java Current and ITF may have played a role in governing the temporal variability of the detrital ε_{Nd}.

Contributions: In this chapter R. Y. Setiawan contributed to perform major laboratory works such as (1) neodymium (Nd) isotope analyses on mixed planktic foraminifera at the GEOMAR Helmholtz Centre for Ocean Research Kiel (2) and on bulk sediments at the Max Planck Research Group for Marine Isotope Geochemistry, Institute for Chemistry and Biology of the Marine Environment (ICBM), University of Oldenburg. K. Pahnke contributed to the strontium (Sr) isotope analyses and total digestion. R. Y. Setiawan wrote the paper with constructive comments from all co-authors.

Chapter 6: Testing the applicability of *G. sacculifer* Ba/Ca in the eastern tropical Indian Ocean (technical report)

R. Y. Setiawan, M. Mohtadi, J. Groeneveld, S. Steinke, H. Kuhnert, D. Hebbeln

Chapter 6, for the first time, investigates and discusses the applicability of the *G. sacculifer* Ba/Ca ratio as a tracer for present and past freshwater discharge in the eastern tropical Indian Ocean. The results suggest that the Ba/Ca ratio of *G. sacculifer* cannot be used as a tracer for freshwater discharge as the presence of seasonal upwelling complicates the interpretation of the proxy. In addition, a series of cleaning experiments were performed to test the use of reductive solutions of hydrazine, hydroxylamine, and DTPA for Ba/Ca ratio extraction. According to the

results of cleaning experiment, hydroxylamine and a cleaning protocol proposed by Barker et al. (2003) can be used to extract Ba/Ca ratio of *G. sacculifer*.

Contributions: For this chapter R. Y. Setiawan performed all laboratory works. J. Groeneveld and H. Kuhnert designed the cleaning experiment and R. Y. Setiawan wrote the report with significant editorial contribution from all co-authors.

2. Regional Hydrography

2.1. Ocean circulation

Today the large-scale circulation in the ETIO is dominated by the South Equatorial Current (SEC) (Qu and Meyers, 2005). The SEC is a vertical water mass extending from surface to the abyss in the eastern Indian Ocean (Talley and Sprintall, 2005). It advects the fresher ITF water westward across the Indian Ocean and flows centered at 12°S (Figure 4) (Talley and Sprintall, 2005; Talley et al., 2011).

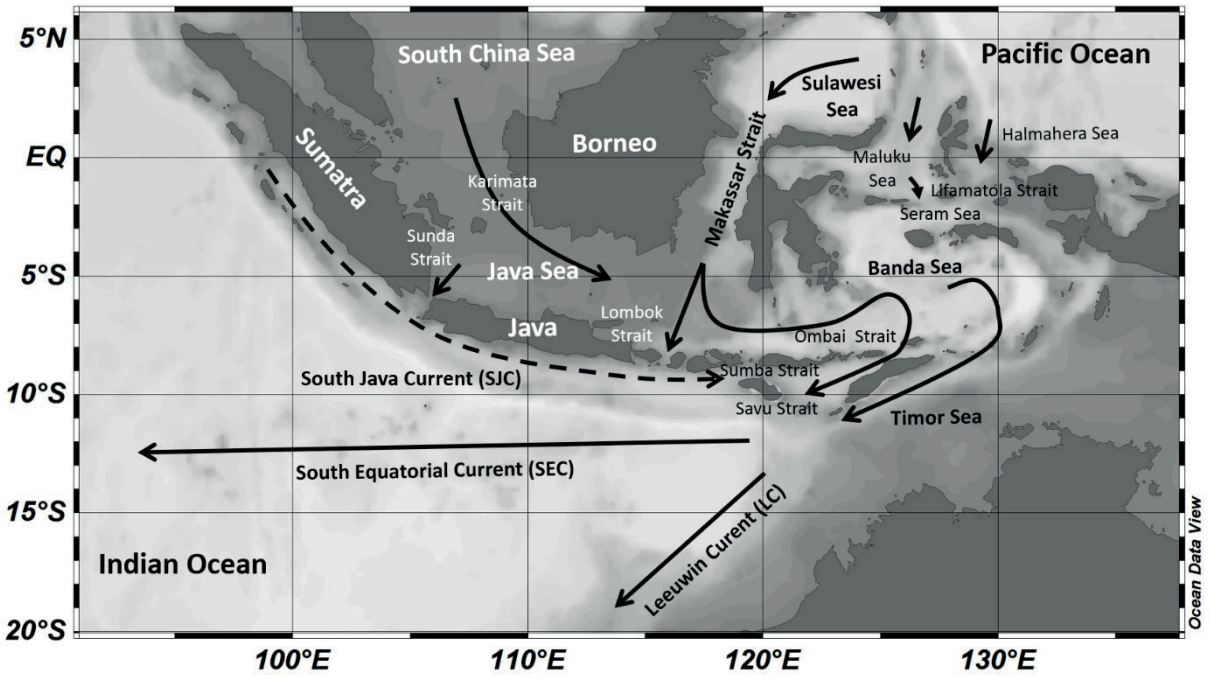

Figure 4. Dashed arrow off southern Sumatra and Java depict the direction of the South Java Current (Sprintall et al., 2010). Solid lines denote the ITF pathways in the Indonesian Seas, and the directions of SEC and LC.

The most important ocean circulation in the ETIO and the Indonesian Seas is the ITF (Figure 4). There are two major routes of the ITF within the Indonesian Seas. The first route is through the Sulawesi Sea into the Makassar Strait, and the second route is via the Maluku Sea into the Lifamatola Strait, or directly through the Halmahera Sea into the internal Seram and Banda Seas. From the Makassar Strait ITF directly exits through the Lombok Strait, whereas from the

Banda Sea the ITF exits into the east Indian Ocean via Timor Passage, or via the Ombai Strait and then through the Sumba Strait and the Savu Strait (Gordon and Fine, 1996; Hautala et al., 1996; Sprintall et al., 2009). Recently, a new ITF branch through the South China Sea and the Karimata Strait has been found (Susanto et al., 2010) and some studies suggest that this small inflow has strong seasonal variability and influence on vertical structure of the main ITF (Tozuka et al., 2009; Fang et al., 2010; Susanto et al., 2013).

Another important current system in the ETIO is the South Java Current (SJC) and UnderCurrent (SJUC) (Quadfasel and Cresswell, 1992; Sprintall et al., 2010). These current systems play a significant role in distributing freshwater into and out of the southeast Indian Ocean (Sprintall et al., 2010). The SJC is a semi-permanent eastward surface flow and transports warm and fresh waters from the high rainfall, warm pool region of the eastern equatorial Indian Ocean up to the Savu Sea and Ombai Strait (Figure 4) (Sprintall et al., 2010). The direction of SJC is reversed only during the SEM season. Sprintall et al. (2010) suggest that the driving force of SJC is interplay processes by various mechanisms relate to remotely driven Kelvin waves, Ekman dynamics, the ITF, and topographic effects.

The SJUC flows eastward at depths of 200-1000 m and is driven by remotely Kelvin waves forced in the equatorial Indian Ocean that travel along the coastal waveguide of Sumatra,- Java and the Lesser Sunda Islands. The properties and velocities of the SJUC are different from the SJC. The SJUC transports high salinity, low oxygen North Indian Intermediate Water (NIIW) eastward reaching the Ombai Strait (Sprintall et al., 2010).

2.2. Water masses

A major water mass that dominates the upper layer (0-150 m) off the Sunda Strait is the Java Sea water mass (Putri, 2005). This water mass is characterized by low salinity (<34 psu) and high SST (>29°C) (Putri, 2005). In the eastern Indian Ocean, the total ITF transport is composed of the Indonesian Throughflow Water (ITW) in the upper layer (0-500 m) and the Indonesian

Intermediate Water (IIW) at deeper layer (>500-1500 m) (Talley and Sprintall, 2005). Both the ITW and IIW are characterized by low salinity (~34.55 psu) and high silica that can be traced along the SEC. Below 1500 m to the bottom, the water column off the eastern Indian Ocean is comprised of the upper Indian Deep Water (IDW). This water mass is characterized by high salinity (>34.6) and cold temperature (<4°C) (Atmadipoera et al., 2009). In the Indian Ocean, the IDW ranges from 500–3800 m in the southern portion of the Indian Ocean to 2000–3800 m in the north, with a core at ~2400 m (Martin and Scher, 2006).

3. Materials and Methods

3.1. Materials of study and sediment sampling

Materials used in this study include the sediment cores (GeoB 10042-1 and GeoB 10043-3) collected from off the Sunda Strait and ten surface sediment samples (Table 1 in chapter 6) collected from off Sumatra during the RV Sonne Expedition 184 in 2005 (Hebbeln et al., 2005). Cores GeoB 10042-1 and GeoB 10043-3 were retrieved from 2454 m and 2171 m, respectively. The core length of GeoB 10042-1 is 540 cm while core GeoB 1043-3 is 390 cm long. Both consist of nannofossil oozes and have ash layers in the upper 18 cm and in the bottom of the cores at a depth between 370 and 382 cm (GeoB 10043-3) and at 470 cm (GeoB 10042-2).

The ten surface sediment samples were retrieved from depths between 911 and 2605 m. In this study, these surface samples were used to perform Ba/Ca analyses.

The working halves of cores GeoB 10042-1 and GeoB 10043-3 were sub-sampled at 5 cm intervals for Mg/Ca analyses. For the analyses of the foraminifera neodymium isotopic composition (ε_{Nd}) only core GeoB 10043-3 was sampled at 5 cm interval. While for the detrital ε_{Nd} and detrital strontium isotope ($^{87}Sr/^{86}Sr$) analyses both cores were sampled only at specific time slices (the Heinrich stadial 1, the Bølling-Allerød, the Younger Dryas, and the early and late Holocene). In addition, XRF analyses were also conducted on the archive halves of cores GeoB 10042-1 and GeoB 10043-3.

3.2. Methods

3.2.1. Accelerator mass spectrometry (AMS) dating

The age models for GeoB 10042-1 and GeoB 10043-3 are based on the radiocarbon ages of planktic foraminifera (Table 1 in chapter 4). For this analysis, *G. ruber* s.s. and *G. sacculifer* (without the sac-like final chamber) were picked from the >150 μm fraction. Radiocarbon dating was performed at the Keck Carbon Cycle Accelerator Mass Spectrometry, University of

California, Irvine (UCI). All AMS ^{14}C ages were converted to 2σ calendar ages with the CALIB 7.0 software using the Marine13 calibration dataset (Reimer et al., 2013) (Table 1 in chapter 4) with a regional reservoir correction of 100 years (Southon et al., 2013).

3.2.2. Stable isotope, Mg/Ca and Ba/Ca analyses

For the stable oxygen isotope ($\delta^{18}O$) and Mg/Ca analyses, around 30-40 individuals of *G. ruber* s.s. were picked from the 250-355 μm size fraction. The samples were then gently crushed using two glass plates, homogenized, and split. About two-third of the tests was used for Mg/Ca analysis and the remaining one- third was used for $\delta^{18}O$ analysis. The $\delta^{18}O$ measurements were carried out using a Finnigan MAT 251 mass spectrometer at the MARUM, University of Bremen. Long-term standard deviation of the carbonate standard is <0.07‰. The $\delta^{18}O$ results are reported relative to the international Pee-Dee Belemnite (PDB) Standard.

For the Mg/Ca analyses, the gently crushed tests were cleaned according to a cleaning protocol suggested by Barker et al. (2003). After chemical cleaning, samples were measured with an inductively coupled plasma–optical emission spectrometer (ICP-OES) (720 Agilent Technology Series) at the MARUM, University of Bremen. The Mg/Ca ratio values are reported as mmol mol^{-1}. The average 1σ error for the Mg/Ca analyses on an external standard measured along with the analyses for cores GeoB 10042-1 and GeoB 10043-3 is 0.04 mmol mol^{-1}.

For the Ba/Ca analyses, approximately 30-40 individuals of *G. sacculifer* (without the sac-like final chamber) were picked from the 250-355 μm size fraction and gently cracked using glass plates. All test fragments were split into five aliquots and these aliquots were subjected to various cleaning steps. Similar to the Mg/Ca analyses, cleaned samples were then measured with an Agilent 720 ICP-OES. The Ba/Ca values are reported as μmol mol^{-1}. The average 1σ error for the Ba/Ca analyses on external standard and ECRM 752-1 standard are 0.02 μmol mol^{-}

^{1} and 0.1 µmol mol^{-1}, respectively. It is important to note here that the sample reproducibility was not measured due to insufficient sample amount.

3.2.3. Neodymium and strontium isotope analyses

3.2.3.1. Neodymium extraction from mixed planktonic foraminifera

In order to reconstruct the bottom water Nd isotopic composition (ε_{Nd}), approximately 20 to 75 mg of mixed planktic foraminifera tests >250 µm were picked and gently cracked using two glass plates. Samples were then cleaned using a method developed by Boyle (1981) and modified (scaled up for larger samples) by Vance and Burton (1999) and Vance et al. (2004). After cleaning, samples were dissolved in HNO_3 and aliquots were separated for element (particularly Al/Ca, Mn/Ca, Fe/Ca), rare earth element (REE) and Nd isotope analyses.

3.2.3.2. Neodymium and Strontium extraction from detrital fraction

In order to investigate the sediment provenance, 50 mg of the freeze-dried and homogenized sediment samples were leached using 25% (v/v) acetic acid and 0.02 M hydroxylamine hydrochloride (HH). The leached sediment samples were then digested in closed polytetrafluorethylene (PTFE) vessels using a mixture of concentrated HF-HNO_3-$HClO_4$. The dissolved samples were then subjected to standard element purification procedures for neodymium and strontium.

3.2.3.3. Neodymium and strontium isotope measurements

Nd isotope measurements were performed using a Nu plasma MC-ICPMS at GEOMAR and a Neptune Plus MC-ICPMS at the Institute for Chemistry and Biology of the Marine Environment (ICBM), University of Oldenburg. The Nd isotopic composition signature is reported as ε_{Nd}, which corresponds to the deviation of a measured $^{143}Nd/^{144}Nd$ of a sample from the Chondritic Uniform Reservoir (CHUR) value of 0.512638 (Jacobsen and Wasserburg, 1980) (ε_{Nd} = {($^{143}Nd/^{144}Nd$) sample / ($^{143}Nd/^{144}Nd$) CHUR -1} × 10,000). The Sr isotopes were

also measured at ICBM and the results were normalized to the widely accepted value of NIST SRM987 standard with an $^{86}Sr/^{88}Sr$ ratio of 0.710245. The external reproducibility (2σ) of the $^{143}Nd/^{144}Nd$ at GEOMAR was between 0.3 and 0.6 ε_{Nd} units, while at ICBM was between 0.2 and 0.3 ε_{Nd} units. The 2σ of $^{87}Sr/^{86}Sr$ measurement at ICBM ranged between 0.00001 and 0.00002.

3.2.4. X-Ray Fluorescence (XRF) core scanning

Elemental XRF scanners are commonly used to detect chemical compositions in sediments as it offers a rapid and non-destructive analyses of a suite of elements at the surface of split cores. The XRF measurements were performed on cores GeoB 10042-1 and GeoB 10043-3, and were carried out with XRF Core Scanner I and II at MARUM, University of Bremen. For the GeoB 10042-1 the measurements were conducted at 2 cm intervals, whereas for the GeoB 10043-3 1 cm intervals have been applied. For this study the elemental ratio of titanium to calcium (Ti/Ca; logarithmic scale) was used as a proxy to determine past changes in terrestrial input.

4. The consequences of opening the Sunda Strait on the hydrography of the eastern tropical Indian Ocean

Riza Yuliratno Setiawan[1*], Mahyar Mohtadi[1], John Southon[2], Jeroen Groeneveld[1,3], Stephan Steinke[1], Dierk Hebbeln[1]

[1] MARUM – Center for Marine Environmental Sciences, University of Bremen, Bremen, Germany

[2] Earth System Science Department, University of California, Irvine, CA 92697, USA

[3]Alfred-Wegener Institute, Helmholtz Center for Polar and Marine Research, Potsdam, Germany

Accepted in *Paleoceanography* on 30 September 2015

Abstract

The advection of relatively fresh Java Sea water through the Sunda Strait is presently responsible for the low-salinity ‘‘tongue’’ in the eastern tropical Indian Ocean with salinities as low as 32‰. The evolution of the hydrologic conditions in the eastern tropical Indian Ocean since the last glacial period, when the Sunda shelf was exposed and any advection via the Sunda Strait was cut off, and the degree to which these conditions were affected by the Sunda Strait opening are not known. Here we have analyzed two sediment cores (GeoB 10042-1 and GeoB 10043-3) collected from the eastern tropical Indian Ocean off the Sunda Strait that cover the past ~40,000 years. We investigate the magnitude of terrigenous supply, sea surface temperature (SST) and seawater $\delta^{18}O$ ($\delta^{18}O_{sw}$) changes related to the sea level-driven opening of the Sunda Strait. Our new spliced records off the Sunda Strait show that during the last glacial, average SST was cooler and $\delta^{18}O_{sw}$ was higher than elsewhere in the eastern tropical Indian Ocean. Seawater $\delta^{18}O$ decreased ~0.5‰ after the opening of the Sunda Strait at ~10 kyr BP accompanied by a SST increase of 1.7°C. We suggest that fresher sea surface conditions have persisted ever since due to a continuous transport of low salinity Java Sea water into the eastern tropical Indian Ocean via the Sunda Strait that additionally increased marine productivity through the concomitant increase in terrigenous supply.

1. Introduction

The Sunda Shelf in the Indo-Pacific Warm Pool (IPWP) is one of the largest shelves in the world with less than 70 m water depth. During the Last Glacial Maximum (LGM), when global sea level was ~130 m below the present level, the wide Sunda Shelf was exposed forming a huge land mass also known as Sundaland [*Tija*, 1980; *Pelejero et al.*, 1999; *Hanebuth et al.*, 2000]. Model results suggest that the exposure of the Sunda Shelf altered the atmospheric circulation by weakening the Indian Ocean Walker Circulation, which was accompanied by increased aridity in the eastern tropical Indian Ocean and higher sea surface salinity (SSS) south of Java [*DiNezio and Tierney*, 2013].

Marine and terrestrial proxy data suggest that the Sunda Shelf was flooded at ~9.5 kyr BP due to eustatic sea level rise [*Hanebuth et al.*, 2000; 2011; *Griffiths et al.*, 2009; 2013; *Linsley et al.*, 2010]. The flooding of the shelf has been suggested to affect seawater $\delta^{18}O$ and rainfall in regions to the east and southeast of the Sunda Shelf, in the Timor Sea [*Xu et al.*, 2008] and the Savu Sea [*Dubois et al.*, 2014], in Flores [*Griffiths et al.*, 2009; 2013], and in the Makassar Strait [*Linsley et al.*, 2010]. However, temperature and rainfall proxy records from Sulawesi [*Russell et al.*, 2014] and from sites to the west and north of the Sunda Shelf do not show a sea-level related variability on glacial-interglacial timescales; e.g., in Borneo [*Carolin et al.*, 2013; *Dubois et al.*, 2014] and western Sumatra [*Maloney*, 1980; *Mohtadi et al.*, 2014; *Niedermeyer et al.*, 2014; *Stuijts et al.*, 1988; *van der Kaars et al.*, 2010]. Records from south of the Sunda Shelf are equivocal [*Kershaw et al.*, 2007; *Mohtadi et al.*, 2011a]. Moreover, some results suggest that the flooding of the Sunda Shelf influenced the Indonesian Throughflow (ITF) by changing a surface-dominated to a thermocline-dominated flow [*Linsley et al.*, 2010; *Xu et al.*, 2008]. In the absence of any influence of the relatively fresh South China Sea (SCS) water, that today adds to the ITF through the Java Sea, glacial ITF transport was dominated by warmer and saltier surface flow [*Xu et al.*, 2008].

The effect of the Sunda Shelf flooding and the opening of the Sunda Strait at ~9.5 kyr BP on the hydrology of the eastern tropical Indian Ocean is not well known. Presently, the Sunda Strait is the most important link between the Java Sea and the Indian Ocean as it transports warm, low salinity Java Sea water into the eastern tropical Indian Ocean [*Putri*, 2005]. This advection of relatively fresh water has significant impacts particularly on the upper ocean stratification in the eastern tropical Indian Ocean off the Sunda Strait [*Putri*, 2005; *Du and Qu*, 2010]. Data from a sedimentary record to the Northwest of the Sunda Strait imply that during periods of lower sea level prior to the Holocene the input of less-saline waters via the Sunda Strait was cut off and saltier sea surface condition prevailed in the eastern tropical Indian Ocean [*Mohtadi et al.*, 2010a; b]. Here we study two additional marine sedimentary archives collected in the eastern tropical Indian Ocean off the Sunda Strait with a higher temporal resolution and more accurate age model for the past 40 kyr to understand the influence of an exposed or a flooded Sunda Shelf on the regional hydrology. Records of bulk sedimentary element composition together with stable oxygen isotope ($\delta^{18}O$) and Mg/Ca ratio of the planktic foraminifera *Globigerinoides ruber* sensu stricto (s.s.) are used to unravel changes in the regional hydrology of the eastern tropical Indian Ocean related to sea level changes and the resulting exposure/flooding of the Sunda Shelf.

2. Study Area

Today the eastern tropical Indian Ocean is greatly influenced by the Australian-Indonesian monsoon (AIM) system. The dynamics of the seasonally reversing monsoon winds over the study area impacts oceanic circulation, sea surface temperature (SST), and SSS along the southern coasts of Java and Sumatra [*Susanto et al.*, 2001; *Qu and Meyers*, 2005; *Du et al.*, 2005; 2008]. During the northwest monsoon (NWM) season (December–February), winds blow from the Eurasian continent, pass the South China Sea and the Bay of Bengal and carry warm and moist air to Indonesia [*Gordon*, 2005; *Qu et al.*, 2005]. Along the coasts of Sumatra

and Java, the almost year-round eastward flowing South Java Current carries low-salinity, warm water from the eastern equatorial Indian Ocean off Sumatra into the southeast Indian Ocean [*Du et al.*, 2005; *Sprintall et al.*, 2009; 2010]. The direction of the SJC is reversed only during the southeast monsoon (SEM) season (June–September), carrying higher salinity water flows westward [*Sprintall et al.*, 2010] (Fig. 1a). During this time southeasterly winds blow from Australia and carry warm and dry air to Indonesia [*Gordon*, 2005; *Qu et al.*, 2005]. A striking feature during the SEM is the appearance of wind-induced upwelling centered south of Java [*Susanto et al.*, 2001].

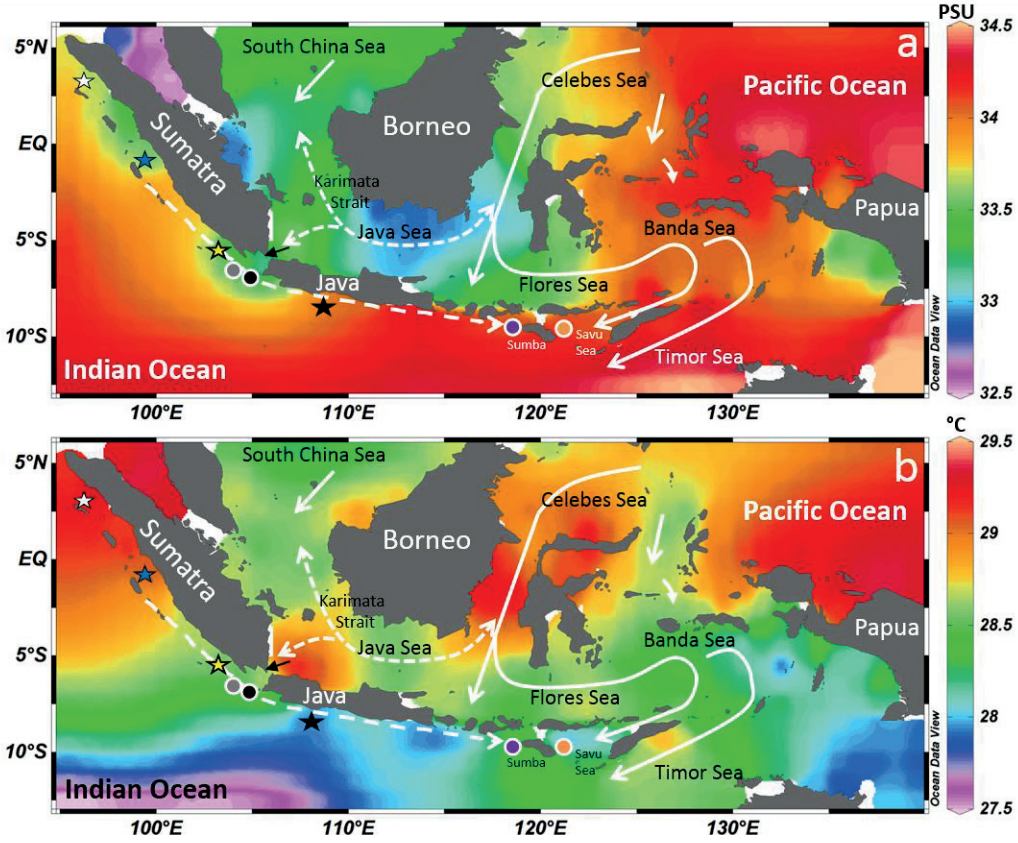

Figure 1. Annual mean maps of (a) sea surface salinity (psu) [*Zweng et al.*, 2013] and (b) sea surface temperature (°C) [*Locarnini et al.*, 2013] obtained from the World Ocean Atlas 2013. The Sunda Strait is indicated by black arrow in the maps. Grey, black, purple, and orange dots denote the positions of GeoB 10042-1 and GeoB 10043-3 (this study), MD98-2165 [*Levi et al.*, 2007], and GeoB 10069-3 [*Gibbons et al.*, 2014], respectively. White, blue, yellow and black stars show the positions of SO189-119KL, SO189-39KL [*Mohtadi et al.*, 2014], GeoB 10038-4 [*Mohtadi et al.*, 2010a; b], and sediment trap JAM1-3 [*Mohtadi et al.*, 2009]. White dashed arrows in the Java Sea and off the southern Sumatra and Java depict the movement of low salinity water and the direction of the South Java Current [*Sprintall et al.*, 2010]. White solid lines denote ITF pathways.

The eastern tropical Indian Ocean is a region where precipitation (P) exceeds evaporation (E) throughout the year [*Hendon*, 2003]. Moreover, Qu and Meyers (2005) suggest that a large P-E difference is confined to the coastal region of Indonesia, with a maximum >10 mm day^{-1} occurring near the coast of Sumatra. This large P-E creates a strong salinity-induced stratification in the surface waters. Further south in the monsoon region of southern Indonesia, the rainy season is principally linked to the NWM due to the southward progression of the Intertropical Convergence Zone (ITCZ), while the dry season peaks during the SEM [*Aldrian and Susanto*, 2003; *Hendon*, 2003].

Another important oceanic circulation component in the study area is the ITF. The ITF transports Pacific Ocean water into the Indian Ocean via multiple passages within the Indonesian Seas [*Vranes and Gordon*, 2005; *Gordon et al.*, 2010]. Presently, the estimated transport is ~15 Sv (1 Sv = 10^6 m^3 s^{-1}) and roughly 80% of that is transported via the main pathway, the Makassar Strait [*Gordon et al.*, 2010]. The ITF modifies the heat and freshwater budgets and air–sea heat fluxes of the Pacific and Indian Oceans, and may play a role in ENSO and Asian monsoon climate phenomena [*Gordon et al.*, 2003]. The relatively cool and fresh ITF exits the Indonesian Seas through Timor Passage, Lombok and Ombai Straits and flows westward across the Indian Ocean near 12°S [*Gordon et al.*, 2010].

Modern oceanographic observations show that the Java Sea water, characterized by low salinity and high temperature water, is the dominant water mass passing through the Sunda Strait continuously during the entire year [*Putri*, 2005]. Moreover, a recent modelling study suggests that from the annual mean southward transport of 0.6 Sv through the Karimata Strait [*Gordon et al.*, 2012], about 0.5 Sv passes later on through the Sunda Strait [*Du and Qu*, 2010]. Combined with runoff from Java and Sumatra, this transport is responsible for the low-salinity ‘‘tongue’’ in the SJC with salinities as low as 32‰ (Fig. 1) [*Wijffels et al.*, 1996], that can extend as far as 13°S [*Gingele et al.*, 2002; *Ding et al.*, 2006]. The large amount of freshwater

in this region results in the development of a thick barrier layer, a layer that separates the base of the mixed-layer from the thermocline. The presence of the barrier layer in the study area impedes the intrusion of thermocline waters to the mixed-layer during the upwelling season and reduces its effect on the SST [e.g. *Du et al.*, 2005].

3. Materials and Method

3.1. Sediment cores GeoB 10042-1 and GeoB 10043-3

The two gravity cores GeoB 10042-1 (7°06.81'S 104° 38.58'E, 2454 m water depth, core length: 540 cm) and GeoB 10043-3 (7°18.57'S 105°03.53'E, 2171 m water depth, core length: 390 cm) were collected from west of the Sunda Strait during the SO-184 field campaign with the German RV SONNE in 2005 (Fig. 1) [*Hebbeln et al.*, 2005]. Both cores, GeoB 10042-1 and GeoB 10043-3, consist of nannofossil ooze. In core GeoB 10043-3 a turbidite layer is observed from 225–232 cm depth.

3.2. Radiocarbon dating

For radiocarbon dating the surface-dwelling planktic foraminifera species *Globigerinoides ruber* sensu stricto (s.s.) and *Globigerinoides sacculifer* (without the sac-like final chamber) were hand-picked under a binocular microscope from the >150 μm fraction. The abundance of these species within the cores was generally low, and occasionally both species were combined to obtain a sufficient amount of datable material. Samples were then measured at the Keck Carbon Cycle Accelerator Mass Spectrometry Laboratory, University of California, Irvine (UCI). Raw ^{14}C ages were converted to 2σ calendar ages with the CALIB 7.0 software using the Marine13 calibration dataset [*Reimer et al.*, 2013] (Table 1) with a regional reservoir correction of 100 years [*Southon et al.*, 2013].

Table 1. AMS ^{14}C and calendar ages obtained from planktic foraminifera shells in cores GeoB 10042-1 and GeoB 10043-3. References: (1) [*Southon et al.*, 2013], (2) this study.

UCIAMS #	Depth (cm)	^{14}C_age (yrs BP)	Error	Calendar Age (yrs BP)	1σ	Species	Reference
GeoB 10042-1							
89145	8	3895	20	3751	65	*G. ruber, G. sacculifer*	1
98276	13	4225	40	4201	91	*G. sacculifer*	1
98279	18	4440	50	4491	89	*G. sacculifer*	1
98281	23	4580	15	4670	124	*G. sacculifer*	1
98284	33	4675	45	4798	81	*G. sacculifer*	1
98288	38	4885	20	5078	78	*G. sacculifer*	1
98291	43	5015	25	5259	67	*G. sacculifer*	1
103693	100	6130	45	6460	76	*G. ruber, G. sacculifer*	2
127996	163	7740	60	8108	82	*G. ruber, G. sacculifer*	2
103694	200	8440	50	8917	89	*G. ruber, G. sacculifer*	2
130252	213	8885	45	9460	49	*G. ruber, G. sacculifer*	2
130253	238	11830	60	13223	74	*G. ruber, G. sacculifer*	2
127997	243	13065	30	14909	140	*G. ruber, G. sacculifer*	2
130254	263	13760	60	15949	120	*G. ruber, G. sacculifer*	2
103695	300	16620	90	19454	139	*G. ruber, G. sacculifer*	2
103696	400	24210	130	27797	113	*G. ruber, G. sacculifer*	2
103698	470	30750	750	34286	677	*G. ruber, G. sacculifer*	2
103700	500	32390	660	35834	712	*G. ruber, G. sacculifer*	2
GeoB 10043-3							
89142	13	545	35	84	59	*G. ruber, G. sacculifer*	1
89143	18	640	35	177	70	*G. ruber, G. sacculifer*	1
98502	23	1150	25	627	37	*G. sacculifer*	1
98506	28	1570	35	1029	62	*G. ruber*	1
98508	33	2070	25	1539	65	*G. sacculifer*	1
98510	38	2240	15	1741	59	*G. sacculifer*	1
98518	43	2525	30	2076	71	*G. sacculifer*	1

98520	48	2760	30	2370	65	*G. sacculifer*	1
103701	150	6520	20	6914	64	*G. ruber, G. sacculifer*	2
103702	200	8330	70	8769	129	*G. ruber, G. sacculifer*	2
103703	223	9140	90	9767	158	*G. ruber, G. sacculifer*	2
127998	273	13265	35	15215	78	*G. ruber, G. sacculifer*	2
103705	300	15235	50	17937	95	*G. ruber, G. sacculifer*	2
127999	328	19280	45	22632	106	*G. ruber, G. sacculifer*	2
103706	367	29740	490	33321	106	*G. ruber, G. sacculifer*	2
103707	385	31140	240	34580	233	*G. ruber, G. sacculifer*	2

3.3. Stable Isotope and Mg/Ca Analyses

The cores GeoB 10042-1 and GeoB 10043-3 were sampled every 5 cm for the planktic foraminifera *G. ruber* s.s. in order to conduct stable oxygen isotope ($\delta^{18}O$) and Mg/Ca analyses. Approximately 30-40 individuals of *G. ruber* s.s. collected from the 250-355 μm size fraction were firstly gently cracked using glass plates, then homogenized and split. About two-third of the material was used for Mg/Ca analysis and the remaining one- third was used for $\delta^{18}O$ analysis. The $\delta^{18}O$ measurements were carried out using a Finnigan MAT 251 mass spectrometer at the MARUM, University of Bremen. Long-term standard deviation of the carbonate standard is <0.07‰. The $\delta^{18}O$ results are reported relative to the international Pee-Dee Belemnite (PDB) Standard.

For Mg/Ca analysis, we followed the foraminifera cleaning procedure proposed by *Baker et al.* [2003]. The samples were rinsed five times with de-ionized water and two times with methanol, with ultrasonic treatment after each rinse. In the following step, organic matter was oxidized by adding a NaOH-buffered 1%-H_2O_2 reagent to the samples and placed in a hot water bath for 10 minutes with a few seconds in an ultrasonic bath. After repeating this step, the samples were rinsed and transferred into new acid-cleaned vials. Then, the samples underwent a weak acid leaching (0.001 M QD HNO_3) with 30 seconds ultrasonic treatment after which the samples

were dissolved using 0.075 M QD HNO_3, centrifuged for 10 minutes at 6000 rpm, and transferred into new acid cleaned vials. Mg/Ca measurements were conducted with an Agilent 720 Inductively Coupled Plasma Optical Emission Spectrometer (ICP-OES) housed at the Department of Geosciences, University of Bremen. The Mg/Ca ratio values are reported as mmol mol^{-1}. The instrumental precision during measurement was monitored by analysis of an in-house standard solution, which was measured after every fifth sample. The average 1σ error for the Mg/Ca analyses on an external standard measured along with the analyses for cores GeoB 10042-1 and GeoB 10043-3 is 0.04 mmol/mol. Sample reproducibility based on replicate samples for GeoB 10043-3 (n=15) and GeoB 10042-1 (n=15) is ±0.13 mmol/mol and ±0.31 mmol/mol, respectively.

Mg/Ca ratio values were converted to temperature (T) following the equation proposed by *Anand et al.* [2003] for *G. ruber* (250–350μm):

$$Mg/Ca = 0.38 \exp^{(0.09*T)} \qquad (1)$$

According to sediment trap and core-top studies by *Mohtadi et al.* (2007; 2009; 2011b), *G. ruber* s.s. records mean annual mixed-layer conditions between 0 and 30 m and the dissolution effect on this species is negligible in the study area. This finding is supported by the presence of aragonitic pteropods throughout our cores that further declines any significant role of calcite dissolution in altering the primary signal preserved in the planktic foraminifera shells. Surface sediment and culture studies have shown a significant effect of salinity on the Mg/Ca ratio of planktic foraminifera shells [e.g. *Kisakürek et al.*, 2008; *Mathien-Blard and Bassinot*, 2009; *Arbuszewski et al.*, 2010]. However, the effect of salinity remains a matter of debate due to the overriding effect of dissolution [see e.g. *Hertzberg and Schmidt*, 2013], lack of in-situ measurements or unrealistic laboratory conditions. Core top studies suggest that shell Mg/Ca of planktic foraminifera is biased only in hyper-saline conditions when salinity surpasses 36

psu [*Ferguson et al.*, 2008; *Gibbons et al.*, 2014]; an out of reach threshold for the rain-laden eastern tropical Indian Ocean.

The stable oxygen isotope composition of foraminifera calcite is a function of temperature and the isotopic composition of the ambient seawater ($\delta^{18}O_{sw}$). In order to calculate the seawater $\delta^{18}O$ ($\delta^{18}O_{sw}$), we used the $\delta^{18}O$-temperature equation of *Bemis et al.* [1998]:

$$T\ (°C) = 14.9 - 4.8\ (\delta^{18}O_{cc} - \delta^{18}O_{sw}) \qquad (2)$$

where $\delta^{18}O_{cc}$ and T are the measured $\delta^{18}O$ of calcite and Mg/Ca-based temperature, respectively. The values were then converted to Standard Mean Ocean Water (SMOW) and corrected for sea-level changes as proposed by *Waelbroeck et al.* [2002]. The errors of the Mg/Ca-based temperature and $\delta^{18}O_{sw}$ reconstructions are estimated by propagating the errors introduced by *Mohtadi et al.* [2014]. The resulting errors for temperature and $\delta^{18}O_{sw}$ are on average ~1°C and 0.3 ‰, respectively.

3.4. X-Ray Fluorescence (XRF) Core Scanning

We used the XRF Core Scanner 1 at the MARUM, University of Bremen, to perform measurements on both cores, GeoB 10042-1 and GeoB 10043-3, in 1 cm-resolution. The scanner uses a KEVEX Psi Peltier Cooled Silicon Detector and a KEVEX X-ray Tube 52500008-02 with the target material molybdenum (Mo). In this study we use the elemental ratio of titanium to calcium (Ti/Ca; logarithmic scale) as a proxy to detect past changes in terrestrial input [*Mohtadi et al.,* 2010a; b] to our sites GeoB 10042-1 and GeoB 10043-3.

3.5. Spliced records and published data

The age-depth models for both cores were generated with a Bayesian approach using the Bacon software [*Blaauw and Christen*, 2011]. This method divides a core into sections and models the

accumulation rate for each of these sections (Fig. 2). Afterward we generated a spliced record for each proxy in both cores by averaging data in 500- year, non-overlapping bins and will refer to the spliced records when discussing our results.

By comparing our record to the other published data from the eastern tropical Indian Ocean by *Levi et al.* [2007] and *Gibbons et al.* [2014], we recalculated SST and $\delta^{18}O_{sw}$ in those records by applying equations (1) and (2). Thus, the resulting values differ from those in the original publications. The binned data were then generated using the same method described above.

4. Results

4.1. Age Model

The age models for sediment cores GeoB 10042-1 and GeoB 10043-3 are based on 18 and 16 calibrated radiocarbon dates, respectively, measured on the mixed-layer dwelling planktic foraminifera species *G. ruber* and/or *Globigerinoides sacculifer* (Table 1; Figure 2). The upper 50 cm of both cores spans the last 5.2 kyr (GeoB 10042-1) and 2.3 kyr (GeoB 10043-3), have previously been studied by *Southon et al.* [2013]. In this study we provide 11 (GeoB 10042-1) and 8 (GeoB 10043-3) new radiocarbon dates.

The resulting age-depth models suggest that cores GeoB 10042-1 and GeoB 10043-3 cover the past 39.4 and 34.4 kyr and indicate that the average sedimentation rates of cores GeoB 10042-1 and GeoB 10043-3 are 23.4 cm kyr^{-1} and 16.4 cm kyr^{-1}. Both sediment cores have a distinct ash layer (GeoB 10043-3: 13-18 cm; GeoB 10042-1: 6-8 cm core depth) that has been linked to the Krakatau eruption in 1883 [*Southon et al.*, 2013]. In addition, another ash layer is observed in core GeoB 10043-3 at a depth between 370 and 382 cm and in core GeoB 10042-1 at 470 cm (Fig. 3).

Both cores reveal low glacial sedimentation rates ranging between 3.4 and 19 cm kyr^{-1} (GeoB 10042-1) and between 3.1 and 11.9 cm kyr^{-1} (GeoB 10043-3) compared to the much higher

Holocene sedimentation rates of 14.7 to 54.3 cm kyr^{-1} (GeoB 10042-1) and of 9.7 to 33.7 cm kyr^{-1} (GeoB 10043-3). Using the age-depth model of GeoB 10042-1, we found a hiatus indicated by a dramatic increase in the sedimentation rate from 3.6 to 31 cm kyr^{-1} around 10 kyr BP associated with abrupt changes in $\delta^{18}O$ and Ti/Ca log ratio (Fig 3).

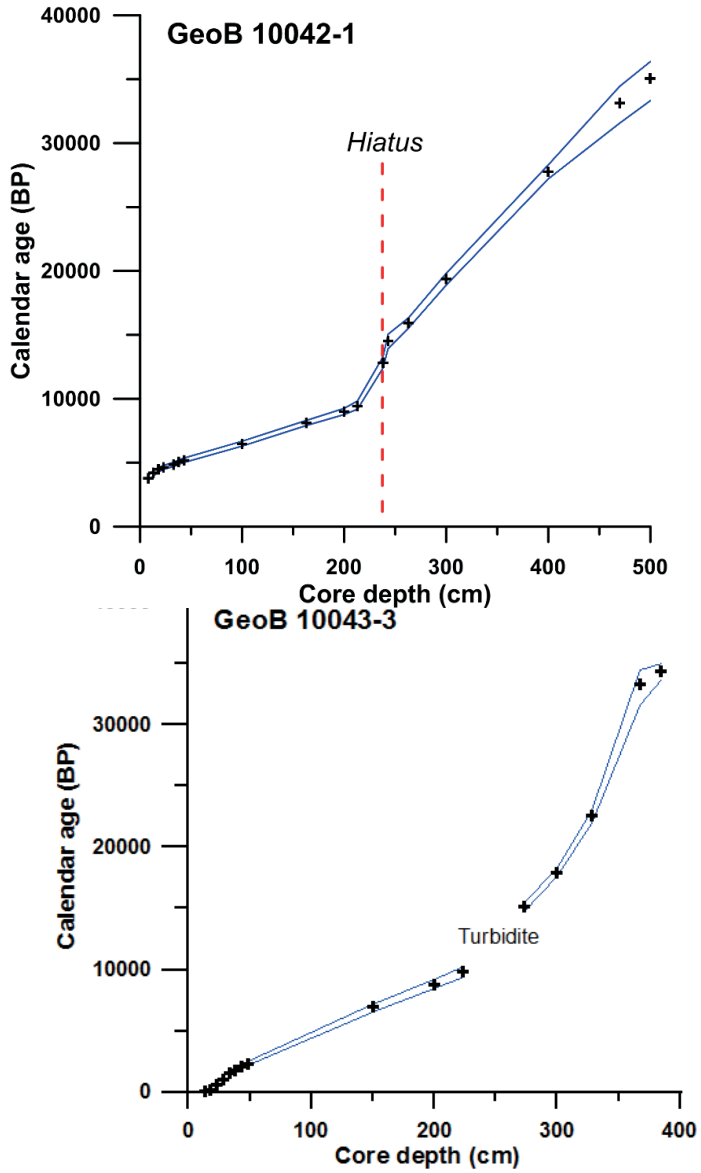

Figure 2. Age-depth model of the GeoB 10042-1 (top) and GeoB 10043-3 (bottom). The turbidite layer in GeoB 10043-3 is between 225 and 232 cm. Blue lines in both age models denote the envelope of 2σ errors. Dashed red line indicates the position of a hiatus.

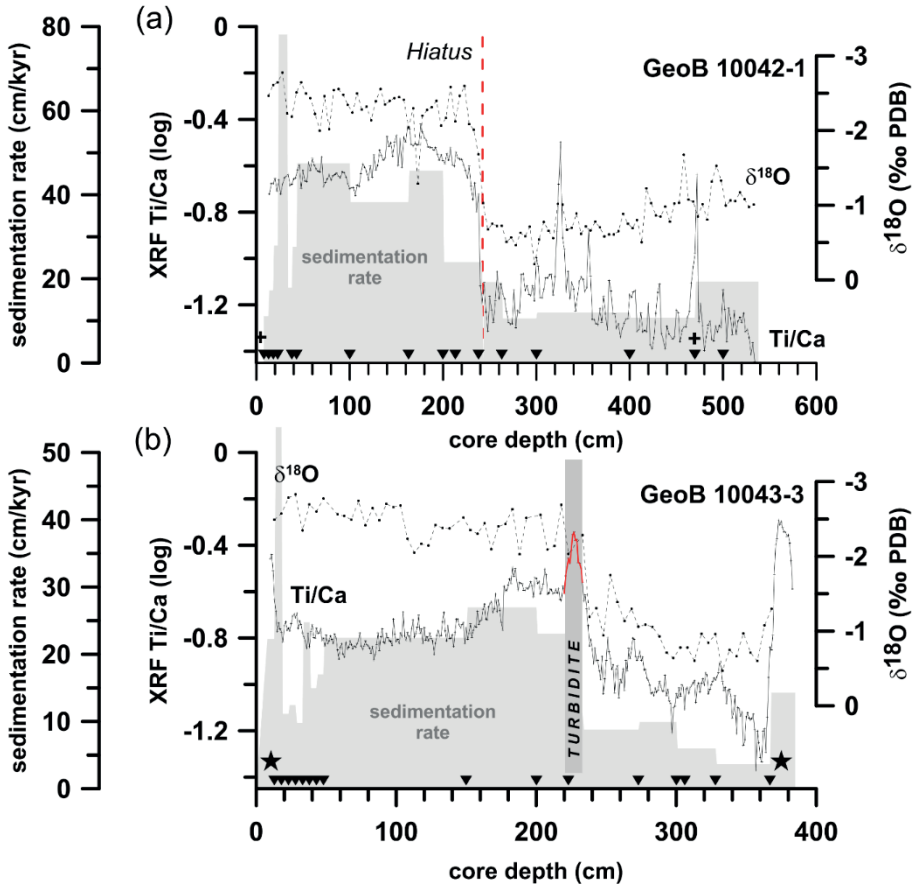

Figure 3. (a) Sedimentation rates (shaded area), $\delta^{18}O$ (dashed line), and Ti/Ca ratio (solid line) of GeoB 10042-1. Crosses denote the positions of volcanic ash layers at 5 cm and 470 cm. The dashed red line shows the position of **a** hiatus. Triangles indicate AMS ^{14}C dating points. (b) Same as top but for GeoB 10043-3. Black stars depict the locations of volcanic ash layer at 10-12 cm and 370-382 cm. The red line and shaded bar show the position of the turbidite layer.

4.2. Shell $\delta^{18}O$ and Mg/Ca ratio of *G. ruber* s.s.

The $\delta^{18}O$ values of *G. ruber* s.s. from cores GeoB 10042-1 and GeoB 10043-3 display a similar variability over the time they overlap (Figs. 3, 4a). In the following, the last glacial and the Holocene always refer to periods >10 kyr BP and <10 kyr BP, respectively. Average last glacial $\delta^{18}O$ values of GeoB 10042-1 and GeoB 10043-3 are -0.92‰ and -0.96‰ and average $\delta^{18}O$ values during the Holocene are -2.34‰ (GeoB 10042-1) and -2.46‰ (GeoB 10043-3). During the last glacial, the average values of Mg/Ca ratio for both cores are 3.58 mmol mol^{-1} (GeoB 10042-1) and 3.78 mmol mol^{-1} (GeoB 10043-3) (Figs. 3, 4b). The averages Mg/Ca ratio values of both cores during the Holocene are 4.18 (GeoB 10042-1) and 4.22 mmol mol^{-1} (GeoB 10043-

3). Estimated Mg/Ca-based SSTs recorded in both sediment cores show a similar pattern for the past ~40 kyr (Fig. 4b). During the last glacial, average SSTs for cores GeoB 10042-1 and GeoB 10043-3 are 24.9°C and 25.5°C (Fig. 4c). During the Holocene, both SSTs show similar, slightly warmer average values of 26.6°C (GeoB 10042-1) and 26.7°C (GeoB 10043-3). Deglacial warming of 2-3°C reached maximum values during the early Holocene at around 9 kyr BP. Subsequently SSTs decreased by about 1°C between 9 and 7 kyr BP followed by a slight increase towards the present.

4.3. Seawater $\delta^{18}O$ ($\delta^{18}O_{sw}$)

During the last glacial, the average $\delta^{18}O_{sw}$ values of GeoB 10042-1 and GeoB 10043-3 are almost identical within the error, i.e. 0.65‰ and 0.69‰ (Figs. 3, 4d). Likewise, similar average $\delta^{18}O_{sw}$ values of 0.26‰ (GeoB 10042-1) and 0.23‰ (GeoB 10043-3) are observed for the Holocene. In GeoB 10043-3, $\delta^{18}O_{sw}$ values remain stable during the course of the last deglaciation until the Younger Dryas (12.8-11.5 kyr) when there is a marked increase, whereas the $\delta^{18}O_{sw}$ record of GeoB 10042-1 reveals a ~0.5‰ increase during the early deglaciation.

4.4. XRF Measurements

In general, both sediment cores indicate similar first order variability in the Ti/Ca log ratio during the past ~40 kyr (Figs. 3, 4e). In both sediment cores the Ti/Ca log ratios are much lower during the last glacial compared to the Holocene. The peak of the Ti/Ca log ratio occurred during the early Holocene. The Ti/Ca log ratios in both cores GeoB 10042-1 and GeoB 10043-3 show a declining trend from the early to mid-Holocene (8-4 kyr BP) followed by a slight increase afterward.

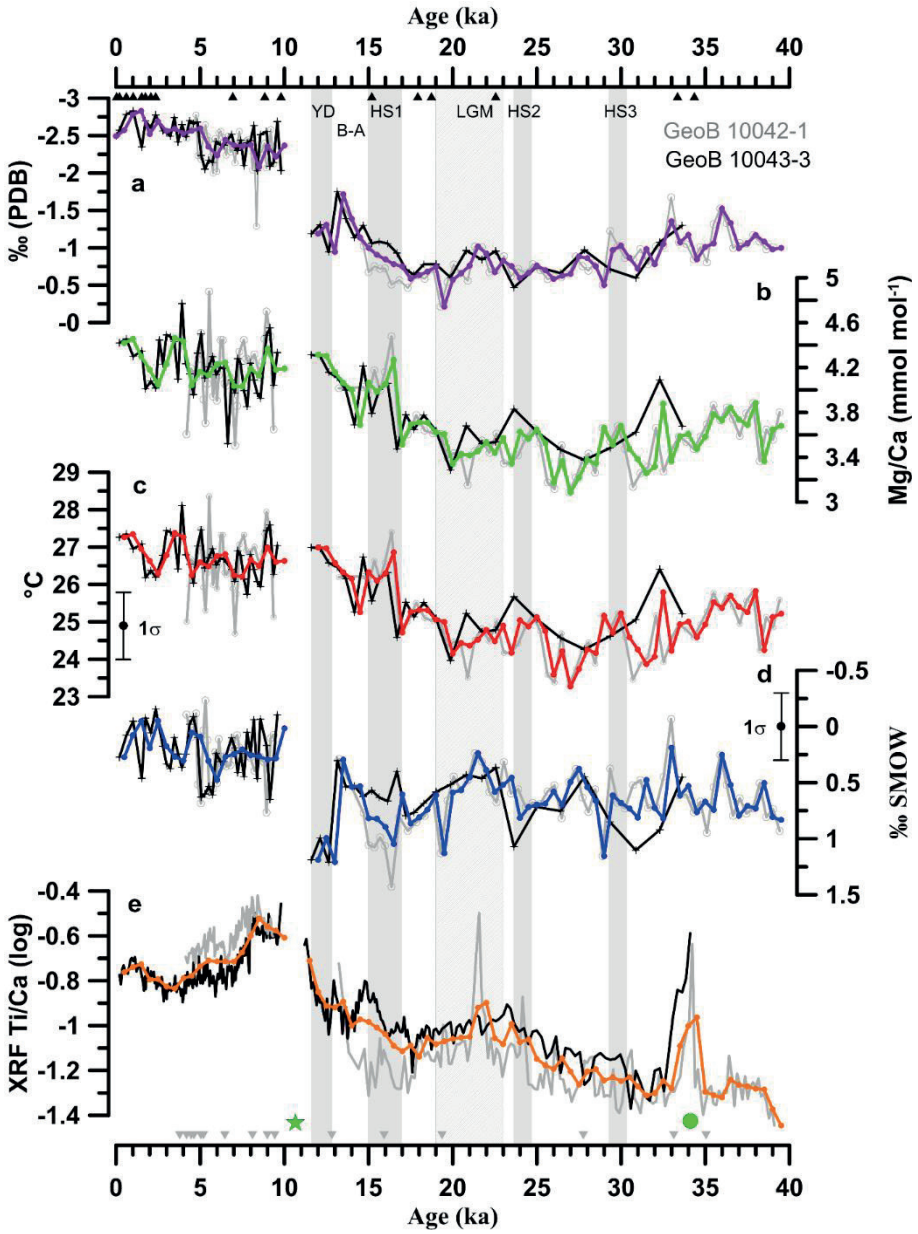

Figure 4. (a) *G. ruber* s.s $\delta^{18}O$, (b) *G. ruber* s.s Mg/Ca ratio, (c) SST calculations based on b, (d) $\delta^{18}O_{sw}$ calculated from a and c, and (e) Ti/Ca (logarithmic scale) of the GeoB 10042-1 (gray) and GeoB 10043-3 (black). Purple, green, red, blue, and orange curves are splice records of a, b, c, d and e. Black (grey) triangles denote AMS ^{14}C dating points for the GeoB 10043-3 (GeoB 10042-1). Shaded bars indicate LGM, Heinrich stadials (HS) 1-4 and the Younger Dryas (YD). Green stars and the green dot denote the positions of turbidite and volcanic ash layers.

5. Discussion

5.1. Hydrologic conditions off the Sunda Strait prior to the Sunda Shelf flooding (10 kyr BP)

During the last glacial, SST variability off the Sunda Strait (Fig. 5a) is similar to other Mg/Ca-based SST reconstructions from the eastern tropical Indian Ocean (Fig. 5b-c) [*Mohtadi et al.*, 2010a; 2014; *Levi et al.*, 2007; *Xu et al.*, 2008]. Furthermore, short-term variations in our SST reconstructions are within the range of SST variability described for the upwelling region covering the south Sumatra-Java-Lesser Sunda Island chain region (between ~23° and 29°C). Reconstructed SSTs from the non-upwelling region off north and central Sumatra are 2-3°C warmer, ranging from ~25° to 30°C [*Mohtadi et al.*, 2014] (Fig. 5c). Within our age model uncertainty (Fig. 2), the onset of deglacial SST warming in our records (~17-18 kyr BP) coincides with warming over Antarctica [*Jouzel et al.*, 2007] and the atmospheric CO_2 rise [*Monnin et al.*, 2001], in line with other records of the eastern tropical Indian Ocean [*Levi et al.*, 2007; *Xu et al.*, 2008; *Mohtadi et al.*, 2010a; 2014; *Gibbons et al.*, 2014].

In order to better reconstruct the hydroclimate conditions off the Sunda Strait we suggest Ti/Ca values reflect terrigenous input and continental runoff, where high Ti/Ca values indicate increased runoff [e.g. *Mohtadi et al.*, 2010b; 2011a] (Fig. 6e). Ideally, there should be an inverse relationship between Ti/Ca and $\delta^{18}O_{sw}$ if both parameters are controlled by changes in rainfall and P-E. However, the overall increasing trend in Ti/Ca indicative of increasing terrigenous input during the last glacial (Fig. 6e) is not paralleled by any trend in our reconstructed glacial $\delta^{18}O_{sw}$ (Fig. 6a). This mismatch is not unexpected as Ti/Ca and runoff in this region include a strong seasonal signal caused by monsoonal precipitation during the NWM from December to March [*Mohtadi et al.*, 2009; 2010b, 2011a]. In contrast, results from sediment surface samples and a nearby sediment trap suggest that Mg/Ca ratio in *G. ruber* reflects mean annual surface conditions [*Mohtadi et al.*, 2009; 2011b]. Thus, our reconstructed $\delta^{18}O_{sw}$ is interpreted to reflect a mixed signal of the monsoon and non-monsoon seasons. Besides the potential bias introduced

by the different seasonality of the two sets of data, it is likely that $\delta^{18}O_{sw}$ off the Sunda Strait is additionally controlled by varying intrusion of saltier waters from below during the SEM upwelling season. Variability in $\delta^{18}O_{sw}$ in this region is also influenced by the changing direction of the South Java Current during different seasons (see section 2, study area). In summary, while the $\delta^{18}O_{sw}$ records from the more enclosed, non-upwelling basins in west and northwest of Sumatra are likely to reflect P-E in the past [*Mohtadi et al.*, 2014], *G. ruber*-based $\delta^{18}O_{sw}$ reconstructions off southwest Sumatra and from the monsoon-influenced region in Indonesia, characterized by seasonal upwelling and changing surface current directions, should be interpreted with caution as a proxy for changing rainfall or P-E.

Within the age uncertainty of our records during the last glacial, $\delta^{18}O_{sw}$ values increase during the Heinrich stadials and the Younger Dryas (Fig. 6a) accompanied by a slight SST increase of 1-2°C (Fig. 5a) that has been also observed in other $\delta^{18}O_{sw}$ and SST records from both the non-upwelling areas (Figs. 5c and 6c) and upwelling areas (Figs. 5b and 6b) of the eastern tropical Indian Ocean [*Levi et al.*, 2007; *Mohtadi et al.*, 2010a; 2014; *Gibbons et al.*, 2014]. This finding suggests widespread changes in the Indonesian hydroclimate during the millennial-scale cold periods of the Northern Hemisphere and supports previous inferences of a modified atmospheric circulation in the topics. Model simulations suggest a weakened and easterly displaced Hadley Circulation as a response to a weak Atlantic Meridional Overturning Circulation [*Zhang and Delworth*, 2005], or a reorganization of the Hadley Circulation and a southward displacement of the ITCZ [*Gibbons et al.*, 2014; *Mohtadi et al.*, 2014]. Further support for a southward displacement of the ITCZ during Heinrich stadials is provided by the speleothem records from the IPWP: Borneo speleothems suggest anomalous dry conditions [*Carolin et al.*, 2013] while speleothem records from Flores [*Ayliffe et al.*, 2013] and northern Australia [*Denniston et al.*, 2013] imply anomalous wet conditions during the Heinrich stadials. According to model simulations of the Heinrich stadials [*Gibbons et al.*, 2014; *Mohtadi et al.*,

2014], the eastern tropical Indian Ocean should have experienced drier and warmer conditions during the entire year, which might explain why our "mean annual" proxies of SST and $\delta^{18}O_{sw}$ record these millennial events. Therefore, the otherwise efficient control of seasonality and advection on the $\delta^{18}O_{sw}$ at our site has been minimized by an overall, year-round dry and warm eastern tropical Indian Ocean during the Younger Dryas and Heinrich stadials.

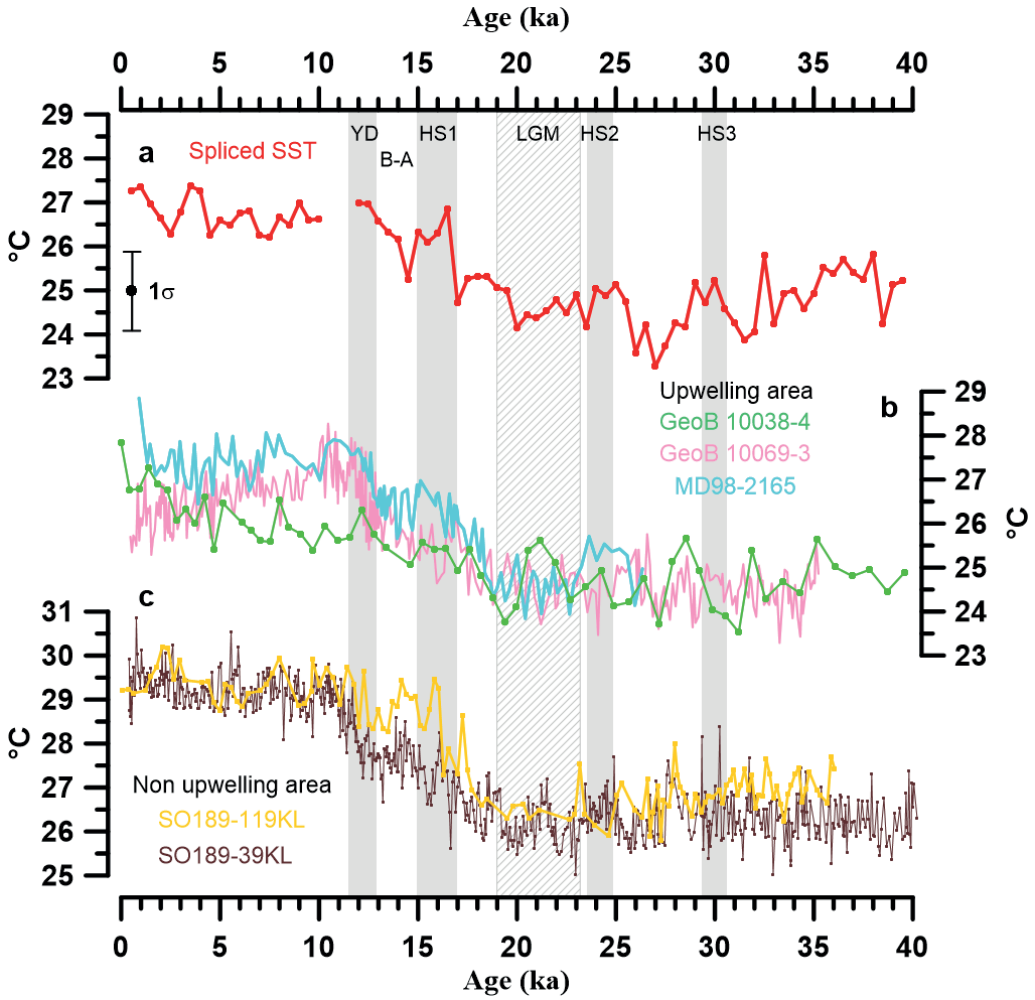

Figure 5. (a) Spliced SST record of the Sunda Strait. (b) Mg/Ca-based SSTs of GeoB 10038-4 (green curve [*Mohtadi et al.*, 2010a], of GeoB 10069-3 (pink curve] [*Gibbons et al.*, 2014] and of MD98-2165 (light blue curve) [*Levi et al.*, 2007]. (c) Mg/Ca-based SSTs of SO189-39KL (brown curve) and SO189-119KL (yellow curve) [*Mohtadi et al.*, 2014]. Shaded bars indicate LGM, Heinrich stadials (HS) 1-4 and the Younger Dryas (YD). Error bar indicates 1σ error (1°C).

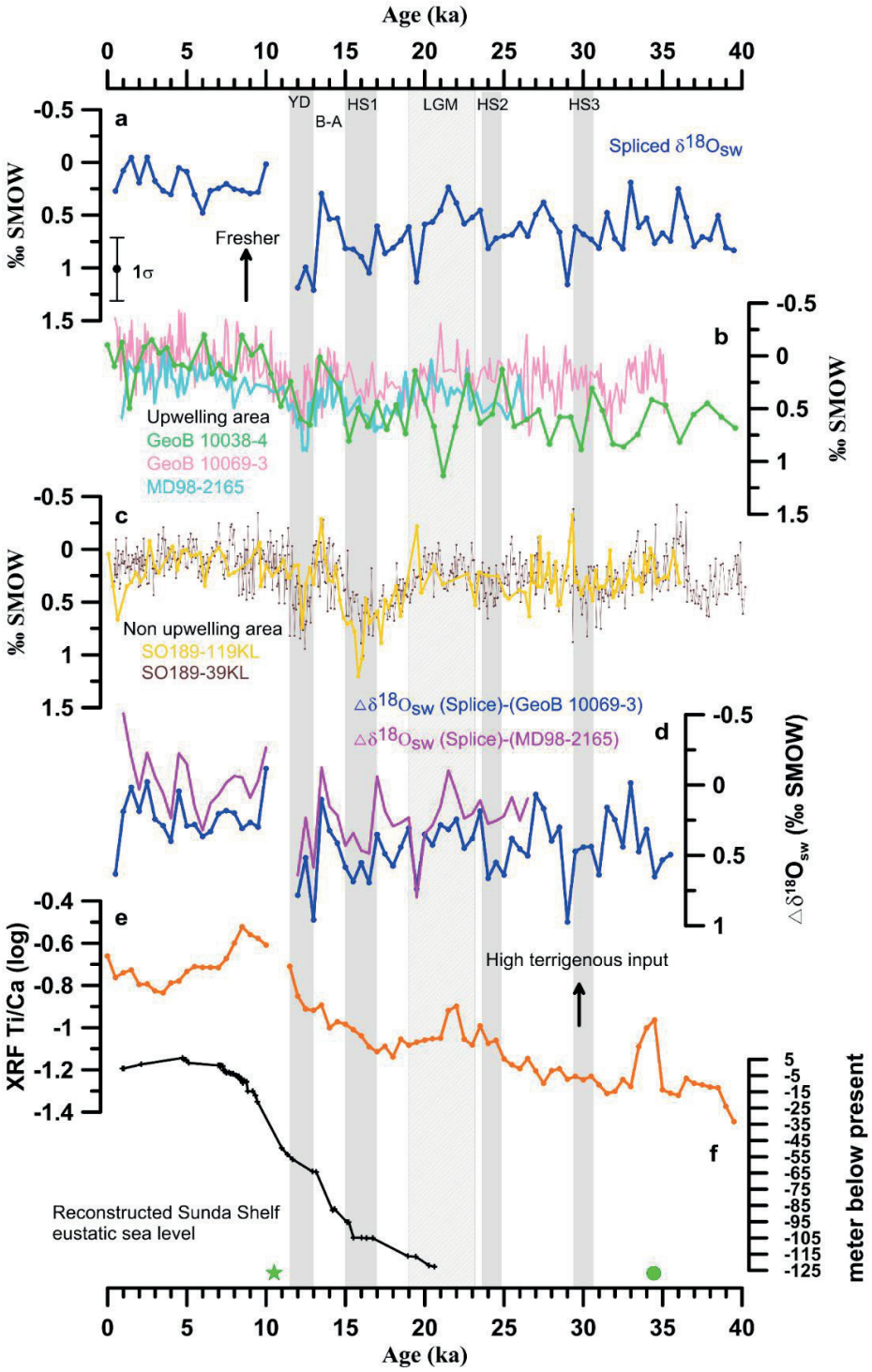

Figure 6. (a) Spliced $\delta^{18}O_{sw}$ record of the Sunda Strait (‰ SMOW). (b) *G. ruber* $\delta^{18}O_{sw}$ (‰ SMOW) of of GeoB 10038-4 (green curve) [*Mohtadi et al.*, 2010a], of GeoB 10069-3 (pink curve) [*Gibbons et al.*, 2014] and of MD98-2165 (light blue curve) [*Levi et al.*, 2007]. (c) *G. ruber* $\delta^{18}O_{sw}$ (‰ SMOW) of SO189-39KL (brown curve) and SO189-119KL (yellow curve) [*Mohtadi et al.*, 2014]. (d) $\delta^{18}O_{sw}$ difference ($\Delta\delta^{18}O_{sw}$; 500-yr average) between the Sunda Strait and the Savu Sea (blue curve) and between the Sunda Strait and Sumba (magenta curve). (e) Spliced record of Ti/Ca from XRF measurement (logarithmic scale). (f) Reconstructed sea level fluctuation of the Sunda Shelf [*Hanebuth et al.*, 2011]. Shaded bars indicate LGM, Heinrich stadials (HS) 1-4 and the Younger Dryas (YD). The green stars and green dot denote the positions of turbidite and volcanic ash layers, respectively. Error bar indicates 1σ error (0.3‰).

5.2. The flooding of the Sunda Shelf

According to our results, the final (or full) opening of the Sunda Strait occurred at ~10 kyr BP (Figs. 4-6). While in other records changes on millennial timescales are much more prominent than on glacial-interglacial scale [*Mohtadi et al.*, 2010a; 2014; *Gibbons et al.*, 2014; *Niedermeyer et al.*, 2014], our $\delta^{18}O_{sw}$ record together with that of the nearby core GeoB 10038-4 [*Mohtadi et al.*, 2010a] reveal fresher conditions since 10 kyr BP compared to the last glacial period (Fig. 6a-c). We attribute this freshening to the inflow of the relatively fresh Java Sea waters through the Sunda Strait at this time. Due to island topographies, almost all of the large rivers in Indonesia drain into the Java Sea and are characterized by fresher conditions compared to the surrounding seas and oceans. The opening of the Sunda Strait with shallow sill depths of only 20-40 m in the east enabled the transport of the fresh Java Sea waters to our core sites.

The spliced Ti/Ca record provides more evidence of this opening during the last deglaciation and shows a prominent change in the terrigenous material supply associated with the rapid sea level rise on the Sunda Shelf between 11 and 9.5 kyr BP (Fig. 6f). The marked change in Ti/Ca around 10 kyr BP is not preserved in a sedimentary archive off south Java [*Mohtadi et al.*, 2011a, not shown]. The increase in Ti/Ca during this period suggests an enhanced supply of terrigenous material from the formerly exposed Sunda Shelf towards our core sites via the Sunda Strait that corresponds to the inundation of inner Sunda Shelf region at ~10.8 kyr BP [for details see *Sathiamurthy and Boris*, 2006; *Hanebuth et al.*, 2011]. Furthermore, sedimentation rates at both sites also indicate a marked change from ~3.5 to 31 cm kyr^{-1} (GeoB 10042-1) and from ~9.8 to 22.5 cm kyr^{-1} (GeoB 10043-3) at this time (Fig. 3). This change is accompanied by a turbidite layer in core GeoB 10043-3 and a hiatus in core GeoB 10042-1 indicating possible erosive mass wasting and slope instability related to the rapid sea level rise and the opening of the Sunda Strait. After the opening, higher sedimentation rates are sustained at site closer to the Sunda Strait and support the inference of additional sediment supply through the Sunda Strait.

Finally, terrigenous proxy records show an increase in kaolinite and quartz content in the nearby core BAR9442 during the Holocene that has also been related to the opening of the Sunda Strait [*Gingele et al.*, 2002].

5.3. Hydrologic conditions off the Sunda Strait after the Sunda Shelf flooding

After the opening of the Sunda Strait at ~10 kyr BP, SST varied from ~26.3° to 27.4°C. Previous studies suggest no ubiquitous Holocene SST evolution in the eastern tropical Indian Ocean region, where some suggest a clear cooling trend to the present [*Gibbons et al.*, 2014], others interpret a continuous warming trend [*Mohtadi et al.*, 2010a; b] or no trend during the Holocene [*Levi et al.*, 2007; *Xu et al.*, 2008; *Mohtadi et al.*, 2014] similar to our new data off the Sunda Strait (Fig. 5). The available Holocene SST data do not reveal a distinct geographical pattern and might be additionally biased by different temporal resolutions of these records.

The Holocene $\delta^{18}O_{sw}$ records off the Sunda Strait characterizing the "open-Sunda-Strait-setting" differ from other records from the eastern tropical Indian Ocean when comparing average glacial and interglacial values. In general lower $\delta^{18}O_{sw}$ values during the post- compared to the pre-opening of the Sunda Strait indicate the permanent influence of the Java Sea waters on the hydrology at our core sites. However, the lack of correspondence between $\delta^{18}O_{sw}$ and Ti/Ca during the Holocene suggests another control on these parameters. In addition to P-E, the pattern of the Holocene Ti/Ca record is similar to the Ti/Ca record in the nearby core GeoB 10038-4 [*Mohtadi et al.*, 2010b] and appears to follow insolation changes with maximum values during the early Holocene and minimum values at ~3 kyr BP. This is similar to various monsoonal proxy-archives that are inferred to reflect the monsoon strength during a particular season [*Dykoski et al.*, 2005; *Fleitmann et al.*, 2007; *Mohtadi et al.*, 2011a]. This trend in Ti/Ca values is not evident in the $\delta^{18}O_{sw}$ record (as discussed in section 5.1) and may reflect differences in the seasonality of these two proxies and other hydrographic controls on seawater $\delta^{18}O$.

5.4. The impact of the Sunda Strait opening on regional hydrography

The contrast between our proxy records off the Sunda Strait and those in other eastern tropical Indian Ocean records on glacial-interglacial timescales suggesting an overriding control of sea-level related changes on the hydrology off the Sunda Strait. Present-day sea surface conditions in the eastern tropical Indian Ocean off the Sunda Strait are always fresher than the Lombok basin off Sumba and the Savu Sea further to the east by ~1 psu (Fig. 1). To track this difference over the past ~40 kyr, we calculated the $\delta^{18}O_{sw}$ difference ($\Delta\delta^{18}O_{sw}$) between the Sunda Strait and the Savu Sea (GeoB 10069-3; blue curve in Fig. 6d) and between the Sunda Strait and the Sumba area (MD98-2165; magenta curve in Fig. 6d). During the Holocene, the $\delta^{18}O_{sw}$ values are indistinguishable within error. During the last glacial, there is a difference between the Sunda Strait sites and the other eastern tropical Indian Ocean sites related to the larger glacial $\delta^{18}O_{sw}$ values off the Sunda Strait (Fig. 6a) compared to the glacial $\delta^{18}O_{sw}$ values at other sites that remained stable (Fig. 6b-c). During the last glacial, $\delta^{18}O_{sw}$ values in the Savu Sea are fresher than elsewhere, possibly due to the position of the Savu Sea record sits near the major exit passage of the relatively fresh ITF (Fig. 6b). This is also shown in the $\Delta\delta^{18}O_{sw}$ contrast between the Sunda Strait and Savu Sea that has been larger than the average difference between the Sunda Strait and the Lombok Basin off Sumba over the past 40 kyr (Fig. 6d).

Model simulations of the LGM climate suggest that the exposure of the Sunda Shelf resulted in cooling over the Maritime Continent that weakened the Walker Circulation over the Indian Ocean and led to a stronger upwelling in the eastern tropical Indian Ocean [*DiNezio et al.*, 2011; *DiNezio and Tierney*, 2013]. However, available proxy records of past upwelling and productivity in the eastern tropical Indian Ocean do not support strong upwelling in our study area during the last glacial [*De Deckker and Gingele*, 2002; *Lückge et al.*, 2009; *Mohtadi et al.*, 2010b]. Whether the higher glacial $\delta^{18}O_{sw}$ values off the Sunda Strait reflect stronger upwelling of deeper and saltier waters in this region or a stronger influence of the saltier surface Indian

Ocean is not known, and will require additional reconstructions of water mass distributions and upwelling histories for the eastern tropical Indian Ocean. It is important to note that differences between $\delta^{18}O_{sw}$ values at different locations are greatest during Heinrich stadials and the Younger Dryas even though the pattern of change in individual records is generally similar (Fig. 6d, increasing $\delta^{18}O_{sw}$). This suggests a stronger zonal gradient in the hydrological cycle of the eastern tropical Indian Ocean during these times that might reflect changes in the atmospheric circulation (Walker and Hadley circulation and the position of the ITCZ, see above and [*DiNezio and Tierney*, 2013; *Gibbons et al.*, 2014; *Mohtadi et al.*, 2014]). Overall, it is not clear to what degree different mechanisms were responsible for the similarities between proxy records from various eastern tropical Indian Ocean sites during the Holocene. Nevertheless, our data indicate that the opening of the Sunda Strait at ~10 kyr BP was a major control on these records, as the fresher Java Sea waters and the resulting fresh water cap introduced into the eastern tropical Indian Ocean reduced local upwelling intensity during the Holocene. Paleoproductivity reconstructions based on diatoms [*Romero et al.*, 2012] and organic carbon [*Lückge et al.*, 2009] in two cores off the Sunda Strait suggest that marine productivity during the Holocene was higher compared to the last glacial. Apparently this higher marine productivity is due to an additional input of (terrigenous) nutrients through the Sunda Strait [*Gingele et al.*, 2002; *Mohtadi et al.*, 2010b; *Romero et al.*, 2012].

Another notable change after the opening of the Strait is a decrease in thermocline temperatures recorded in a nearby core off the Sunda Strait [*Mohtadi et al.*, 2010b]. It is possible that the opening of the Sunda Strait and the subsequent addition of freshwater to this area facilitated the development of the barrier layer (see section 2 for details) and a diverging evolution of the thermocline and surface temperatures during the Holocene. The degree to which this freshwater forcing might have been responsible for the observed changes in the upper water column has to be explored by a (transient) model-data assessment in future studies.

6. Conclusion

We have reconstructed sea surface conditions of the eastern tropical Indian Ocean off the Sunda Strait for the past 40,000 years. Our results show a major change in hydrology off the Sunda Strait with fresher conditions during the Holocene compared to the last glacial period. The surface ocean was cooler and saltier than elsewhere in the eastern tropical Indian Ocean prior to the opening of the Sunda Strait with average SST of 25°C and seawater $\delta^{18}O$ of ~0.7‰. The opening of the Sunda Strait at ~10 kyr BP altered surface hydrology with the inflow of low salinity Java Sea water into the eastern tropical Indian Ocean changing average seawater $\delta^{18}O$ and SST by ~-0.5‰ and 1.7°C. Our results suggest that the opening of the Sunda Strait and the increase in terrigenous supply may have been responsible for higher marine productivity in the eastern tropical Indian Ocean during the Holocene.

Acknowledgments

We are grateful to M. Segl, B. Meyer-Schack, and S. Pape for technical assistance. R.Y. Setiawan acknowledges financial support from the Deutscher Akademischer Austauschdienst (DAAD grant A/10/7596). This study was supported by the German Ministry of Education and Research (project PABESIA) and the Deutsche Forschungsgemeinschaft (DFG grant HE3412/15-1). The data of this study are archived and can be retrieved at PANGAEA (www.pangaea.de).

5. Modification of the deep water neodymium isotope composition along the eastern margin of the tropical Indian Ocean (In preparation)

Riza Yuliratno Setiawan[1*]; Ed C. Hathorne[2]; Katharina Pahnke[3]; Mahyar Mohtadi[1]; Dierk Hebbeln[1]

[1]MARUM – Center for Marine Environmental Sciences, University of Bremen, Bremen, Germany

[2]GEOMAR Helmholtz Centre for Ocean Research Kiel, Kiel, Germany

[3]Max Planck Research Group for Marine Isotope Geochemistry, Institute for Chemistry and Biology of the Marine Environment (ICBM), University of Oldenburg, Oldenburg, Germany

*E-mail: riza.y.setiawan@gmail.com

Abstract

The eastern tropical Indian Ocean (ETIO) is an important region for the global thermohaline circulation as it hosts the exit passages of the Indonesian Throughflow (ITF). With respect to global sea level rise during the last deglaciation, the Sunda shelf flooding and the opening of the Sunda Strait at ~10 kyr have been suggested to impact the ITF flow and sea surface conditions of the eastern tropical Indian Ocean (ETIO), respectively. Nonetheless, the impact of opening the Sunda Strait on deep waters is still unknown until today. Here we study two sediment cores GeoB 10042-1 (2454 m water depth) and GeoB 10043-3 (2171 m water depth) collected from the ETIO off the Sunda Strait. We analyzed the neodymium isotope ratio ($^{143}Nd/^{144}Nd$, expressed as ε_{Nd}) of authigenic coatings of mixed planktic foraminifera and of detrital silicates. Our new data show prominent modifications on the bottom water (foraminifera ε_{Nd}) off the Sunda Strait during the last deglaciation and the Holocene coincided with a strong- and a weak thermocline ITF flow, respectively. In addition, large terrigenous material input driven by the opening of the Sunda Strait might partly modify our Holocene foraminifera ε_{Nd}. Moreover, our new detrital ε_{Nd} data indicate to be more sensitive to the deep ITF flow and to the opening of the Sunda Strait.

1. Introduction

The Indonesian throughflow (ITF) plays a significant role in the global thermohaline circulation by transporting water mass and heat from the Pacific to the Indian Oceans (Gordon 2005). As a consequence, this transport has been suggested to impact the state of the Pacific and Indian Oceans (Sprintall et al., 2014; Sprintall and Revelard, 2014) and global climate system (Qu et al., 2005). Today, the ITF transports cool and fresh upper thermocline North Pacific waters to the Indian Ocean via multiple passages of the Indonesian Seas (Gordon et al., 2003) and is influenced by freshwater flow from the Java Sea. However, the conditions were different during the Last Glacial Maximum (LGM). Without any influence from the low salinity Java Sea water, the ITF transport was dominated by warm, saltier surface flow (Xu et al., 2008).

The Sunda Shelf flooding at ~9.5 kyr has been suggested to alter the hydrographic conditions of the seas around Indonesia (Linsley et al., 2010; DiNezio and Tierney, 2013). This shelf flooding reconnected the South China Sea and the Makassar Strait and allows the transport of low salinity Java Sea into the eastern tropical Indian Ocean (ETIO) through the opening of the Sunda Strait. The opening of the Sunda Strait is of particular interest because it has been suggested to impact past and modern oceanography in the ETIO off the Sunda Strait (Putri, 2005; Setiawan et al., 2015). However, the impact of the opening of the Sunda Strait on bottom water is unknown until today.

The radiogenic neodymium isotope composition (ε_{Nd}) is an important water mass tracer as it can be used to reconstruct past changes of deep ocean circulation, such as in the Indian Ocean (e.g. Jeandel et al., 1998; Frank et al., 2006; Martin and Scher, 2006; Piotrowski et al., 2009; Wilson et al., 2012). Neodymium isotopes have a shorter residence time (~500 years) than the global ocean mixing time (e.g. Tachikawa et al., 1999; 2003) and are insensitive to biological fractionation (Jeandel et al., 1995; Frank, 2002). This short residence time makes the isotopic composition of Nd a suitable quasi-conservative water mass tracer. A water mass acquires its

Nd isotopic composition from the surrounding continents through weathering processes and the dissolved ε_{Nd} in the ocean is a function of water mass flow path (Frank, 2002).

Previous studies have shown that the spatial variability of the ε_{Nd} in the surface waters of the ETIO off Indonesia ranges from -9.9 to -1.5 ε_{Nd} units (Amakawa et al., 2000), whereas the distribution of ε_{Nd} in water column ranges from -7.3 to -2.2 ε_{Nd} units (Jeandel et al., 1998). Furthermore, both studies have indicated that the high seawater ε_{Nd} values in the ETIO waters reflect the strong influence of the Indonesian volcanic islands on the seawater ε_{Nd}. A study by Ehlert et al. (2011) reveals that radiogenic ε_{Nd} values dominated the Java-Nusa Tenggara Lesser Sunda Islands and suggests that the ITF plays an important role for the distribution of high radiogenic ε_{Nd} in the ETIO. Recently, Stumpf et al. (2015) suggest that the detrital ε_{Nd} of eastern Indian Ocean is sensitive to changes in ITF intensity and documented an intensification of the ITF during the early MIS3 until 47.4 kyr. Nevertheless, high-resolution records of bottom water ε_{Nd} in the ETIO during the last deglaciation are still lacking. Here, for the first time, we present a reconstruction of bottom water Nd isotope compositions obtained from the authigenic coatings of planktonic foraminifera and of detrital silicates in the ETIO covering the past 19 kyr. We provide evidence that the opening of the Sunda Strait and the ITF exerted pronounced modifications on the bottom water ε_{Nd} in the ETIO off the Sunda Strait. Our results reveal that the detrital silicates are sensitive to ocean current in the region.

2. Study Area

Today the eastern tropical Indian Ocean (ETIO) off southern Indonesia is strongly influenced by the Australian-Indonesian Monsoon (AIM) system. The dynamics of the seasonally reversing AIM winds have prominent impacts on the oceanic circulation over the study area. During the northwest monsoon (NWM) season (December–February), the winds blow from the Eurasian continent, over the South China Sea and the Bay of Bengal and carry warm and moist air to Indonesia (Gordon, 2005; Qu et al., 2005). Along the coasts of Sumatra and Java, the

eastward flowing South Java Current (SJC) carries low-salinity, warm water from the eastern equatorial Indian Ocean off Sumatra into the southeast Indian Ocean for 8 months of the year (Du et al., 2005; Sprintall et al., 2009; 2010). During the southeast monsoon (SEM) season (June–September) the direction of the SJC is reversed, carrying higher salinity southeast Indian Ocean water westward (Sprintall et al., 2010) (Fig. 1). During this time of the year southeasterly winds blow from Australia and carry warm and dry air to Indonesia (Gordon, 2005; Qu et al., 2005) and wind-induced upwelling centered south of Java occurs (Susanto et al., 2001).

The Indonesian throughflow (ITF) transports Pacific Ocean water into the Indian Ocean via multiple passages within the Indonesian Seas (Gordon et al., 2010; Vranes and Gordon, 2005), forming the return pathway in the global thermohaline circulation (e.g. Sprintall et al., 2014). The main pathways of the ITF in the west are the Sulawesi Sea and Makassar Strait, whereas in the east the ITF passes through the Maluku and Halmahera Seas (e.g. Gordon et al., 2010). The ITF flows westward as part of the South Equatorial Current (SEC) entering the Agulhas current system and eventually the Atlantic Ocean (Talley and Sprintall, 2005).

The ITF water masses are the Indonesian Throughflow Water (ITW) in the upper layer (0-500 m) and of the Indonesian Intermediate Water (IIW) at a deeper layer (~600-1500 m) (Talley and Sprintall, 2005). Both the ITW and IIW are characterized by low salinity and high silica that can be traced along the SEC. In the Indian Ocean the IIW is defined in a latitude band between 8°S and 18°S, with a core at 14°S. Furthermore, the IIW is formed as a result of diapycnal mixing between water masses from the North Pacific and South Pacific that occurred in the Banda Sea (Talley and Sprintall, 2005). Below 1500 m to the bottom, the water column off the eastern Indian Ocean is comprised of the upper Indian Deep Water (IDW) (Talley and Sprintall, 2005; Atmadipoera et al., 2009). This water mass is characterized by high salinity (>34.6) and cold temperature (<4°C) (Atmadipoera et al., 2009). In the Indian Ocean, the IDW

ranges from 500–3800 m in the southern portion of the Indian Ocean to 2000–3800 m in the north, with a core at ~2400 m (Martin and Scher, 2006).

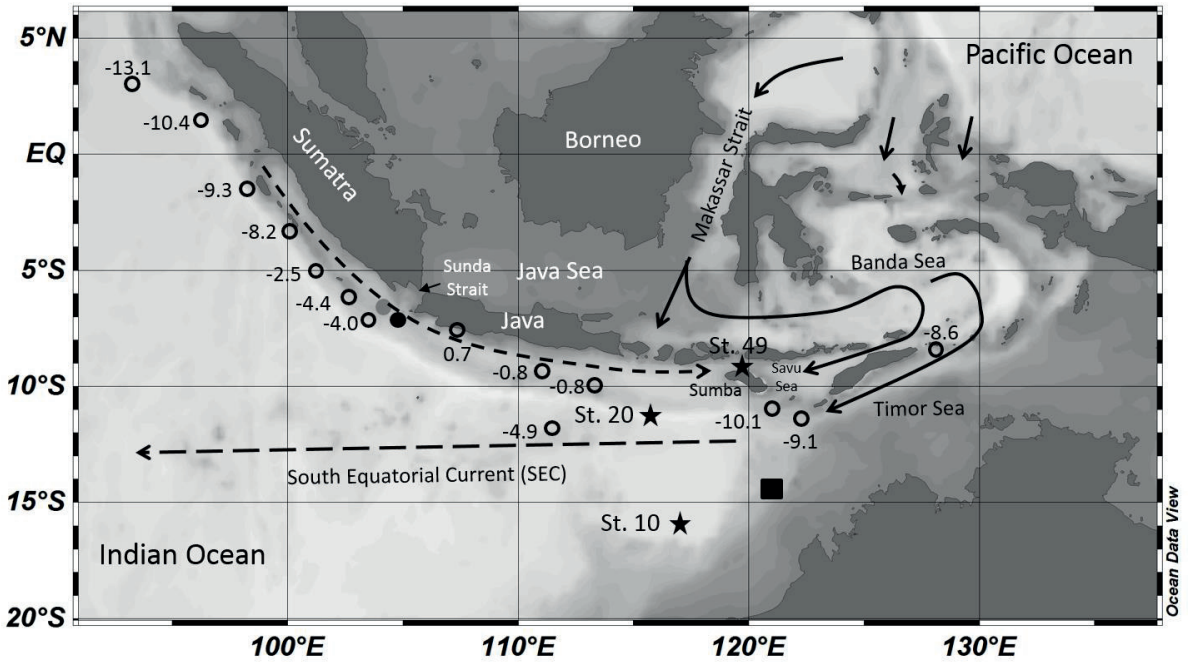

Fig. 1. Grey and black dots denote the location of GeoB 10042-1 and GeoB 10043-3, respectively. Black stars indicate the stations of seawater ε_{Nd} measurements (Jeandel et al., 1998). Circles and numbers show the positions of surface sediment samples and the values of clay-sized detrital ε_{Nd} of corresponding surface samples (Ehlert et al., 2011). Black box denotes the location of sediment core FR10/95-GC5 (Ehlert et al., 2011). Solid line indicates the pathway of the ITF. Dashed lines show the direction of South Java Current (Sprintall et al., 2010) and South Equatorial Current (SEC).

3. Materials and Methods

3.1. Sediment cores GeoB 10042-1 and GeoB 10043-3

The two gravity cores GeoB 10042-1 (7°06.81'S 104° 38.58'E, 2454 m water depth, core length: 540 cm) and GeoB 10043-3 (7°18.57'S 105°03.53'E, 2171 m water depth, core length: 390 cm) were collected from west of the Sunda Strait during the SO-184 field campaign with the German RV SONNE in 2005 (Fig. 1; Hebbeln et al., 2005). Both cores consist of

nannofossil ooze. A small turbidite layer is observed in GeoB 10043-3 at a depth of 225–232 cm.

3.2. Age Model

The age model for both cores is based on radiocarbon dating of the surface-dwelling planktic foraminifera species *Globigerinoides ruber* sensu stricto (s.s.) and *Globigerinoides sacculifer* (without the sac-like final chamber) from the >150 μm fraction. Details on the datings are published in Setiawan et al. (2015).

3.3. Neodymium and strontium isotope analyses

3.3.1. Neodymium extraction from mixed planktonic foraminifera

In order to reconstruct the bottom water Nd isotopic composition (ε_{Nd}), approximately 20 to 75 mg of mixed planktic foraminifera tests >250 μm were hand picked. Tests were then gently cracked using two glass plates and any visible contaminant grains removed. Samples were then treated with ultrasonication repeatedly in de-ionized water and once with methanol to remove clays and silicate particles. After that, organic matter was removed by oxidation using a hot H_2O_2–NaOH solution. A reductive solution of hydrazine was applied to remove ferromanganese oxide. The samples were then dissolved in dilute nitric acid (<0.5M HNO_3). A few larger samples were split into 2 aliquots and one was reductively cleaned following Vance et al. (2004) adapted from Boyle (1981). The dissolved samples were then centrifuged and the supernatant was immediately siphoned off to prevent the leaching of remaining phases. Then, the supernatant was dried and re-dissolved in 1 ml 2% nitric acid, a small aliquot taken for elemental analysis and the remainder purified for Nd isotope analysis.

3.3.2. Neodymium and Strontium extraction from detrital fraction

We also analyze detrital ε_{Nd} to investigate the sediment provenance of cores GeoB 10042-1 and 10043-3. Briefly, in order to remove carbonate, the freeze-dried and homogenized sediment

samples were leached using 25% (v/v) acetic acid and 0.02 M hydroxylamine hydrochloride (HH). The leached sediment was then digested in closed PTFE vessels. The samples and the certified standard BCR-2 (50 mg) as well as a blank were treated with 1 mL HNO_3 over night to oxidize any organic matter. After that 2 mL HF and 2 mL $HClO_4$ were added and the vessels were closed and heated in an oven for 12 h at 180°C. All acids were of suprapure quality. After digestion acids were evaporated on a heated metal block (180°C), residues were redissolved and fumed off three times with 3 mL half-concentrated HCl, and finally taken up in 1N HNO_3.

3.3.3. Column chromatography and isotope measurement

We applied a two-step ion chromatography to separate Nd and Sr from other elements using AG50W-X12 resin. Then, Nd and Sr were purified using Eichorm Ln Spec resin and Sr Spec resin, respectively. Nd isotope measurements were performed using a Nu plasma MC-ICPMS at GEOMAR and a Neptune Plus MC-ICPMS at the Institute for Chemistry and Biology of the Marine Environment (ICBM), University of Oldenburg, Germany. Sr isotopes were measured at ICBM. For instrumental mass bias, the measured $^{143}Nd/^{144}Nd$ ratios were corrected to a $^{146}Nd/^{144}Nd$ ratio of 0.7219 and normalized to the accepted $^{143}Nd/^{144}Nd$ of 0.512115 for the JNdi-1 standard (Tanaka et al., 2000). Measured $^{87}Sr/^{86}Sr$ ratios were mass bias corrected with $^{86}Sr/^{88}Sr$ of 0.1194 and were normalized to the widely accepted value of 0.710245 (NIST NBS987). The external reproducibility (2σ) of the $^{143}Nd/^{144}Nd$ at GEOMAR was between 0.3 and 0.6 ε_{Nd} units, while at ICBM was between 0.2 and 0.3 ε_{Nd} units. The 2σ of $^{87}Sr/^{86}Sr$ measurement at ICBM ranged between 0.00001 and 0.00002 (Table 2).

4. Results

4.1. Neodymium Isotope Composition of Mixed Planktic Foraminifera

The mixed planktic foraminifera ε_{Nd} has been shown in numerous settings to reliably record the isotopic composition of bottom waters (Roberts et al., 2012; Piowtroski et al.,2012; Kraft et al.,

2013; Molina-Kescher et al., 2014). The foraminifera ε_{Nd} of core GeoB 10043-3 shows a distinct change from the glacial to the Holocene (Fig. 2 and Table 1). During the last glacial, the foraminifera ε_{Nd} along the Sumatra-Java continental margin exhibits more radiogenic ε_{Nd} values ($-3.0<\varepsilon_{Nd}<-2.0$) compared to the mid-late Holocene (past 5 kyr B.P.; $\varepsilon_{Nd} < -3.0$). Interestingly, the foraminifera ε_{Nd} values were rather stable at around -3.8 through the past ~2.4 kyr.

4.2. Neodymium and Strontium Isotope Composition of the Detrital Silicates

In general, the Nd isotopic compositions (ε_{Nd}) of detrital silicate of cores GeoB 10042-1 and GeoB 10043-3 demonstrate similar trend compared to detrital $^{87}Sr/^{86}Sr$ (Fig. 2). The detrital ε_{Nd} values in both cores are more radiogenic during the last glacial, with average ε_{Nd} of -3.2 and -4.3 respectively for GeoB 10042-1 and GeoB 10043-3. While during the Holocene, the average detrital ε_{Nd} are -5.3 (GeoB 10042-1) and -6.6 (GeoB 10043-3). The late Holocene period in both cores is marked by the least radiogenic ε_{Nd} values.

During the past 22 kyr the variability of detrital $^{87}Sr/^{86}Sr$ of both cores ranges from more radiogenic values (0.715) during the Holocene to less radiogenic (0.707) during the last glacial (Fig. 2c). However, there is a disagreement in the late Holocene value where detrital $^{87}Sr/^{86}Sr$ of GeoB 10043-3 indicates unradiogenic value of 0.707.

Table 1. Measurement results of foraminifera ε_{Nd}.

Depth (cm)	Age (kyr)	Foraminifera ε_{Nd} (Non Red; Kiel)	2σ	Foraminifera ε_{Nd} (Red; Oldenburg)	2σ	Foraminifera ε_{Nd} (Non Red; Oldenburg)	2σ
18	0,21	-3,8	0,2				
23	0,62	-3,9	0,2			-3,2	0,3
28	1,02	-3,8	0,2				
38	1,75	-3,8	0,2				
43	2,07	-3,8	0,2				
48	2,36	-3,8	0,2				
53	2,57	-3,4	0,2				
58	2,79	-3,6	0,2				
63	3,00	-3,8	0,2				
68	3,23	-3,7	0,2				
73	3,47	-4,3	0,2				
78	3,69	-3,4	0,2				
83	3,92	-3,0	0,2				
88	4,15	-3,9	0,2				
93	4,37	-3,1	0,2				
98	4,60	-3,4	0,2				
103	4,84	-3,6	0,2				
108	5,06	-3,1	0,2				
113	5,28	-3,5	0,2				
118	5,51	-3,3	0,2				
123	5,73	-2,9	0,2				
128	5,96	-3,4	0,2				
133	6,20					-3,0	0,2
138	6,42	-3,1	0,2				
148	6,86	-2,7	0,2				
153	7,06	-3,2	0,2				
158	7,22	-2,9	0,2				
168	7,60	-3,0	0,2				
173	7,79					-2,3	0,0
183	8,19	-2,5	0,2				
188	8,39	-2,8	0,2				
193	8,57	-2,4	0,2				
198	8,76	-2,6	0,2				
208	9,15	-2,9	0,2				
238	11,61	-2,4	0,2				
243	12,12	-2,3	0,2				
253	13,14	-2,2	0,2				
258	13,66	-2,5	0,2				
263	14,17					-2,4	0,7
268	14,68	-2,2	0,2	-2,2	0,2		
273	15,19	-2,4	0,2	-1,9	0,3	-2,1	0,1
283	16,14	-2,5	0,2			-2,0	0,1
288	16,69	-2,7	0,2				
303	18,28	-3,0	0,2				
308	19,00	-2,9	0,2				

Table 2. Measurement results of detrital ε_{Nd} and detrital $^{87}Sr/^{86}Sr$

Core	Depth (cm)	Age (kyr)	Detrital ε_{Nd}	2σ	Detrital $^{87}Sr/^{86}Sr$	2σ
GeoB 10042-1	23	4,64	-7,1	0,3	0,715870247	1,6665E-05
	208	9,19	-5,9	0,2	0,713071058	1,0973E-05
	228	9,84	-4,7	0,3	0,711154846	1,6665E-05
	233	10,00	-3,5	0,3	0,709561295	1,6665E-05
	238	13,24	-2,8	0,3	0,708241799	1,6665E-05
	243	14,70	-1,9	0,2	0,707054116	1,6665E-05
	258	15,68	-0,9	0,2	0,707455004	1,6665E-05
	268	16,37	-4,5	0,3	0,709658037	1,6665E-05
	313	20,47	-4,5	0,3	0,709920532	1,6665E-05
	328	21,74	-4,4	0,2	0,709238038	1,6665E-05
GeoB 10043-3	78	3,69	-6,6	0,3	0,707648598	1,6665E-05
	243	12,12	-4,6	0,3	0,710482993	1,6665E-05
	248	12,63	-4,1	0,2	0,710590855	1,6665E-05
	258	13,66	-4,8	0,3	0,711115735	1,6665E-05
	263	14,17	-5,3	0,3	0,712181092	1,0973E-05
	278	15,63	-3,1	0,3	0,70795216	1,0973E-05
	288	16,69	-4,7	0,2	0,709801962	1,0973E-05
	318	20,80	-3,2	0,3	0,70776255	1,6665E-05

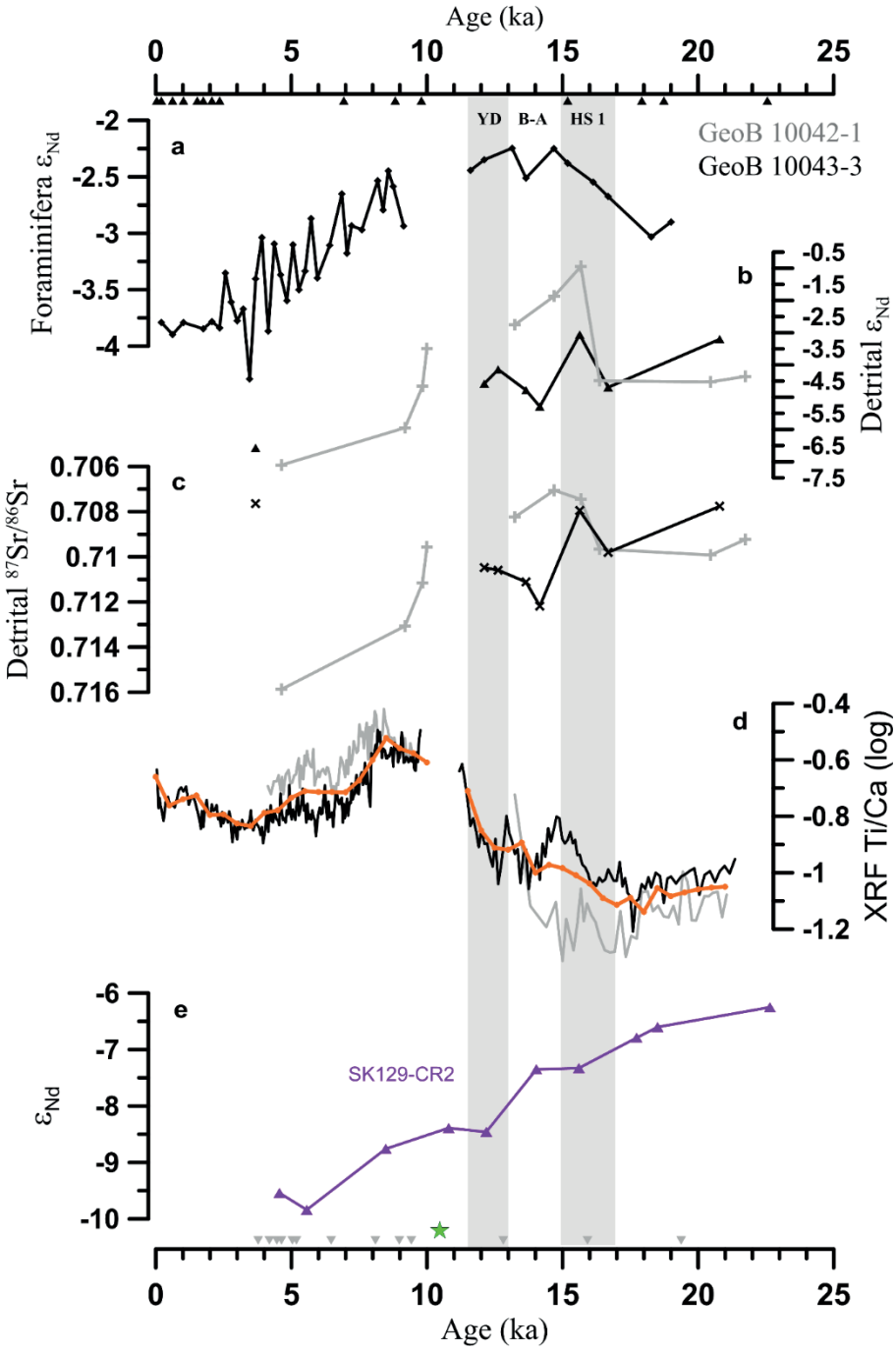

Fig. 2. (a) Foraminifera ε_{Nd} of GeoB 10043-3. (b) Detrital ε_{Nd} of GeoB 10042-1 (grey) and GeoB 10043-3 (black). (c) Detrital $^{87}Sr/^{86}Sr$ of GeoB 10042-1 (grey) and GeoB 10043-3 (black). (d) XRF Ti/Ca (logarithmic scale) of GeoB 10042-1 (grey) and GeoB 10043-3 (black) and its spliced record (orange) (according to Setiawan et al., 2015). ε_{Nd} of Fe–Mn leachates at 3800 m (Piotrowski et al., 2009). The data gap around 10 kyr B.P. in (a) to (d) is due to a hiatus (GeoB 10042-1) and a turbidite, (GeoB 10043-3 that have been observed (Setiawan et al., 2015).

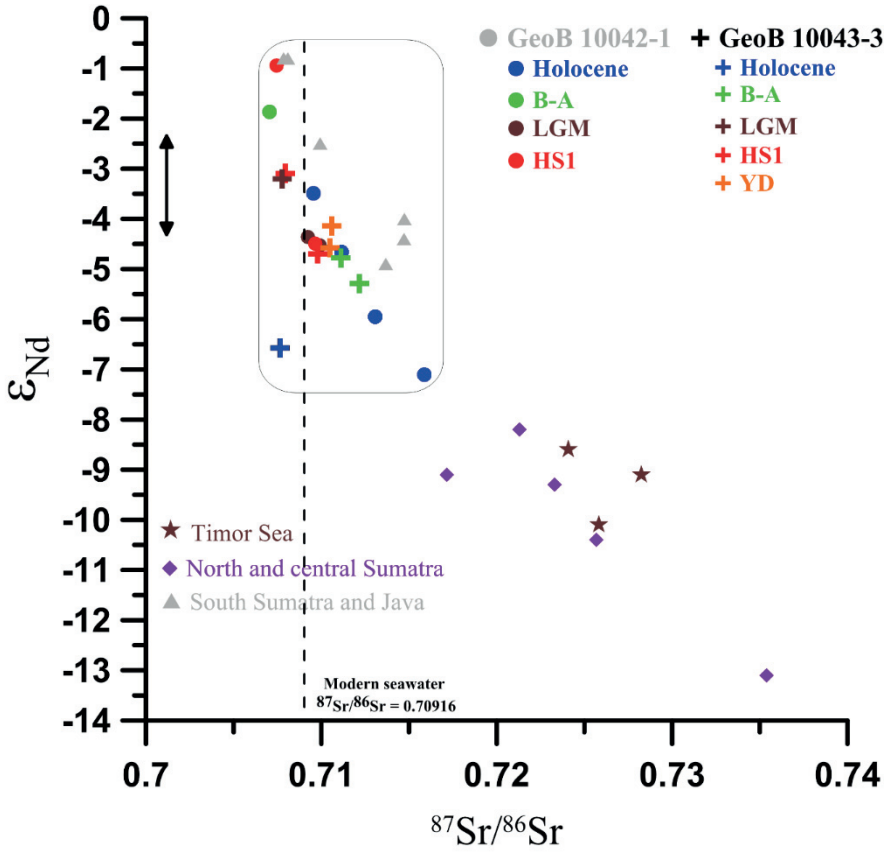

Fig. 3. Detrital ε_{Nd} versus $^{87}Sr/^{86}Sr$ of cores GeoB 10042-1 (dots) and GeoB 10043-3 (crosses) and of surface sediment samples collected along north and central Sumatra, south Sumatra and Java, and in the Timor Sea (Ehlert et al., 2011).

5. Discussion

5.1. Modification of the foraminifera ε_{Nd} off the Sunda Strait

Our foraminifera ε_{Nd} data from the ETIO off the Sunda Strait exhibit significant variability during the past 19 kyr (Fig. 2a). In contrast, during the past ~2.4 kyr foraminifera ε_{Nd} values show less variable with an average ε_{Nd} value of -3.8. This present day ε_{Nd} value is within the range for the measured seawater ε_{Nd} values at a depth between 450 m and 1500 m nearby our core location (St. 20 in Fig. 1; Table 3) and is within the range for the modern Indonesian Intermediate Water (IIW; $-3.8<\varepsilon_{Nd}<-5.2$) (Jeandel et al., 1998). Below 2000 m to the bottom the seawater ε_{Nd} values range between $\varepsilon_{Nd} = -6.0$ and $\varepsilon_{Nd} = -7.3$. As the studied area is an active

upwelling region, we hypothesize that the deep waters (upper IDW) at our core site (2171 m) acquired the radiogenic isotope signatures from the surface and intermediate waters through vertical transport of particles. We further hypothesize that sinking particles not only adsorbed the dissolved Nd isotope composition of the intermediate water and but also released the Nd. In the end it will influence the Nd isotope composition of deep waters. It is unlikely that the source for the radiogenic seawater ε_{Nd} at depth of 2171 m is from a Nd release from seafloor sediments or pore waters (e.g. Elderfield and Sholkovitz, 1987) as the seawater ε_{Nd} values below our core (depths > 2400 m) show less radiogenic values ranging from -7.1 to -6.0 (St. 20 in Fig. 1; Table 3). In addition, the increase of Nd concentration with depth at St. 20 (Fig. 1; Table 3) suggests that . Furthermore, less variable in the foraminifera ε_{Nd} values during the past ~2.4 kyr suggests no alteration of the bottom waters at our core site.

During the period between ~18 and ~15 kyr foraminifera ε_{Nd} data show an uninterrupted increase trend from ε_{Nd} = -3.0 to ε_{Nd} = -2.2. The high radiogenic ε_{Nd} values are observed during this period compared to modern ε_{Nd} value. The average ε_{Nd} during this period is -2.5, and is offset 1.3 ε_{Nd} unit from the modern ε_{Nd} value of the upper IDW (ε_{Nd} = -3.8). Interestingly, these last glacial values are in good accordance with the water column ε_{Nd} data from the Sumba Strait (St. 49 in Fig. 1; Jeandel et al., 1998). In accordance with this observation, the flow of cool, fresh thermocline ITF has been suggested to intensify during the last deglaciation (see Holbourn et al., 2011 for details). Therefore it is plausible that the radiogenic seawater ε_{Nd} of the Sumba Strait may have been transported by a smooth increase of the ITF flow reaching our core and our foraminifera recorded this ε_{Nd} signature. As a result, during the last glacial the ε_{Nd} of bottom water at our core site resembles the intermediate depth of seawater ε_{Nd} of the Sumba Strait. In addition, enhanced intensity in the thermocline ITF flow closely relates to enhanced NW monsoon in Indonesia (Gordon et al., 2003). The presence of fresher Java Sea water at the southern Makassar Strait during the NW monsoon prohibited the transport of warm, saltier

surface ITF flow. As a consequence, sea surface of the ETIO off southern Indonesia is cool and fresh (Song and Gordon, 2004).

Table 3. Seawater ε_{Nd} of the eastern Indian Ocean (Jeandel et al., 1998).

Station	Latitude (°N)	Longitude (°E)	water depth (m)	ε_{Nd}	2σ
10	-16,3	117,366667	104	-5,3	0,2
	-16,3	117,366667	180	-5,2	0,4
	-16,3	117,366667	402	-4,8	0,3
	-16,3	117,366667	700	-4,8	0,2
	-16,3	117,366667	999	-5,3	0,6
	-16,3	117,366667	1999	-5	0,2
	-16,3	117,366667	3003	-6,1	0,2
20	-11,5	115,95	59	-4,5	0,5
	-11,5	115,95	99	-3,4	0,5
	-11,5	115,95	200	-2,9	0,4
	-11,5	115,95	452	-3,7	0,4
	-11,5	115,95	701	-3,6	0,3
	-11,5	115,95	1099	-3,6	0,3
	-11,5	115,95	1501	-3,8	0,3
	-11,5	115,95	2499	-6	0,3
	-11,5	115,95	3000	-6,1	0,2
	-11,5	115,95	5000	-7,3	0,2
	-11,5	115,95	5353	-7,1	0,2
49	-9	123	500	-2,8	0,2
	-9	123	546	-2,8	0,3
	-9	123	600	-2,2	0,2
	-9	123	791	-2,5	0,2

During the period between ~7.7 and ~2.6 kyr, the ε_{Nd} value of upper IDW at our core site is modified. As shown in Fig. 2a, our foraminera ε_{Nd} values demonstrate a gradual change from ε_{Nd} = -2.3 (7.7 kyr) to ε_{Nd} = -3.4 (2.6 kyr). The average ε_{Nd} during this period is -3.3, 0.5 ε_{Nd} unit offset from the present-day value of the upper IDW (ε_{Nd} = -3.8). We postulate that the general trend of the decreased foraminera ε_{Nd} values may reflect the reduced contribution of the intermediate waters of the Sumba Strait at our core site. The foraminera ε_{Nd} values also exhibit high variability during this period. We hypothesize that this variability might be a result of an

additional terrigenous input from the Sunda Shelf. According to our previous study (Setiawan et al., 2015), the final (or full) opening of the Sunda Strait occurred at ~10 kyr. The Ti/Ca record provides evidence of this opening during the last deglaciation that clearly shows a prominent change in the terrigenous material supply associated with the rapid sea level rise on the Sunda Shelf between 11 and 9.5 kyr (Fig. 2d). The sharp increase in Ti/Ca during this period suggests a massive supply of terrigenous material from the formerly exposed Sunda Shelf towards our core sites via the Sunda Strait that corresponds to the inundation of inner Sunda Shelf region at ~10.8 kyr BP, resulted a turbidite layer in core GeoB 10043-3 and a hiatus in core GeoB 10042-1. When the terrigenous material sinks to the bottom, it released Nd and changed the Nd isotopic composition of the deep water off the Sunda Strait.

In order to investigate the influence other water masses of the Indian Ocean, we compare our foraminifera ε_{Nd} to Nd isotopes of Fe–Mn leachates from the equatorial Indian Ocean (3800 m) (Piotrowski et al., 2009). Piotrowski et al. (2009) provides insight into glacial-interglacial evolution of the bottom water ε_{Nd} of the equatorial Indian Ocean, although the evidence is lacking during the late Holocene (Fig. 2e). In brief, Piotrowski et al. (2009) suggest that more Atlantic waters reaching the Indian Ocean during the Holocene than the last glacial. This suggestion is based on the observation that shows the identical ε_{Nd} values in magnitude and direction between the deep central Indian Ocean (SK129-CR2) and the South Atlantic deep Cape Basin (RC11-83/TNO57-21) during glacial-interglacial timescales, with ε_{Nd} variability between -6 (Glacial) and -9.5 (Holocene). They hypothesized that this similarity is an indication of the North Atlantic Deep Water (NADW) propagation into the Indian Ocean via the Southern Ocean, more specifically more (less) NADW waters reaching the Indian Ocean during the Holocene (the last glacial). However, a pronounced lack of correspondence between our ε_{Nd} record and the equatorial Indian Ocean ε_{Nd} record during the past 19 kyr suggests that our ε_{Nd} record represents regional hydrography without any significant influence from deep-water

circulation of the Indian Ocean. Indeed, our new results suggest that ε_{Nd} of authigenic coatings of planktic foraminifera at 2171 m is sensitive to the ITF thermocline flow.

5.2. Variability of the detrital ε_{Nd} off the Sunda Strait

In order to investigate changes in the sediment provenance, we compare our detrital ε_{Nd} and $^{87}Sr/^{86}Sr$ data to the previously published ε_{Nd} and $^{87}Sr/^{86}Sr$ data from the region. As shown in Fig. 3, the distribution of our detrital ε_{Nd} and $^{87}Sr/^{86}Sr$ values is within the range as the detrital clay-size fractions of core top sediments off southern Sumatra and Java (Ehlert et al., 2011), except for the late Holocene. Our detrital ε_{Nd} and $^{87}Sr/^{86}Sr$ values vary between -4.9 and -0.8 and between 0.707 and 0.715, respectively. Within the ETIO there is a distinct isotopic signature between southern Sumatra/Java (gray triangles) and northern and central Sumatra (purple diamonds and black dots), Timor Sea (brown stars), and northeast Australia (pink triangles). Based on the clay-sized detrital ε_{Nd} and $^{87}Sr/^{86}Sr$, Ehlert et al. (2011) suggest there is only one sedimentary province for the radiogenic ε_{Nd} values and less radiogenic $^{87}Sr/^{86}Sr$ in the Indonesian Archipelago. In the southern Indonesia, this province covers the south Sumatra-Java-Lesser Sunda Island chain region, whereas in the northern site it covers the Java Sea, Makassar Strait, and Banda Sea. From this observation and considering that our study area is strongly influenced by the Australian-Indonesian Monsoon system, we suggest that the source for the radiogenic detrital ε_{Nd} in our cores is possibly either from the sediments of the Sunda Arc volcanics continental margin off south Sumatra and Java or from the Java Island. This region as well as the Indonesian islands mainly consist of Tertiary to Quaternary volcanic rocks (Vroon et al., 1995) and has been recognized as a source for the radiogenic ε_{Nd} value (Jeandel et al., 1998; Lacan and Jeandel, 2005; Frank et al., 2006).

Ehlert et al. (2011) show that off south Java is characterized by more radiogenic clay-sized detrital ε_{Nd} values ranging from -0.8 to 0.7 (Fig. 1). Whereas off Sumatra is characterized by less radiogenic clay-sized detrital ε_{Nd} values ranging from -13.1 to -2.5. Nearby the Sunda Strait,

the values of the clay-sized detrital ε_{Nd} are -4.0 and -4.4. These values are in good agreement with the average value of the detrital ε_{Nd} of cores GeoB 10042-1 and GeoB 10043-3 during the LGM (ε_{Nd}= -4.0), suggesting the same sediment provenance possibly from the continental margin off south Sumatra and Java. During the HS 1 our detrital ε_{Nd} values altered. A significant change in the detrital ε_{Nd} value (from -4.5 to -0.9) is observed in core GeoB 10042-1. We postulate that this radiogenic detrital sediment (detrital ε_{Nd} = -0.9) probably originated from south Java and transported to our core by deep currents, possibly by a strong ITF flow at deeper depths. The deepest exit portal of the ITF in the eastern Indian Ocean is via Timor Passage (1250 m eastern sill depth at the Leti Strait and 1890 m at the western end). Thus, it is possible that during the HS 1 the detrital sediments off Java were transported to core GeoB 10042-1 by a strong ITF flow at ~1900 m. It is likely that the elevated ITF flow during the HS 1 occurred not only at the thermocline depth (see section 5.1) but also at ~1900 m depth.

Detrital sediments can also be delivered to our cores via wind. Grain-size analyses from off south Java suggest that sediments deposited during the HS 1 contain coarser terrigenous components, suggesting an eolian source of the terrigenous sediment fraction (Mohtadi et al., 2011). Therefore it is also possible that the more radiogenic detrital ε_{Nd} value (-0.9) in GeoB 10042-1 during the HS 1 was a result of wind transport, possibly from the Java Island. For both hypotheses we speculate that much of the detrital sediments were deposited at core GeoB 10042-1 as the change in the GeoB 10043-3 detrital ε_{Nd} value is not robust. We further postulate that it is unlikely that the radiogenic detrital ε_{Nd} was transported to our cores through river runoff as the model simulations and marine sediment proxies suggest that the ETIO experienced reduced rainfall and warmer conditions during the HS 1 as a consequence of southward migration of the ITCZ (Gibbons et al., 2014; Mohtadi et al., 2014).

During the Holocene the detrital ε_{Nd} and detrital $^{87}Sr/^{86}Sr$ values of GeoB 10042-1 show a prominent change (from -3.5 to -7.1 ε_{Nd} units and from 0.709 to 0.715), indicating a change in

the provenance of the sediment. In addition, the Holocene detrital ε_{Nd} value of GeoB 10043-3 also indicates an unradiogenic value (-6.6) compared to the last glacial. We suggest that a sharp change in the sediment provenance at our cores was triggered by the opening of the Sunda Strait at ~10 kyr (see section 5.1). As indicated in Fig. 2d, the transported sediments into our cores presumably contained unradiogenic detrital ε_{Nd}, possibly from Sumatra (Ehlert et al., 2011), and hence resulted less radiogenic detrital ε_{Nd} values. However, we cannot unambiguously explain an offset in the $^{87}Sr/^{86}Sr$ value of GeoB 10043-3 during the Holocene. During this period the $^{87}Sr/^{86}Sr$ value of GeoB 10043-3 indicates unradiogenic value (0.707).

6. Conclusion

We have investigated the modification of bottom water ε_{Nd} in the eastern tropical Indian Ocean off the Sunda Strait. Our foraminifera ε_{Nd} suggests no alteration of the bottom waters (2171 m) during the past ~2.4 kyr. Furthermore our new ε_{Nd} data show that pronounced modifications of the bottom water at our core site occurred during the period between ~7.7 and ~2.6 kyr and during the last deglaciation as consequences of a strong- and a weak thermocline ITF flow, respectively. Our detrital ε_{Nd} and detrital $^{87}Sr/^{86}Sr$ values are also in good agreement with the core top clay-sized detrital ε_{Nd} and $^{87}Sr/^{86}Sr$ values from south Sumatra and Java, suggesting that the source for the radiogenic detrital ε_{Nd} in our cores is presumably from the sediments of the Sunda Arc volcanics continental margin off south Sumatra and Java. Moreover we postulate that a sharp change in the detrital ε_{Nd} (GeoB 10042-1) off the Sunda Strait during the HS 1 might reflect stronger ITF flow at a depth of ~1900 m. Meanwhile, variability of the detrital ε_{Nd} during the Holocene indicates a prominent change in the provenance of the sediment. The XRF Ti/Ca ratio data suggest that the opening of the Sunda Strait at ~10 kyr B.P. might be responsible for the changes in the sediment provenance during this period.

Acknowledgments

We are grateful to M. Schulz and P. Böning for technical assistance. R.Y. Setiawan acknowledges financial support from the Deutscher Akademischer Austauschdienst (DAAD grant A/10/7596). This study was supported by the German Ministry of Education and Research (project PABESIA) and the Deutsche Forschungsgemeinschaft (DFG grant HE3412/15-1). The data of this study are archived and can be retrieved at PANGAEA (www.pangaea.de).

6. Testing the applicability of *G. sacculifer* Ba/Ca as an indicator of freshwater discharge in the eastern tropical Indian Ocean

R. Y. Setiawan, M. Mohtadi, J. Groeneveld, S. Steinke, H. Kuhnert, D. Hebbeln

Technical Report

Abstract

The Ba/Ca ratio of planktic foraminifera carbonate serves as a new geochemical proxy for seawater Ba/Ca and thus providing information on modern and past salinity and freshwater discharge. In this study we have investigated the applicability of Ba/Ca ratio of core-top *G. sacculifer* collected from the eastern tropical Indian Ocean (ETIO) for paleoceanographic reconstructions. In doing so, we conducted a series of cleaning experiments for Ba/Ca extraction by using different reductive solutions. Our new results suggest that the Ba/Ca ratio of *G. sacculifer* cannot be utilized as a tracer for modern and past salinity changes in the ETIO region off the Sunda Strait. We suggest that the existence of seasonal upwelling adds an additional signal to the seawater Ba/Ca in the ETIO, and thus complicates the interpretation of *G. sacculifer* Ba/Ca as a freshwater tracer. Moreover, our cleaning experiment results show that the cleaning protocol of Barker et al. (2003), DTPA, and hydroxylamine can be used to extract valuable Ba/Ca ratios from planktic foraminifera shells.

1. Introduction

Ba/Ca ratios of planktic foraminifera have been used to trace modern and past salinity changes (Bahr et al., 2013; Saraswat et al, 2013; Schmidt and Lynch-Stieglitz, 2011; Weldeab et al., 2007; Hall and Chan, 2004). The main reason to use this ratio is that Ba/Ca ratio in foraminiferal shells reflects the seawater barium (Ba) concentration as the Ba concentration in estuarine/coastal settings is elevated relative to the open ocean and inversely correlated with salinity (Lea and Spero, 1994). In addition, the incorporation of Ba into foraminifera shells is independent of temperature, salinity, pH, and symbiont photosynthesis (Hönisch et al., 2011; Lea and Spero, 1994; 1992), thus, making it a seemingly well suited salinity indicator. Ba is supplied to the oceans through riverine input (Edmond et al., 1979; Shaw et al., 1998; Hanor,

2000) and hydrothermal vents (von Damm et al., 1985; Elderfield and Schultz, 1996). The mineral barite ($BaSO_4$) has been suggested as the primary carrier of particulate Ba in the water column (Dehairs et al., 1980; Bishop, 1988; Dymond et al., 1992) and it precipitates in the water column, on the sea floor and within marine sediments (Griffith and Paytan, 2012). Within the water column the euphotic zone is typically enriched in particulate Ba compared to the deep ocean (Dehairs et al., 1980; Collier and Edmond, 1984) and the enrichment is associated with the oxygen minimum zone (Paytan and Griffith, 2007). Therefore upwelling regions usually contain high Ba concentrations what possibly also can influence the Ba/Ca ratio of planktic foraminifera (Saraswat et al, 2013).

Ba/Ca ratios extracted from foraminiferal shells can be biased by contaminant phases such as clay minerals, organic matter, or ferromanganese coatings. Hence, the removal of those contaminants requires a multiple step cleaning procedure of the samples. Commonly two different cleaning methods to extract reliable Ba/Ca ratio from foraminifera shells are used (Bahr et al., 2013; Schmidt and Lynch-Stieglitz, 2011; Weldeab et al., 2007; Martin and Lea, 2002; Lea and Boyle, 1991). The major difference between these two methods is in the use of an additional step using diethylenetriamine-pentaacetic acid (DTPA) (Martin and Lea, 2002; Lea and Boyle, 1993; 1991). DTPA has been suggested to effectively remove sedimentary barite that associated with shells, a potential source of contamination (Lea and Boyle, 1993; 1991). However, Martin and Lea (2002) also suggest that the effect of employing reductive and DTPA cleanings might bias the measured Mg/Ca, Cd/Ca, Ba/Ca, and Mn/Ca ratios on two different benthic species show inconsistent results. On the other hand other authors (Bahr et al., 2013; Schmidt and Lynch-Stieglitz, 2011; Weldeab et al., 2007) have omitted the DTPA cleaning step due to its corrosiveness that can cause shell dissolution. In the perspective of foraminifera cleaning, another cleaning protocol proposed by Barker et al. (2003) to clean foraminifera for Mg/Ca measurements has been widely used is. According to their cleaning

experiments, a reductive cleaning step systematically lowered the foraminifera Mg/Ca ratio by 10-15%. Thus their proposed cleaning method for foraminifera does not include a reductive step. Nonetheless, this finding contrasted the study of Martin and Lea (2002) that suggested that a reductive step does not reduce the values of the Mg/Ca ratio in foraminifera.

Here, for the first time, we examine the applicability of Ba/Ca ratio of planktic foraminifera *G. sacculifer* as a tracer for freshwater discharge in the region of eastern tropical Indian Ocean (ETIO) off the Sunda Strait. In this study we also conducted a set of cleaning experiments on ten surface sediment samples collected from off Sumatra to constrain the most suitable cleaning method for the analysis of Ba/Ca in planktic foraminifera. This region is particularly appropriate to address this issue as there is a persistent advection of low salinity Java Sea waters into the investigated area. However, our new data suggest that *G. sacculifer* Ba/Ca ratios cannot be used to trace freshwater discharge into the ETIO.

2. Study Area

Surface sediment samples used in the present study have been collected from the eastern tropical Indian Ocean (ETIO) off Sumatra (Fig. 1). Today, the ETIO is a region where precipitation (P) exceeds over evaporation (E) (Hendon, 2003). Qu et al. (2005) suggest that the rainy season over ETIO region off southern Sumatra is principally linked to the northwest monsoon (NWM) (December-February) season due to the southward progression of the Intertropical Convergence Zone (ITCZ). During this season the winds blow from the Eurasian continent, pass the South China Sea and the Bay of Bengal, carrying large amounts of moisture to Indonesia and causing heavy rainfall over the region (Gordon, 2005; Qu et al., 2005). In contrast, the dry season is associated with the southeast monsoon (SEM) (June-August) season (Aldrian and Susanto, 2003; Hendon, 2003). During the SEM season the southeasterly winds carry warm and dry air from Australia that also generate coastal upwelling along the south coasts of the Java-Lesser Sunda Island chain (Susanto et al., 2001). This upwelling only occurs

during the southeast monsoon season and has been suggested to enhance chlorophyll a concentration (Hendiarti et al., 2004; Susanto and Marra, 2005) as well as pelagic fish catch (Hendiarti et al., 2005) in the region off south Java.

Modern oceanography shows a persistent advection of low-salinity Java Sea waters into the ETIO via the Sunda Strait. Together with runoff from Java and Sumatra, this freshwater advection is responsible for the low-salinity ‘‘tongue’’ (32‰) in the ETIO of the Sunda Strait (Gingele et al., 2002; Ding et al., 2006). Furthermore, this freshwater discharge has been suggested to generate a maximum transport of suspended material during the transition phase between the rainy and dry seasons (March and April) (Hendiarti et al., 2004).

3. Materials and Methods

3.1. Surface sediments samples

A total of 69 surface sediment samples were collected from the ETIO off western and southern Indonesia during the expeditions of RV SONNE 184 and 189 in 2005 and 2006, respectively (Hebbeln et al., 2005; Wiedicke-Hombach et al., 2007). In the present study we only analyzed 10 surface sediment samples from off western and southern Sumatra. The locations and detailed information of the investigated surface samples are presented in Fig. 1 and Table 1 (supplementary material).

3.2. Cleaning of foraminifera shells

We used *Globigerinoides sacculifer* (without sac) from 10 surface sediment samples in order to test the effect of reductive cleaning solution on the Ba/Ca ratio (Table 1; supplementary material). For each surface sediment sample approximately 30-40 individuals of *G. sacculifer* were picked from the 250-355 μm size fraction and then were gently cracked using glass plates.

Then, all shell fragments were split into five aliquots and these split aliquots were subjected to five different cleaning methods.

For the first aliquot we cleaned the tests of *G. sacculifer* using the cleaning procedure proposed by Barker et al. (2003) and we named it as a "Mg/Ca" cleaning. In brief, the samples were ultrasonically cleaned five times with de-ionized water and twice with distilled methanol to remove detrital and clay particles. Organic matter was oxidized by adding a NaOH-buffered 1%-H_2O_2 reagent to the samples and placed in a hot water bath for 10 minutes with a few seconds in an ultrasonic bath. After repeating this step, samples were rinsed and transferred into new acid-cleaned vials. Samples then underwent a weak acid leaching (0.001 M QD HNO_3) with 30 seconds ultrasonic treatment. Following this step, samples were dissolved using 0.075 M QD HNO_3, centrifuged for 10 minutes at 6000 rpm, transferred into new acid cleaned vials and diluted with water.

For another three aliquots we modified the cleaning procedure of Barker et al. (2003) by adding a reductive step after the oxidation step. In this reductive step we performed a set of experiments by employing two different reductive reagents, i.e. hydrazine and hydroxylamine, and DTPA (diethylene triamine penta-acetic acid). Each of the three aliquots received a different solution during this reductive treatment. The detailed composition of each reductive solution is given in Table 2. For experiments with hydrazine and hydroxylamine we added 100 µl of each solution into two aliquots, whereas for the DTPA only 50 µl was added to an aliquot. In the following step, these three samples were placed in a hot bath (~98 °C) for 30 minutes and were sonicated briefly every 2 minutes. After this step all reductive reagents and DTPA were removed and the samples were rinsed 3 times with de-ionized water. For the next steps, i.e. weak acid leaching and dissolution, we followed Barker et al. (2003).

Finally, for the last aliquot we purely cleaned the shells only using de-ionized water for all cleaning steps of Barker et al (2003).

Table 2. Detailed reductive solutions used in this study.

Reductive reagent	Composition	Reference
100 µL of buffered hydrazine solution	750 µL anhydrous hydrazine (NH_2NH_2) + ~0.5 N (~0.25 M) ammonium citrate ($C_6H_{17}N_3O_7$) + 10 mL concentrated (~30%) ammonium hydroxide (NH_4OH)	Martin and Lea (2002)
100 µL of hydroxylamine solution	0.2 M NH_2OH + 1 M CH_3COONa	Shen et al. (2001), Steinke et al. (2010)
50 µL of buffered DTPA (diethylene triamine penta-acetic acid)	0.01N (0.002 M) DTPA + 0.1N sodium hydroxide (NaOH)	Martin and Lea (2002)

3.3. Measurement

For the five different cleaning experiments *G. sacculifer* Ba/Ca ratios were measured using an Agilent 720 Inductively Coupled Plasma Optical Emission Spectrometer (ICP-OES) housed at the Department of Geosciences, University of Bremen. The Ba/Ca values are reported as µmol mol^{-1}. The instrumental precision during measurement was monitored by analysis of an in-house standard solution, which was measured after every fifth sample, as well as the ECRM 752-1 standard (Greaves et al., 2008). The average 1σ error for the Ba/Ca analyses on external standard and ECRM 752-1 standard are 0.02 µmol mol^{-1} and 0.1 µmol mol^{-1}, respectively. It is important to notice that we did not measure reproducibility due to insufficient sample material.

3.4. Calculation of seawater $\delta^{18}O$

All of the *G. sacculifer* Mg/Ca ratios of surface sediment samples used in this study have been measured by Mohtadi et al. (2011). According to Mohtadi et al. (2011) *G. sacculifer* data

represent mean annual mixed-layer conditions at ~50 m. In order to calculate the seawater $\delta^{18}O$ ($\delta^{18}O_{sw}$), we used the $\delta^{18}O$-temperature equation of Bemis et al. (1998):

$$T\ (°C) = 14.9 - 4.8\ (\delta^{18}O_{cc} - \delta^{18}O_{sw}) \qquad (2)$$

where $\delta^{18}O_{cc}$ and T are the measured $\delta^{18}O$ of calcite and Mg/Ca-based temperature, respectively. The values were then converted to Standard Mean Ocean Water (SMOW). The errors of the calculations of Mg/Ca-based temperature and $\delta^{18}O_{sw}$ are estimated by propagating the errors introduced by Mohtadi et al. (2014). The resulting errors for temperature and $\delta^{18}O_{sw}$ are on average 1°C and 0.23 ‰, respectively.

4. Results

4.1. Planktic foraminifera *G. sacculifer* element to calcium ratios

The results of Ba/Ca ratio measurements of five different cleaning protocols are given in Table 1 and shown in Fig. 1. In general most of the Ba/Ca ratio values of different cleaning methods show a consistent pattern. The *G. sacculifer* Ba/Ca ratio values cleaned with hydroxylamine and of Mg/Ca cleaning are always higher than Ba/Ca values cleaned with water. Whereas Ba/Ca values cleaned with hydrazine and DTPA are always lower than that cleaned with water.

For the Mg/Ca cleaning and the cleaning experiment with water the values of Ba/Ca ratio range between 1.59 and 7.60, and between 1.45 and 3.53 μmol mol^{-1}, respectively. Whereas for the cleaning experiment using reductive solutions (Table 2), the Ba/Ca ratio values vary between 1.28 and 73.39 μmol mol^{-1}. This extremely high value (73.39 μmol mol^{-1}) is found in the GeoB 10033-3 (cleaning experiment with hydrazine). Another high Ba/Ca ratio value (12.32 μmol mol^{-1}) is also appeared in GeoB 10042-2 (cleaning experiment with hydrazine).

Most of the values of *G. sacculifer* Al/Ca ratio are under detection limit (negative values). The Mn/Ca ratio values of *G. sacculifer* vary between 0.4 and 682.24 μmol mol^{-1}. Our results

revealed that there are only two surface sediment samples (GeoB 10033-3 and GeoB 10034-3) which have high Mn/Ca value > 100 μmol mol^{-1} (Table 1). For the Fe/Ca ratios, our data also show that most of the values are negative and only two surface sediment samples (GeoB 10038-3 and SO189-02MC) which have Fe/Ca ratio value > 100 μmol mol^{-1}. Overall, there is no significant correlation between these three element ratios and Ba/Ca ratio ($r^2 \leq 0.01$; not shown).

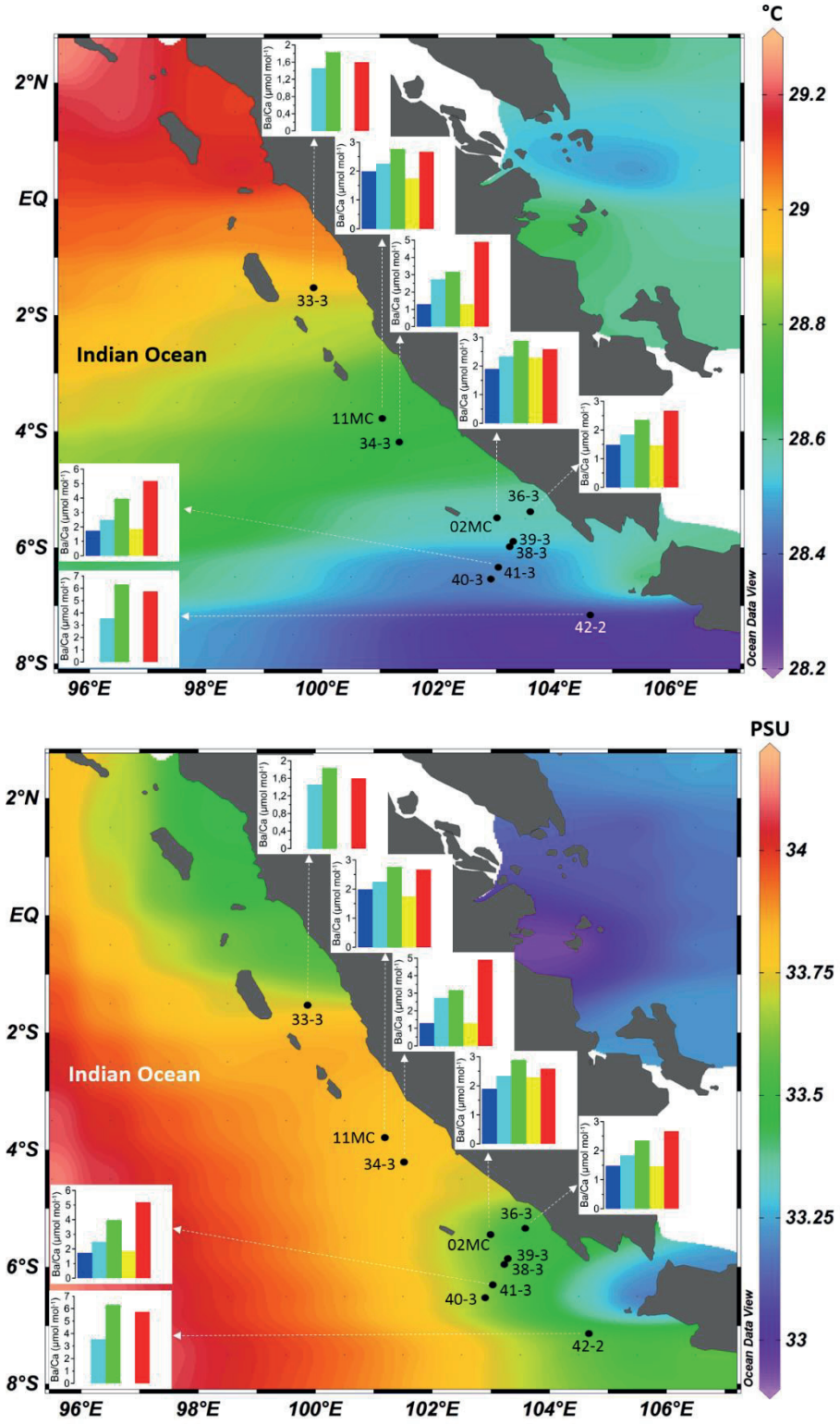

Fig. 1. Annual mean maps of (a) sea surface temperature (°C) (Locarnini et al., 2013) and (b) sea surface salinity (psu) (Zweng et al., 2013) obtained from the World Ocean Atlas 2013.

Black dots show the positions of surface sediment samples used in this study. Blue, cyan, green, yellow, and red bars are the values of Ba/Ca ratios resulted from cleaning experiments with hydrazine, water, hydroxylamine, DTPA, and of normal cleaning, respectively.

4.2. Planktic foraminifera *G. sacculifer* $\delta^{18}O_{sw}$

The $\delta^{18}O_{sw}$ values of *G. sacculifer* from all surface sediment samples used in this study range between 0.01 and 0.43 (‰ SMOW). The lowest and highest values are observed in GeoB 10036-3 and GeoB 10033-3, respectively.

5. Discussion

An issue in using elemental ratios as paleo-proxies is the possibility of contamination caused by silicate material during foraminifera cleaning (Barker et al., 2003) and/or post-depositional Mn-rich carbonate (Pena et al., 2005; 2008). Such contaminations can be assessed through Al/Ca ratio of foraminifera to detect silicate contamination and through Mn/Ca and Fe/Ca ratios to detect contamination by Mn-rich carbonate or early diagenetic ferromanganese oxides. We used the criteria of Ni et al. (2007) that suggests Al/Ca ratio of <100 μmol mol^{-1} indicates not contamination by silicates. We also used a threshold of Boyle (1983) and Boyle and Rosenthal (1996) that suggests that a Mn/Ca ratio of 100-150 μmol mol^{-1} is not contaminated by $MnCO_3$. Our data show that there are two surface sediment samples containing high Al/Ca ratio values, i.e. GeoB 10033-3 cleaned with hydrazine and GeoB 10038-3 of normal cleaning. In addition, Mn/Ca ratios of GeoB 10034-3 (normal cleaning and cleaned with water) also exhibit high values. Therefore we discarded the Ba/Ca ratio values of these samples when discussing our results. We also excluded all of the Ba/Ca ratio values of GeoB 10040-3 and GeoB 10039-3 as the values show an opposite trend compared to general pattern resulted from the experiments (see section 4.1).

Higher Fe/Ca ratio values are observed in cleaning experiment with hydroxylamine in GeoB 10038-3 and SO189-02MC. However, we assume that Ba/Ca analyses for these surface samples were unaffected by silicate contamination as the Al/Ca ratio values are under the detection limit of the ICP-OES. Overall, the elemental ratios of the contamination indicators (Mn/Ca and Fe/Ca ratios) suggest that our *G. sacculifer* Ba/Ca ratio can be used for further analyses.

5.1. Testing *G. sacculifer* Ba/Ca as a proxy for salinity

Although seawater Ba concentration for the investigated area is unknown, we examined the applicability of *G. sacculifer* Ba/Ca ratio as a proxy for paleo-salinity by comparing it to the *G. sacculifer* $\delta^{18}O_{sw}$ from the same surface sediment samples. Compared to GeoB 10033-3, GeoB 10034-3, and SO189-11MC, the positions of surface sediments GeoB 10036-3, GeoB 10038-3, GeoB 10039-3, GeoB 10041-3, GeoB 10042-2, and SO189-02MC are suitable for this investigation as these sediments geographically should be influenced by the transport of low salinity Java Sea water into the ETIO via the Sunda Strait (Fig. 1). This inference is in accordance with the observation (Table 1) that demonstrates the *G. sacculifer* $\delta^{18}O_{sw}$ values of GeoB 10033-3, GeoB 10034-3, and SO189-11MC are on average higher (0.23-0.43 ‰) compared to those located near the Sunda Strait (0.01-0.40 ‰). In addition, precipitation and runoff in Sumatra and Java are enhanced during NWM season, hence, we expect that the transported freshwater to the Sunda Strait is enriched in Ba.

In line with our expectation the average Ba/Ca ratio value of each different cleaning method for surface sediments located in the proximity of the Sunda Strait indicates slightly higher Ba/Ca ratio values compared to surface sediments located far from the Sunda Strait (Table 3), with an exception in Ba/Ca value cleaned with hydrazine that shows identical value. It is important to note here that we excluded Ba/Ca values of GeoB 10042-2 in this calculation. Even if we added this surface sample to the calculation, the yielded difference in the average Ba/Ca for two different locations becomes larger. Indeed, this finding strengthens our assumption that the

fresher Java Sea waters transported to the Sunda Strait are slightly enriched in Ba concentration. However, this observation may also lead to a suggestion that *G. sacculifer* Ba/Ca in the GeoB 10042-2 as well as *G. sacculifer* Ba/Ca of the surface samples close to the Sunda Strait are substantially affected by the upwelling and from the advection of fresher Java Sea waters.

In line with our expectation the average Ba/Ca ratio value of each different cleaning method for surface sediments located in the proximity of the Sunda Strait indicates slightly higher Ba/Ca ratio values compared to surface sediments located far from the Sunda Strait (Table 3), with an exception in Ba/Ca value cleaned with hydrazine that shows identical value. It is important to note here that we excluded Ba/Ca values of GeoB 10042-2 in this calculation. Even if we added this surface sample to the calculation, the yielded difference in the average Ba/Ca for two different locations becomes larger. Indeed, this finding strengthens our assumption that the fresher Java Sea waters transported to the Sunda Strait are slightly enriched in Ba concentration. However, this observation may also lead to a suggestion that *G. sacculifer* Ba/Ca in the GeoB 10042-2 as well as *G. sacculifer* Ba/Ca of the surface samples close to the Sunda Strait are substantially affected by the upwelling and from the advection of fresher Java Sea waters.

Table 3. Average Ba/Ca ratio values of different cleaning experiments for surface sediments located proximal to and distal from the Sunda Strait.

Average Ba/Ca ratio value cleaned with Surface sediments location:	Hydrazine (µmol mol^{-1})	Water (µmol mol^{-1})	Hydroxylamine (µmol mol^{-1})	DTPA (µmol mol^{-1})	Mg/Ca cleaning (µmol mol^{-1})
Near the Sunda Strait (GeoB 10036-3, GeoB 10038-3, GeoB 10041-3, and SO189-02MC)	1.63	2.30	2.79	2.05	3.48
Far from the Sunda Strait (GeoB 10033-3, GeoB 10034-3, SO189-11MC)	1.64	2.14	2.49	1.51	3.05

The correlation plot between *G. sacculifer* $\delta^{18}O_{sw}$ and *G. sacculifer* Ba/Ca of different cleaning procedures for surface sediments nearby the Sunda Strait is shown in Fig. 2. Positive correlations are observed in Ba/Ca of Mg/Ca cleaning (r^2=0.65, n=4), in Ba/Ca cleaned with water (r^2=0.97, n=5) and hydroxylamine (r^2=0.57, n=6). However, we expect that higher Ba/Ca ratios should correspond to lower $\delta^{18}O_{sw}$ values. Hence, we suggest that the Ba/ca ratios do not represent salinity. A weak correlation is also observed between *G. sacculifer* $\delta^{18}O_{sw}$ values and the values of Ba/Ca ratios cleaned with hydrazine (r^2<0.01, n=4) and DTPA (r^2=0.27, n=4). In summary, according to our new results, we suggest that *G. sacculifer* Ba/Ca cannot be applied as a tracer for freshwater discharge in the ETIO off the Sunda Strait due to the fact that Ba/Ca ratio of *G. sacculifer* appears to be influenced not only by freshwater discharge and but also by upwelling. Moreover, cleaning experiments, as indicated by Table 3, suggest that a Mg/Ca cleaning method introduced by Barker et al. (2003), DTPA and hydroxylamine can be used to extract Ba/Ca ratio from the planktic foraminifera shells for the region of ETIO due to their reliability to preserve seawater Ba/Ca. The similar Ba/Ca values between "freshwater discharge" region (proximity to the Sunda Strait) and "non-freshwater discharge" region (distal from the Sunda Strait) in the hydrazine experiment imply that this reductive reagent cannot be used for cleaning the Ba/Ca foraminifera.

5.2. Testing *G. sacculifer* Ba/Ca as an indicator for marine productivity

In order to investigate the potential use of *G. sacculifer* Ba/Ca as a proxy for marine productivity we compare our Ba/Ca data to the published data of marine productivity indicators in the ETIO like bulk content of organic carbon ($C_{org.}$), the isotopic composition of nitrogen ($\delta^{15}N$) (Baumgart et al., 2010), opal contentand planktic foraminifera *G. ruber* $\delta^{13}C$ (Mohtadi et al., 2011). Our comparison suggests that there is a lack of correlation between *G. sacculifer* Ba/Ca and those marine productivity indicators (Fig. 3). For Ba/Ca cleaned with reductive reagents of hydrazine and hydroxylamine, and DTPA the resulted r^2 are 0.07, 0.04, and 0.31, respectively.

Furthermore, the r^2 for Ba/Ca cleaned with water and of normal cleaning are 0.09 and 0.12, respectively. Although we do not have values for Ba/Ca ratio cleaned with hydrazine and DTPA, interestingly, the Ba/Ca ratios of GeoB 10042-2, which is located closed to the south Java upwelling core, differs from the other samples. The Ba/Ca ratios of GeoB 10042-2 indicate higher values than the other regions (Fig. 1 and Table 1)

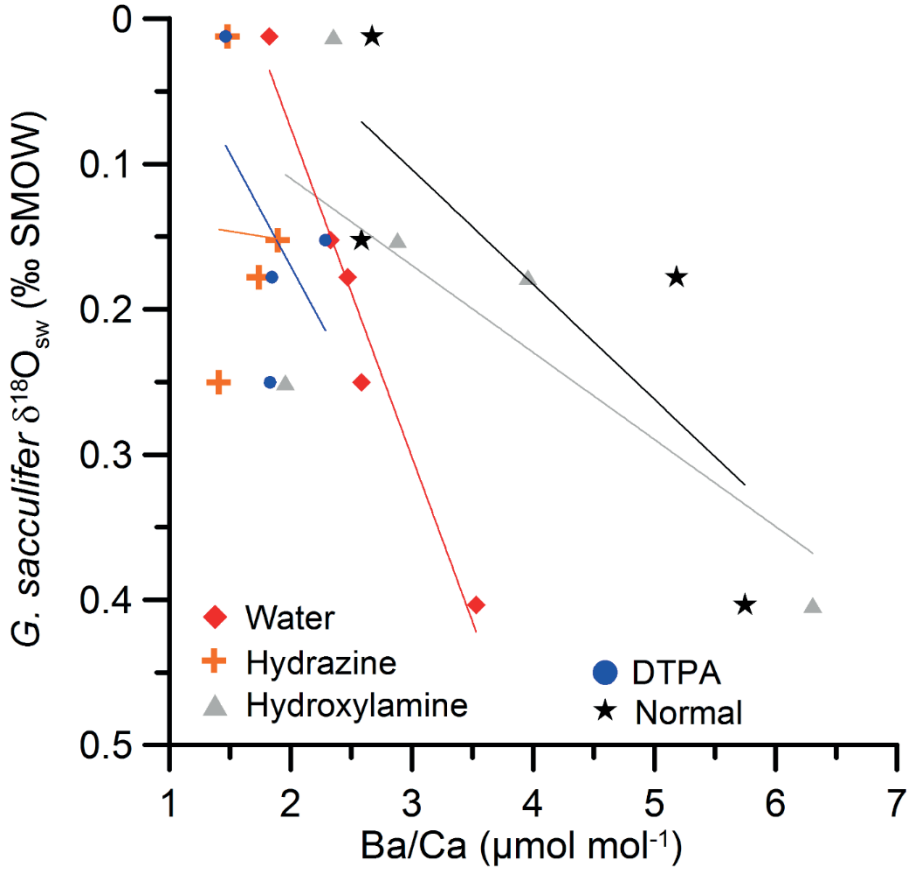

Fig. 2. Correlation plots between *G. sacculifer* seawater $\delta^{18}O$ (‰ SMOW) and *G. sacculifer* Ba/Ca ratios of different cleaning experiments.

Congruent with this observation opal concentration in surface sediment GeoB 10042-2 also exhibits a relatively high concentration (5.2 %) compared to other surface sediment samples used in this study (Table 1). The highest opal concentration (7.2 %) in the studied area is found in GeoB 10038-3. In addition to opal, a systematic trend in concentration is pronounced in the

region off Sumatra, with higher (lower) concentration is observed in the southern (northern) Sumatra. Mohtadi et al. (2007) suggest that opal is a reliable proxy for marine productivity in the ETIO as its spatial distribution is tightly coupled to the south Java-Lesser Sunda Island upwelling that occurs during SEM season. In corroboration with this suggestion a sediment trap study by Romero et al. (2009) also revealed that the highest flux of opal occurred during the SEM season (>150 mg m^{-2} d^{-1}). Furthermore, according to the findings of Mohtadi et al. (2007) there is a strong NW-SE gradient in the spatial distribution of opal concentration in the ETIO. High opal concentrations of 6.37, 7.26, and 9.02 % are found in the surface sediments off south Java, Lombok Basin, and in the Savu Sea, respectively, whereas low opal concentrations (≤ 4.2 %) are observed in the surface sediments off western Sumatra, where the upwelling influence is diminished.

It is likely that high Ba/Ca ratio values in GeoB 10042-2 are strongly coupled to the south Java upwelling. During the upwelling season the primary productivity in the regions off south Java and Lesser Sunda Island chain are increased. The upwelling-induced chlorophyll a bloom leads to enhanced barite precipitation and flux in the water column (Ganeshram et al., 2003; Paytan and Griffith, 2007). Therefore it is plausible that the higher Ba/Ca ratios of *G. sacculifer* in GeoB 10042-2 may reflect higher seawater Ba concentration in the region. However, as the position of GeoB 10042-2 is also close to the Sunda Strait, we believe that the higher value of Ba/Ca ratios in *G. sacculifer* may also be influenced by freshwater advection of Java Sea waters into the Sunda Strait (detailed explanation in the next section). In order to validate this observation a similar study on other multiple planktic foraminifera species collected from the upwelling region of southern Java-Lesser Sunda Island chain (e.g. southern Bali, Lombok and Sumba) is ultimately needed.

Fig. 3. Correlation plots between *G. sacculifer* seawater $\delta^{18}O$ (‰ SMOW) and *G. sacculifer* Ba/Ca ratios of different cleaning experiments.

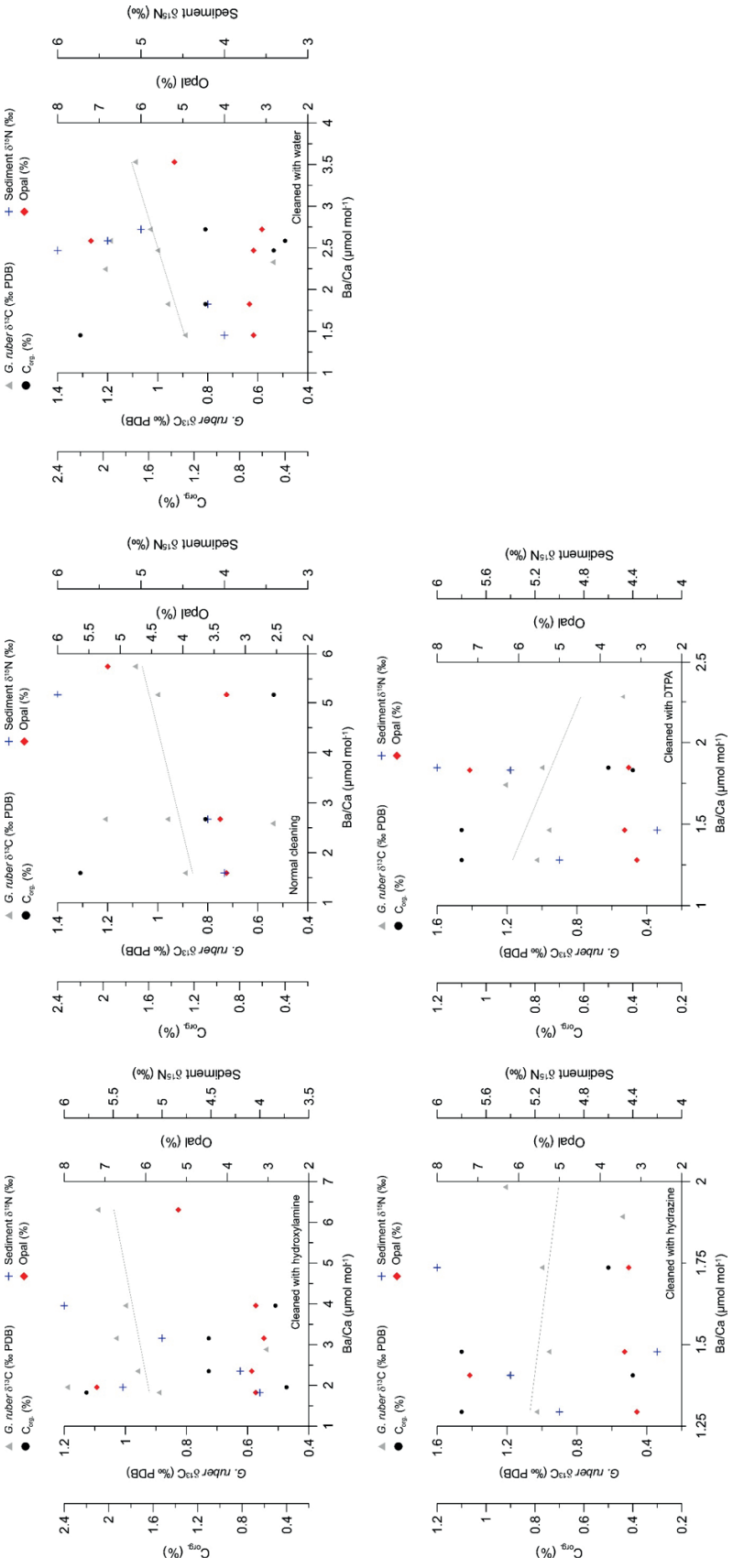

Spatial distribution of the surface sediment $\delta^{15}N$ off Sumatra also shows similar NW-SE gradient as opal (GeoB 10033-3, GeoB 10034-3, GeoB 10040-3 and GeoB 10041-3; Table 1). In addition, the $\delta^{15}N$ values also exhibits a nearshore-offshore trend (GeoB 10036-3, GeoB 10039-3, GeoB 10038-3, GeoB 10041-3, and GeoB 10040-3). For both patterns the highest $\delta^{15}N$ value is observed in the GeoB 10041-3 (6.0 ‰). Unfortunately, the $\delta^{15}N$ data of GeoB 10042-2 was not available, hence, we cannot suggest whether this increase relates to upwelling or not. Higher values for both parameters are found in the GeoB 10033-3, GeoB 10034-3, and SO189-11MC, which are located distal from the upwelling region. This finding suggests that upwelling is a not major contributor for the high values of $C_{org.}$ and *G. sacculifer* $\delta^{13}C$. Meanwhile, spatial distribution of the $C_{org.}$ and *G. sacculifer* $\delta^{13}C$ shows an opposite trend compared to opal concentration. Higher values for both parameters are found in the GeoB 10033-3, GeoB 10034-3, and SO189-11MC, which are located distal from the upwelling region. This finding suggests that upwelling is a not major contributor for the high values of $C_{org.}$ and *G. sacculifer* $\delta^{13}C$.

6. Conclusion

Our present study investigates the potential use of Ba/Ca ratio of planktic foraminifera *G. sacculifer* to trace modern and past salinity and productivity in the ETIO off Sumatra. Our new data provide evidence that the Ba/Ca ratio of *G. sacculifer* cannot be used to reconstruct freshwater discharge. Furthermore, the results indicate that the Ba/Ca ratio of *G. sacculifer* has a potential to trace modern and past marine productivities in the ETIO off south Java and Lesser Sunda Islands. We also have conducted a set of cleaning experiment on planktic foraminifera *G. sacculifer* to test the use of reductive solutions of hydrazine, hydroxylamine, and DTPA for Ba/Ca ratio extraction. According to our experiment results, we conclude that a cleaning

protocol of Barker et al. (2003), DTPA, and hydroxylamine can be used to extract Ba/Ca ratio from planktic foraminifera tests in the ETIO.

Acknowledgments

We are grateful to S. Pape for technical assistance. R.Y. Setiawan acknowledges financial support from the Deutscher Akademischer Austauschdienst (DAAD grant A/10/7596). This study was supported by the German Ministry of Education and Research (project PABESIA) and the Deutsche Forschungsgemeinschaft (DFG grant HE3412/15-1). The data of this study are archived and can be retrieved at PANGAEA (www.pangaea.de).

7. Synthesis

This study provides new evidence and understanding on hydrological changes in the eastern tropical Indian Ocean (ETIO). There are two pivotal findings resulting from this study. First, the new reconstruction of sea surface conditions off the Sunda Strait for the past ~40 kyr reveals that the ETIO has experienced saltier sea surface condition, as indicated by high values of seawater $\delta^{18}O$ ($\delta^{18}O_{sw}$), and decreased precipitation (low Ti/Ca ratio) during Heinrich stadials 1-3 and the Younger Dryas (YD) (Mohtadi et al., 2010a; b; Mohtadi et al., 2014). In contrast, off the Sunda Strait sea surface waters were less saline (indicated by low $\delta^{18}O_{sw}$) during the Holocene compared to the last glacial. Moreover, results of this study provide robust evidence suggesting that the opening of the Sunda Strait at ~10 kyr is a primary factor inducing fresher surface condition in the ETIO region off the Sunda Strait through a persistent transport of low salinity Java Sea water. Consequently, the variability of the $\delta^{18}O_{sw}$ values off the Sunda Strait should be interpreted with caution as a proxy for changing rainfall or P-E.

The second pivotal finding of this study is a novel millennial-scale reconstruction of past bottom water conditions off the Sunda Strait. This study underlines the potential of using the neodymium isotope ratio (ε_{Nd}) of authigenic coatings of mixed planktic foraminifera and of detrital silicates as tracers for the ITF flow and sediment provenance in the ETIO, respectively. For the first time, results of this study provide an evidence for modifications of the deep-water neodymium isotope composition (indicated here by foraminifera ε_{Nd}) off the Sunda Strait during the past ~19 kyr. Furthermore, results of this study also reveal that foraminifera ε_{Nd} and detrital ε_{Nd} are sensitive to large terrigenous input and the ITF flow.

Based on the two pivotal findings mentioned above, it is clear that the opening of the Sunda Strait has played an important role in the hydrology development of the ETIO. Moreover, this study provides robust evidence on the impacts of the opening of the Sunda Strait on the surface and bottom water hydrography, and shows that the ETIO is a sensitive region to climate

changes. These two studies promote the importance of using different proxies for the hydrology development investigations and most importantly, results of this study lay the foundation for future research in the region.

This study also shows that in the ETIO the Ba/Ca ratio of the planktic foraminifera *G sacculifer* does not serve as a suitable tracer for modern and past freshwater discharge as seawater Ba/Ca in this region is also influenced by upwelling. It is likely that the modern oceanographic setting off south Sumatra and Java complicates the use of *G. sacculifer* Ba/Ca to trace modern and past changes in freshwater discharge. Furthermore, results of cleaning experiment demonstrate that the *G. sacculifer* Ba/Ca ratio values of different cleaning methods show a consistent pattern, i.e. the Ba/Ca ratio values cleaned with hydroxylamine and of normal cleaning are always higher than Ba/Ca values cleaned with water. Whereas Ba/Ca values cleaned with hydrazine and DTPA are always lower than those cleaned with water. Also, reductive solution of hydroxylamine and cleaning protocol of Barker et al. (2003) can be used to extract Ba/Ca from planktic foraminifera shells.

8. Outlook

The eastern tropical Indian Ocean (ETIO) has been investigated intensively during the past decade. Foremost among these investigations is the reconstruction of sea surface conditions based on fossil planktic foraminifera *G. ruber* s.s. (Mohtadi et al., 2007; 2009; 2010a; 2010b; 2011a; 2011b; 2014; Kwiatkowski et al., 2015). However, until today only the study presented here provides a robust evidence on the persistent transport of low salinity Java Sea water via the Sunda Strait throughout the Holocene as reflected in the variability of $\delta^{18}O_{sw}$ data. Simulation and observation studies suggest that the strength of the transport of low salinity Java Sea water is influenced by the Australian-Indonesian Monsoon (AIM) winds (Putri, 2005), and this freshwater flux influences the South Java Current (SJC) by lowering surface salinity down to 32‰ (Wijffels et al., 1996). Therefore, it is essential to reconstruct the Holocene variability of $\delta^{18}O_{sw}$ on a set of thermocline and deeper dwelling foraminifera (e.g. *P. obliquiloculata*, *N. dutertrei*, *G. tumida* and *G. truncatulinoides*) that calcify at different depths in order to constrain the impact of freshwater advection on the deeper water column. Such a study may suggest that a prominent freshening at thermocline depth implies a stronger freshwater advection due to anomalous SEM winds and may serve as the first study in deciphering the Holocene water column stratification of the ETIO in great detail.

It is well known that the ETIO is influenced by complex climate systems like ENSO and IOD and it has been suggested that *G. ruber* s.s. reflects annual mean mixed-layer conditions between 0 and 30 m in this region (Mohtadi et al., 2009; 2011b). For long-term research goals, it is necessary to conduct long-term in situ observations paired with a quantitative analysis of planktic foraminifera fluxes in order to ground-truth the extent to which this proxy is controlled by different climate phenomena. Furthermore, it is also vital to reconstruct long-term IOD variability from the non-ENSO and monsoon region (off northern and central Sumatra) in order to gain a comprehensive knowledge on the evolution of IOD.

The use of the radiogenic neodymium isotope composition (ε_{Nd}) in this study provides novel insights about the modification of the bottom waters (as reflected in foraminiferal ε_{Nd} data) during the past 19 kyr. Indeed, results of this study lay the foundation for future research in the ETIO as this is the first study in utilizing foraminfera ε_{Nd} for bottom water reconstruction in the region. However, the long-term (glacial-interglacial) variability and modification of bottom water ε_{Nd} are still unknown. It is critical to investigate the long-term variability of the bottom water ε_{Nd} as the ETIO region is the only tropical pathway of the global thermohaline circulation. Talley and Sprintall (2005) suggest that the deepest ITF pathway is through the Maluku Sea into the Banda Sea, and then exiting via Leti and Timor Straits (1250 and 1890 m). Thus, variability of the bottom water ε_{Nd} at depths of 1250 m and 1890 m may partly reflect the thermohaline circulation and thus, might reveal its sensitivity to climate changes. Also, core top foraminifera ε_{Nd} data for the ETIO region are not available to date. Hence, it is also necessary to perform neodymium isotope analyses on core top foraminifera in order to better constrain the signature of bottom water ε_{Nd} and to investigate the influence of boundary exchange on bottom water ε_{Nd} in the ETIO region (Lacan and Jeandel, 2005).

9. References

Abram, N. J., M. K. Gagan, Z. Liu, W. S. Hantoro, M. T. McCulloch, and B. W. Suwargadi (2007), Seasonal characteristics of the Indian Ocean Dipole during the Holocene epoch, *Nature, 445(7125)*, 299-302.

Abram, N. J., H. V. McGregor, M. K. Gagan, W. S. Hantoro, and B. W. Suwargadi (2009), Oscillations in the southern extent of the Indo-Pacific Warm Pool during the mid-Holocene, *Quaternary Science Reviews, 28*(25–26), 2794-2803.

Aldrian, E., and R. D. Susanto (2003), Identification of three dominant rainfall regions within Indonesia and their relationship to sea surface temperature. *International Journal of Climatology*, *23*, 1435–1452.

Amakawa, H., D. S. Alibo, and Y. Nozaki (2000), Nd isotopic composition and REE pattern in the surface waters of the eastern Indian Ocean and its adjacent seas, *Geochimica et Cosmochimica Acta, 64(10)*, 1715-1727.

Anand, P., H. Elderfield, and M. H. Conte (2003), Calibration of Mg/Ca thermometry in planktonic foraminifera from a sediment trap time series, *Paleoceanography*, *18*, 1050, doi:10.1029/2002PA000846.

Arbuszewski, J., P. deMenocal, A. Kaplan, and E. C. Farmer (2010), On the fidelity of shell-derived δ^{18}Oseawater estimates, *Earth and Planetary Science Letters*, *300*, 185-196.

Arsouze, T., J. C. Dutay, F. Lacan, and C. Jeandel (2009), Reconstructing the Nd oceanic cycle using a coupled dynamical – biogeochemical model, *Biogeosciences, 6*(12), 2829-2846.

Atmadipoera, A., R. Molcard, G. Madec, S. Wijffels, J. Sprintall, A. Koch-Larrouy, I. Jaya, and A. Supangat (2009), Characteristics and variability of the Indonesian throughflow water at the outflow straits, *Deep Sea Research Part I: Oceanographic Research Papers, 56(11)*, 1942-1954.

Ayliffe, L. K., et al. (2013), Rapid interhemispheric climate links via the Australasian monsoon during the last deglaciation, *Nature Communications*, *4*, doi: 10.1038/ncomms3908.

Barker, S., M. Greaves, and H. Elderfield (2003), A study of cleaning procedures used for foraminiferal Mg/Ca paleothermometry, *Geochemistry, Geophysics, Geosystems, 4(9)*, 1-20.

Bemis, B. E., H. J. Spero, J. Bijma, and D. W. Lea (1998), Reevaluation of the oxygen isotopic composition of planktonic foraminifera: Experimental results and revised paleotemperature equations, *Paleoceanography*, *13*, 150-160.

Bishop, J. K. B. (1988), The barite-opal-organic carbon association in oceanic particulate matter, *Nature, 332(6162)*, 341-343.

Blaauw, M., and J. A. Christen (2011), Flexible paleoclimate age-depth models using an autoregressive gamma process. *Bayesian Analysis*, *6*, 457-474.

Boyle, E. A. (1981), Cadmium, zinc, copper, and barium in foraminifera tests, *Earth and Planetary Science Letters, 53(1)*, 11-35.

Bush, A. B. G., and R. G. Fairbanks (2003), Exposing the Sunda shelf: Tropical responses to eustatic sea level change, *Journal of Geophysical Research Atmospheres*, *108*, 4446, doi: 10.1029/2002JD003027.

Cannon, C. H., R. J. Morley, and A. B. G. Bush (2009), The current refugial rainforests of Sundaland are unrepresentative of their biogeographic past and highly vulnerable to disturbance, *Proceedings of the National Academy of Sciences, 106(27)*, 11188-11193.

Carolin, S. A., K. M. Cobb, J. F. Adkins, B. Clark, J. L. Conroy, S. Lejau, J. Malang, and A. A. Tuen (2013), Varied Response of Western Pacific Hydrology to Climate Forcings over the Last Glacial Period, *Science*, *340*, 1564-1566.

De Deckker, P., and F. X. Gingele (2002), On the occurrence of the giant diatom *Ethmodiscus rex* in an 80-ka record from a deep-sea core, southeast of Sumatra, Indonesia: implications for tropical palaeoceanography, *Marine Geology, 183*, 31-43.

Denniston, R. F., K.-H. Wyrwoll, Y. Asmerom, V. J. Polyak, W. F. Humphreys, J. Cugley, D. Woods, Z. LaPointe, J. Peota, and E. Greaves (2013), North Atlantic forcing of millennial-scale Indo-Australian monsoon dynamics during the Last Glacial period, *Quaternary Science Reviews*, *72*, 159-168.

DiNezio, P. N., A. Clement, G. A. Vecchi, B. Soden, A. J. Broccoli, B. L. Otto-Bliesner, and P. Braconnot (2011), The response of the Walker circulation to Last Glacial Maximum forcing: Implications for detection in proxies, *Paleoceanography, 26*, PA3217, doi: 10.1029/2010pa002083.

DiNezio, P. N., and J. E. Tierney (2013), The effect of sea level on glacial Indo-Pacific climate, *Nature Geoscience*, *6*, 485-491.

Ding, X., F. Bassinot, F. Guichard, Q. Y. Li, N. Q. Fang, L. Labeyrie, R. C. Xin, M. K. Adisaputra, and K. Hardjawidjaksana (2006), Distribution and ecology of planktonic foraminifera from the seas around the Indonesian Archipelago, *Marine Micropaleontology*, *58*, 114–134.

Du, Y., T. Qu, and G. Meyers (2008), Interannual Variability of Sea Surface Temperature off Java and Sumatra in a Global GCM, *Journal of Climate*, *21*, 2451-2465.

Du, Y., T. Qu, G. Meyers, Y. Masumoto, and H. Sasaki (2005), Seasonal heat budget in the mixed layer of the southeastern tropical Indian Ocean in a high-resolution ocean general circulation model, *Journal of Geophysical Research Oceans*, *110,* 1978-2012.

Dubois, N., D. W. Oppo, V. V. Galy, M. Mohtadi, S. van der Kaars, J. E. Tierney, Y. Rosenthal, T. I. Eglinton, A. Lückge, and B. K. Linsley (2014), Indonesian vegetation response to changes in rainfall seasonality over the past 25,000 years, *Nature Geoscience*, *7*, 513-517.

Dykoski, C. A., R. L. Edwards, H. Cheng, D. Yuan, Y. Cai, M. Zhang, Y. Lin, J. Qing, Z. An, and J. Revenaugh (2005), A high-resolution, absolute-dated Holocene and deglacial Asian monsoon record from Dongge Cave, China, *Earth and Planetary Science Letters, 233*, 71-86.

Dymond, J., E. Suess, and M. Lyle (1992), Barium in Deep-Sea Sediment: A Geochemical Proxy for Paleoproductivity, *Paleoceanography, 7(2)*, 163-181.

Ehlert, C., M. Frank, B. A. Haley, U. Böniger, P. De Deckker, and F. X. Gingele (2011), Current transport versus continental inputs in the eastern Indian Ocean: Radiogenic isotope signatures of clay size sediments, *Geochemistry, Geophysics, Geosystems, 12(6)*, 1-17.

England, M. H., and F. Huang (2005), On the Interannual Variability of the Indonesian Throughflow and Its Linkage with ENSO. *Journal of Climate*, *18*, 1435–1444.

Fan, W., Z. Jian, F. Bassinot, and Z. Chu (2013), Holocene centennial-scale changes of the Indonesian and South China Sea throughflows: Evidences from the Makassar Strait, *Global and Planetary Change*, *111*, 111-117.

Ferguson, J. E., G. M. Henderson, M. Kucera, and R. E. M. Rickaby (2008), Systematic change of foraminiferal Mg/Ca ratios across a strong salinity gradient, *Earth and Planetary Science Letters*, *265*, 153-166.

Ffield, A., K. Vranes, A. L. Gordon, R. D. Susanto, and S. L. Garzoli (2000), Temperature variability within Makassar Strait, *Geophyical. Research Letters*, *27*, 237-240.

Fleitmann, D., et al. (2007), Holocene ITCZ and Indian monsoon dynamics recorded in stalagmites from Oman and Yemen (Socotra), *Quaternary Science Reviews, 26*, 170-188.

Frank, M. (2002), Radiogenic isotopes: tracers of past ocean circulation and erosional input, *Reviews of Geophysics, 40(1),* 1-1-1-38.

Frank, M., N. Whiteley, T. van de Flierdt, B. C. Reynolds, and K. O'Nions (2006), Nd and Pb isotope evolution of deep water masses in the eastern Indian Ocean during the past 33 Myr, *Chemical Geology, 226(3–4)*, 264-279.

Gibbons, F. T., D. W. Oppo, M. Mohtadi, Y. Rosenthal, J. Cheng, Z. Liu, and B. K. Linsley (2014), Deglacial $\delta^{18}O$ and hydrologic variability in the tropical Pacific and Indian Oceans, *Earth and Planetary Science Letters*, *387*, 240-251.

Gingele, X. F., P. De Deckker, A. Girault, and F. Guichard (2002), History of the South Java Current over the past 80 ka, *Palaeogeography, Palaeoclimatology, Palaeoecology*, *183*, 247-260.

Gordon, A. L., R. D. Susanto, and A. Ffield (1999), Throughflow within Makassar Strait, *Geophysical Research Letters, 26(21)*, 3325-3328.

Gordon, A. L., R. D. Susanto, and K. Vranes (2003), Cool Indonesian throughflow as a consequence of restricted surface layer flow, *Nature, 425(6960)*, 824-828.

Gordon, A. L., J. Sprintall, H. M. Van Aken, D. Susanto, S. Wijffels, R. Molcard, A. Ffield, W. Pranowo, and S. Wirasantosa (2010), The Indonesian throughflow during 2004–2006 as observed by the INSTANT program, *Dynamics of Atmospheres and Oceans*, *50*, 115-128.

Gordon, A. L., R. D. Susanto, and K. Vranes (2003), Cool Indonesian throughflow as a consequence of restricted surface layer flow, *Nature*, *425*, 824-828.

Greaves, M., et al. (2008), Interlaboratory comparison study of calibration standards for foraminiferal Mg/Ca thermometry, *Geochemistry, Geophysics, Geosystems*, *9*, Q08010, doi:10.1029/2008GC001974.

Griffith, E. M., and A. Paytan (2012), Barite in the ocean – occurrence, geochemistry and palaeoceanographic applications, *Sedimentology, 59(6)*, 1817-1835.

Griffiths, M. L., et al. (2009), Increasing Australian-Indonesian monsoon rainfall linked to early Holocene sea-level rise, *Nature Geoscience*, *2*, 636-639.

Griffiths, M. L., R. N. Drysdale, M. K. Gagan, J.-x. Zhao, J. C. Hellstrom, L. K. Ayliffe, and W. S. Hantoro (2013), Abrupt increase in east Indonesian rainfall from flooding of the Sunda Shelf ~9500 years ago, *Quaternary Science Reviews*, *74*, 273-279.

Hall, J. M., and L. H. Chan (2004), Ba/Ca in Neogloboquadrina pachyderma as an indicator of deglacial meltwater discharge into the western Arctic Ocean, *Paleoceanography, 19(1)*, 1-9.

Hanebuth, T., K. Stattegger, and P. M. Grootes (2000), Rapid Flooding of the Sunda Shelf: A Late-Glacial Sea-Level Record, *Science*, *288*, 1033-1035.

Hanebuth, T. J. J., and K. Stattegger (2004), Depositional sequences on a late Pleistocene–Holocene tropical siliciclastic shelf (Sunda Shelf, southeast Asia), *Journal of Asian Earth Sciences, 23(1)*, 113-126.

Hanebuth, T. J. J., K. Stattegger, and A. Bojanowski (2009), Termination of the Last Glacial Maximum sea-level lowstand: The Sunda-Shelf data revisited, *Global and Planetary Change, 66(1–2)*, 76-84.

Hanebuth, T. J. J., H. K. Voris, Y. Yokoyama, Y. Saito, and J. Okuno (2011), Formation and fate of sedimentary depocentres on Southeast Asia's Sunda Shelf over the past sea-level cycle and biogeographic implications, *Earth-Science Reviews, 104*, 92-110.

Hebbeln, D., and cruise participants (2006), Report and preliminary results of RV SONNE Cruise SO-184, Pabesia, Durban (South Africa) - Cilacap (Indonesia) - Darwin (Australia), July 8th - September 13th, 2005, 142 pp, Universität Bremen.

Hendon, H. H. (2003), Indonesian Rainfall Variability: Impacts of ENSO and Local Air–Sea Interaction, *Journal of Climate*, *16*, 1775-1790.

Hertzberg, J. E. and M.W. Schmidt (2013), Refining *Globigerinoides ruber* Mg/Ca paleothermometry in the Atlantic Ocean, *Earth and Planetary Science Letters*, *383*, 123-133.

Holbourn, A., W. Kuhnt, and J. Xu (2011), Indonesian Throughflow variability during the last 140 ka: the Timor Sea outflow, *Geological Society, London, Special Publications, 355(1)*, 283-303.

Iskandar, I., S. A. Rao, and T. Tozuka (2009), Chlorophyll-a bloom along the southern coasts of Java and Sumatra during 2006, *International Journal of Remote Sensing, 30(3)*, 663-671.

Jeandel, C., J. K. Bishop, and A. Zindler (1995), Exchange of neodymium and its isotopes between seawater and small and large particles in the Sargasso Sea, *Geochimica et Cosmochimica Acta, 59(3)*, 535-547.

Jeandel, C., D. Thouron, and M. Fieux (1998), Concentrations and isotopic compositions of neodymium in the eastern Indian Ocean and Indonesian straits, *Geochimica et Cosmochimica Acta, 62(15)*, 2597-2607.

Jouzel, J., et al. (2007), Orbital and Millennial Antarctic Climate Variability over the Past 800,000 Years, *Science*, *317*, 793-796.

Kershaw, A. P., S. van der Kaars, and J. R. Flenley (2007), The Quaternary history of far eastern rainforests, in Tropical Rainforest Responses to Climatic Change, pp. 77-115, Springer Berlin Heidelberg.

Kisakürek, B., A. Eisenhauer, F. Böhm, D. Garbe-Schönberg, and J. Erez (2008), Controls on shell Mg/Ca and Sr/Ca in cultured planktonic foraminiferan, *Globigerinoides ruber* (white), *Earth and Planetary Science Letters*, *273*, 260-269.

Kraft, S., M. Frank, E. C. Hathorne, and S. Weldeab (2013), Assessment of seawater Nd isotope signatures extracted from foraminiferal shells and authigenic phases of Gulf of Guinea sediments, *Geochimica et Cosmochimica Acta, 121(0)*, 414-435.

Kwiatkowski, C., M. Prange, V. Varma, S. Steinke, D. Hebbeln, and M. Mohtadi (2015), Holocene variations of thermocline conditions in the eastern tropical Indian Ocean, *Quaternary Science Reviews, 114(0)*, 33-42.

Lacan, F., and C. Jeandel (2005), Neodymium isotopes as a new tool for quantifying exchange fluxes at the continent–ocean interface, *Earth and Planetary Science Letters, 232(3–4)*, 245-257.

Lea, D. W., and H. J. Spero (1994), Assessing the reliability of paleochemical tracers: Barium uptake in the shells of planktonic foraminifera, *Paleoceanography, 9(3)*, 445-452.

Levi, C., L. Labeyrie, F. Bassinot, F. Guichard, E. Cortijo, C. Waelbroeck, N. Caillon, J. Duprat, T. de Garidel-Thoron, and H. Elderfield (2007), Low-latitude hydrological cycle and rapid climate changes during the last deglaciation, *Geochemistry, Geophysics, Geosystems*, *8*, Q05N12. doi: 10.1029/2006GC001514.

Linsley, B. K., Y. Rosenthal, and D. W. Oppo (2010), Holocene evolution of the Indonesian throughflow and the western Pacific warm pool, *Nature Geoscience*, *3*, 578-583.

Locarnini, R. A., A. V. Mishonov, J. I. Antonov, T. P. Boyer, H. E. Garcia, O. K. Baranova, M. M. Zweng, C. R. Paver, J. R. Reagan, D. R. Johnson, M. Hamilton, and D. Seidov, 2013. World Ocean Atlas 2013, Volume 1: Temperature. S. Levitus, Ed., A. Mishonov Technical Ed.; NOAA Atlas NESDIS 73, 40 pp.

Luo, J.-J., R. Zhang, S. K. Behera, Y. Masumoto, F.-F. Jin, R. Lukas, and T. Yamagata (2010), Interaction between El Niño and Extreme Indian Ocean Dipole, *Journal of Climate, 23(3)*, 726-742.

Lückge, A., M. Mohtadi, C. Rühlemann, G. Scheeder, A. Vink, L. Reinhardt, and M. Wiedicke (2009), Monsoon versus ocean circulation controls on paleoenvironmental conditions off southern Sumatra during the past 300,000 years, *Paleoceanography, 24*, PA1208, doi:1210.1029/2008PA001627.

Maloney, B. K. (1980), Pollen analytical evidence for early forest clearance in North Sumatra, *Nature, 287*, 324-326.

Martin, P. A., and D. W. Lea (2002), A simple evaluation of cleaning procedures on fossil benthic foraminiferal Mg/Ca, *Geochemistry, Geophysics, Geosystems, 3(10)*, 1-8.

Mathien-Blard, E. and F. Bassinot (2009), Salinity bias on the foraminifera Mg/Ca thermometry: Correction procedure and implications for past ocean hydrographic reconstructions, *Geochemistry, Geophysics, Geosystems*, *10*, Q12011, doi:12010.11029/12008GC002353.

Martin, E. E., and H. Scher (2006), A Nd isotopic study of southern sourced waters and Indonesian Throughflow at intermediate depths in the Cenozoic Indian Ocean, *Geochemistry, Geophysics, Geosystems, 7(9)*,1-14.

McBride, J. L., M. R. Haylock, and N. Nicholls (2003), Relationships between the Maritime Continent Heat Source and the El Niño–Southern Oscillation Phenomenon, *Journal of Climate*, *16*, 2905-2914.

Meyers, G., R. J. Bailey, and A. P. Worby (1995), Geostrophic transport of Indonesian throughflow, *Deep Sea Research Part I: Oceanographic Research Papers, 42(7)*, 1163-1174.

Mohtadi, M., S. Steinke, J. Groeneveld, H. G. Fink, T. Rixen, D. Hebbeln, B. Donner, and B. Herunadi (2009), Low-latitude control on seasonal and interannual changes in planktonic foraminiferal flux and shell geochemistry off south Java: A sediment trap study, *Paleoceanography*, *24*, PA1201, doi:10.1029/2008PA001636.

Mohtadi, M., S. Steinke, A. Lückge, J. Groeneveld, and E. C. Hathorne (2010a), Glacial to Holocene surface hydrography of the tropical eastern Indian Ocean, *Earth and Planetary Science Letters*, *292*, 89-97.

Mohtadi, M., A. Lückge, S. Steinke, J. Groeneveld, D. Hebbeln, and N. Westphal (2010b), Late Pleistocene surface and thermocline conditions of the eastern tropical Indian Ocean, *Quaternary Science Reviews, 29*, 887-896.

Mohtadi, M., D. W. Oppo, S. Steinke, J.-B. W. Stuut, R. De Pol-Holz, D. Hebbeln, and A. Lückge (2011a), Glacial to Holocene swings of the Australian-Indonesian monsoon, *Nature Geoscience*, *4*, 540-544.

Mohtadi, M., D. W. Oppo, A. Lückge, R. DePol-Holz, S. Steinke, J. Groeneveld, N. Hemme, and D. Hebbeln (2011b), Reconstructing the thermal structure of the upper ocean: Insights from planktic foraminifera shell chemistry and alkenones in modern sediments of the tropical eastern Indian Ocean, *Paleoceanography, 26*, PA3219, doi:3210.1029/2011pa002132.

Mohtadi, M., M. Prange, D. W. Oppo, R. De Pol-Holz, U. Merkel, X. Zhang, S. Steinke, and A. Lückge (2014), North Atlantic forcing of tropical Indian Ocean climate, *Nature*, *509*, 76-80.

Molina-Kescher, M., M. Frank, and E. Hathorne (2014), South Pacific dissolved Nd isotope compositions and rare earth element distributions: Water mass mixing versus biogeochemical cycling, *Geochimica et Cosmochimica Acta, 127(0)*, 171-189.

Monnin, E., A. Indermühle, A. Dällenbach, J. Flückiger, B. Stauffer, T. F. Stocker, D. Raynaud, and J.-M. Barnola (2001), Atmospheric CO_2 Concentrations over the Last Glacial Termination, *Science*, *291*, 112-114.

Neale, R., and J. Slingo (2003), The Maritime Continent and Its Role in the Global Climate: A GCM Study, *Journal of Climate, 16(5)*, 834-848.

Ni, Y., G. L. Foster, T. Bailey, T. Elliott, D. N. Schmidt, P. Pearson, B. Haley, and C. Coath (2007), A core top assessment of proxies for the ocean carbonate system in surface-dwelling foraminifers, Paleoceanography, 22(3), 1-14.

Niedermeyer, E. M., A. L. Sessions, S. J. Feakins, and M. Mohtadi (2014), Hydroclimate of the western Indo-Pacific Warm Pool during the past 24,000 years, *Proceedings of the National Academy of Sciences*, *111*, 9402-9406.

Osborne, A. H., D. R. Newkirk, J. Groeneveld, E. E. Martin, R. Tiedemann, and M. Frank (2014), The seawater neodymium and lead isotope record of the final stages of Central American Seaway closure, *Paleoceanography, 29(7)*, 715-729.

Paillard, D., L. Labeyrie, and P. Yiou (1996), Macintosh Program performs time-series analysis, *Eos Transactions AGU*, *77*, 379–379.

Pelejero, C., M. Kienast, L. Wang, and J. O. Grimalt (1999), The flooding of Sundaland during the last deglaciation: imprints in hemipelagic sediments from the southern South China Sea, *Earth and Planetary Science Letters*, *171*, 661-671.

Pena, L. D., E. Calvo, I. Cacho, S. Eggins, and C. Pelejero (2005), Identification and removal of Mn-Mg-rich contaminant phases on foraminiferal tests: Implications for Mg/Ca past temperature reconstructions, *Geochemistry, Geophysics, Geosystems, 6(9)*, 1-25.

Pena, L. D., I. Cacho, E. Calvo, C. Pelejero, S. Eggins, and A. Sadekov (2008), Characterization of contaminant phases in foraminifera carbonates by electron microprobe mapping, *Geochemistry, Geophysics, Geosystems, 9(7)*, 1-12.

Piotrowski, A. M., A. Galy, J. A. L. Nicholl, N. Roberts, D. J. Wilson, J. A. Clegg, and J. Yu (2012), Reconstructing deglacial North and South Atlantic deep water sourcing using foraminiferal Nd isotopes, *Earth and Planetary Science Letters, 357–358(0)*, 289-297.

Piotrowski, A. M., V. K. Banakar, A. E. Scrivner, H. Elderfield, A. Galy, and A. Dennis (2009), Indian Ocean circulation and productivity during the last glacial cycle, *Earth and Planetary Science Letters, 285(1–2)*, 179-189.

Putri, M. R. (2005), Study of Ocean Climate Variability (1959-2002) in the Eastern Indian Ocean, Java Sea and Sunda Strait Using the HAMburg Shelf Ocean Model, Dissertation, Univ. Hamburg, 104 pp.

Qu, T., and G. Meyers (2005), Seasonal Characteristics of Circulation in the Southeastern Tropical Indian Ocean, *Journal of Physical Oceanography, 35(2)*, 255-267.

Qu, T., Y. Du, J. Strachan, G. Meyers, and J. Slingo (2005), Sea surface temperature and its variability in the Indonesian region. *Oceanography, 18*, 50–61.

Rasmusson, E. M., and T. H. Carpenter (1982), Variations in Tropical Sea Surface Temperature and Surface Wind Fields Associated with the Southern Oscillation/El Niño, *Monthly Weather Review, 110(5)*, 354-384.

Reimer, P. J., et al. (2013), IntCal13 and Marine13 Radiocarbon Age Calibration Curves 0–50,000 Years cal BP. *Radiocarbon, 55*, 1869-1887.

Rempfer, J., T. F. Stocker, F. Joos, J.-C. Dutay, and M. Siddall (2011), Modelling Nd-isotopes with a coarse resolution ocean circulation model: Sensitivities to model parameters and source/sink distributions, *Geochimica et Cosmochimica Acta, 75(20)*, 5927-5950.

Roberts, N. L., A. M. Piotrowski, H. Elderfield, T. I. Eglinton, and M. W. Lomas (2012), Rare earth element association with foraminifera, *Geochimica et Cosmochimica Acta, 94*(0), 57-71.

Romero, O. E., M. Mohtadi, P. Helmke, and D. Hebbeln (2012), High interglacial diatom paleoproductivity in the westernmost Indo-Pacific Warm Pool during the past 130,000 years, *Paleoceanography, 27*, PA3209, doi:3210.1029/2012pa002299.

Russell, J. M., H. Vogel, B. L. Konecky, S. Bijaksana, Y. Huang, M. Melles, N. Wattrus, K. Costa, and J. W. King (2014), Glacial forcing of central Indonesian hydroclimate since 60,000 y B.P, *Proceedings of the National Academy of Sciences*, *111*, 5100-5105.

Saji, N. H., B. N. Goswami, P. N. Vinayachandran, and T. Yamagata (1999), A dipole mode in the tropical Indian Ocean, *Nature, 401(6751)*, 360-363.

Schmidt, M. W., and J. Lynch-Stieglitz (2011), Florida Straits deglacial temperature and salinity change: Implications for tropical hydrologic cycle variability during the Younger Dryas, *Paleoceanography, 26(4)*, 1-16.

Setiawan, R. Y., and A. Habibi (2011), Satellite Detection of Summer Chlorophyll-a Bloom in the Gulf of Tomini, *Selected Topics in Applied Earth Observations and Remote Sensing, IEEE Journal of, 4*(4), 944-948.

Setiawan, R. Y., and H. Kawamura (2011), Summertime Phytoplankton Bloom in the South Sulawesi Sea, *Selected Topics in Applied Earth Observations and Remote Sensing, IEEE Journal of, 4*(1), 241-244.

Setiawan, R. Y., M. Mohtadi, J. Southon, J. Groeneveld, S. Steinke, D. Hebbeln (2015), The consequences of opening the Sunda Strait on the hydrography of the eastern tropical Indian Ocean, *Paleoceanography: under review after revision*.

Song, Q., A. L. Gordon, and M. Visbeck (2004), Spreading of the Indonesian Throughflow in the Indian Ocean, *Journal of Physical Oceanography, 34(4)*, 772-792.

Southon, J., M. Mohtadi, and R. De Pol-Holz (2013), Planktic Foram Dates from the Indonesian Arc: Marine ^{14}C Reservoir Ages and a Mythical AD 535 Volcanic Eruption. *Radiocarbon, 55*, 1869-1887.

Sprintall, J., and A. Révelard (2014), The Indonesian Throughflow response to Indo-Pacific climate variability, *Journal of Geophysical Research: Oceans, 119(2)*, 1161-1175.

Sprintall, J., A. L. Gordon, A. Koch-Larrouy, T. Lee, J. T. Potemra, K. Pujiana, and S. E. Wijffels (2014), The Indonesian seas and their role in the coupled ocean-climate system, *Nature Geosci, 7(7)*, 487-492.

Sprintall, J., S. Wijffels, R. Molcard, and I. Jaya (2010), Direct evidence of the South Java Current system in Ombai Strait, *Dynamics of Atmospheres and Oceans*, *50*, 140-156.

Sprintall, J., S. E. Wijffels, R. Molcard, and I. Jaya (2009), Direct estimates of the Indonesian Throughflow entering the Indian Ocean: 2004–2006, *Journal of Geophysical Research Oceans*, *114*, C07001, doi:10.1029/2008JC005257.

Steinke, S., M. Kienast, J. Groeneveld, L.-C. Lin, M.-T. Chen, and R. Rendle-Bühring (2008), Proxy dependence of the temporal pattern of deglacial warming in the tropical South China Sea: toward resolving seasonality, *Quaternary Science Reviews*, *27*, 688-700.

Steinke, S., M. Prange, C. Feist, J. Groeneveld, and M. Mohtadi (2014), Upwelling variability off southern Indonesia over the past two millennia, *Geophysical Research Letters, 41(21)*, 7684-7693.

Stuijts, I., J. C. Newsome, and J. R. Flenley (1988), Evidence for late quaternary vegetational change in the Sumatran and Javan highlands, *Review of Palaeobotany and Palynology*, *55*, 207-216.

Stumpf, R., S. Kraft, M. Frank, B. Haley, A. Holbourn, and W. Kuhnt (2015), Persistently strong Indonesian Throughflow during marine isotope stage 3: evidence from radiogenic isotopes, *Quaternary Science Reviews, 112(0)*, 197-206.

Susanto, R. D., Z. Wei, R. Adi, B. Fan, S. Li, and G. Fang (2013), Observations of the Karimata Strait througflow from December 2007 to November 2008, *Acta Oceanologica Sinica*, *32*, 1-6.

Susanto, R. D., G. Fang, I. Soesilo, Q. Zheng, F. Qiao, Z. Wei, and B. Sulistyo (2010), New Surveys of a Branch of the Indonesian Throughflow, *Eos Transactions AGU*, *91*, 261-263.

Susanto, R. D., and J. Marra, (2005), Effect of the 1997/98 El Niño on chlorophyll a variability along the southern coasts of Java and Sumatra. *Oceanography, 18*, 124–127.

Susanto, R. D., A. L. Gordon, and Q. Zheng (2001), Upwelling along the coasts of Java and Sumatra and its relation to ENSO, *Geophysical Research Letters*, *28*, 1599-1602.

Susanto, R. D., T. S. Moore, and J. Marra (2006), Ocean color variability in the Indonesian Seas during the SeaWiFS era, *Geochemistry, Geophysics, Geosystems, 7(5)*, 1-16.

Tachikawa, K., C. Jeandel, and M. Roy-Barman (1999), A new approach to the Nd residence time in the ocean: the role of atmospheric inputs, *Earth and Planetary Science Letters, 170(4)*, 433-446.

Tachikawa, K., V. Athias, and C. Jeandel (2003), Neodymium budget in the modern ocean and paleo-oceanographic implications, *Journal of Geophysical Research: Oceans, 108(C8)*, 1-13.

Talley, L. D., and J. Sprintall (2005), Deep expression of the Indonesian Throughflow: Indonesian Intermediate Water in the South Equatorial Current, *Journal of Geophysical Research: Oceans, 110(C10)*, 1-30.

Tjia, H. D. (1980), The Sunda Shelf, SE Asia. *Zeitschrift für Geomorphologie*, *24*, 405–427.

Vance, D., A. E. Scrivner, P. Beney, M. Staubwasser, G. M. Henderson, and N. C. Slowey (2004), The use of foraminifera as a record of the past neodymium isotope composition of seawater, *Paleoceanography, 19(2)*, 1-17.

van der Kaars, S., F. Bassinot, P. De Deckker, and F. Guichard (2010), Changes in monsoon and ocean circulation and the vegetation cover of southwest Sumatra through the last 83,000 years: The record from marine core BAR94-42, *Palaeogeography, Palaeoclimatology, Palaeoecology*, *296*, 52-78.

Vranes, K., and A. L. Gordon (2005), Comparison of Indonesian Throughflow transport observations, Makassar Strait to eastern Indian Ocean, *Geophysical Research Letters*, *32*, L10606, doi:10.1029/2004GL022158.

Vroon, P. Z., M. J. van Bergen, G. J. Klaver, and W. M. White (1995), Strontium, neodymium, and lead isotopic and trace-element signatures of the East indonesian sediments: provenance and implications for banda arc magma genesis, *Geochimica et Cosmochimica Acta, 59(12)*, 2573-2598.

Waelbroeck, C., L. Labeyrie, E. Michel, J. C. Duplessy, J. F. McManus, K. Lambeck, E. Balbon, and M. Labracherie (2002), Sea-level and deep water temperature changes derived from benthic foraminifera isotopic records, *Quaternary Science Reviews*, *21*, 295-305.

Weldeab, S., D. W. Lea, R. R. Schneider, and N. Andersen (2007), 155,000 Years of West African Monsoon and Ocean Thermal Evolution, *Science, 316(5829)*, 1303-1307.

Wilson, D. J., A. M. Piotrowski, A. Galy, and I. N. McCave (2012), A boundary exchange influence on deglacial neodymium isotope records from the deep western Indian Ocean, *Earth and Planetary Science Letters, 341–344(0)*, 35-47.

Xu, J., A. Holbourn, W. Kuhnt, Z. Jian, and H. Kawamura (2008), Changes in the thermocline structure of the Indonesian outflow during Terminations I and II, *Earth and Planetary Science Letters*, *273*, 152-162.

Yuan, D., J. Wang, T. Xu, P. Xu, Z. Hui, X. Zhao, Y. Luan, W. Zheng, and Y. Yu (2011), Forcing of the Indian Ocean Dipole on the Interannual Variations of the Tropical Pacific Ocean: Roles of the Indonesian Throughflow, *Journal of Climate, 24(14)*, 3593-3608.

Zhang, R., and T. L. Delworth (2005), Simulated Tropical Response to a Substantial Weakening of the Atlantic Thermohaline Circulation, *Journal of Climate*, *18*, 1853-1860.

Zweng, M. M, J.R. Reagan, J. I. Antonov, R. A. Locarnini, A.V. Mishonov, T. P. Boyer, H. E. Garcia, O. K. Baranova, D. R. Johnson, D. Seidov, M. M. Biddle (2013), World Ocean Atlas 2013, Volume 2: Salinity. S. Levitus, Ed., A. Mishonov Technical Ed.; NOAA Atlas NESDIS 74, 39 pp.